WIRELESS

communications

Principles & Practice

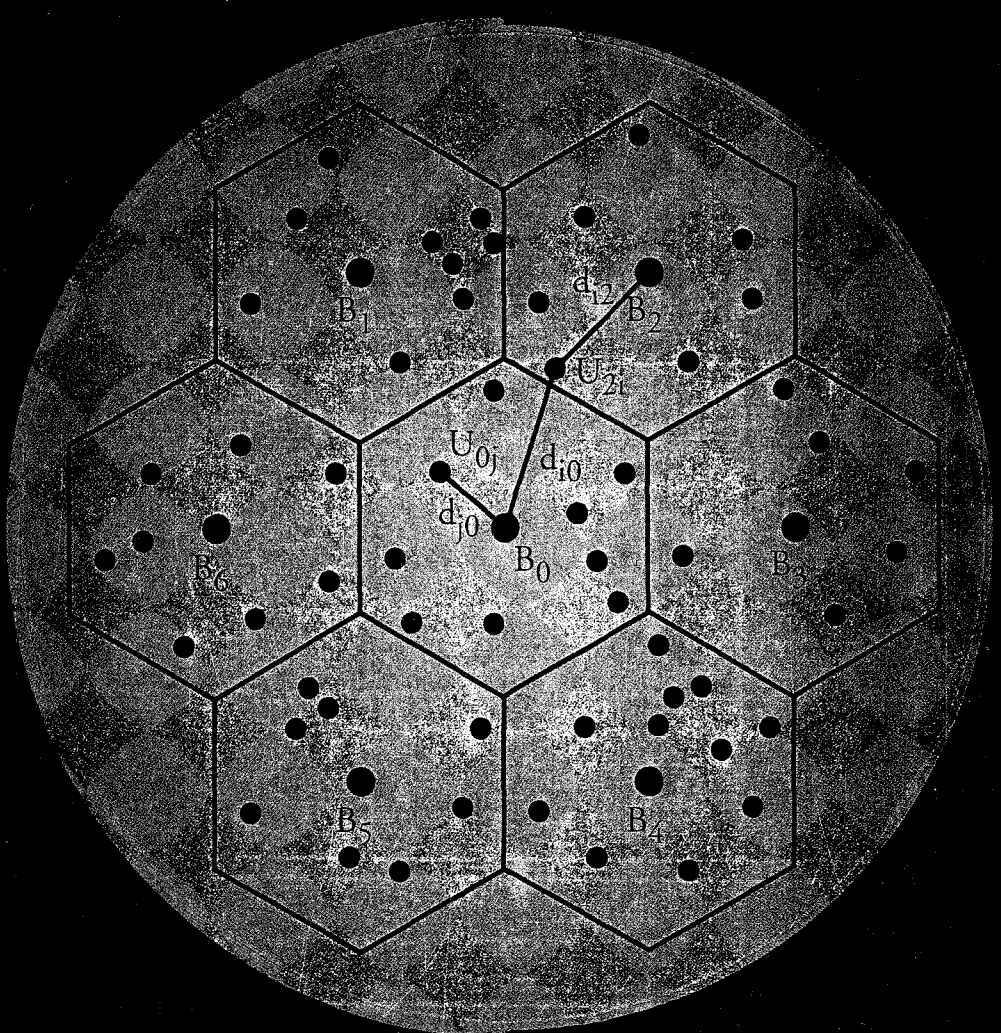

Theodore S. Rappaport

Wireless Communications

Principles and Practice

Theodore S. Rappaport

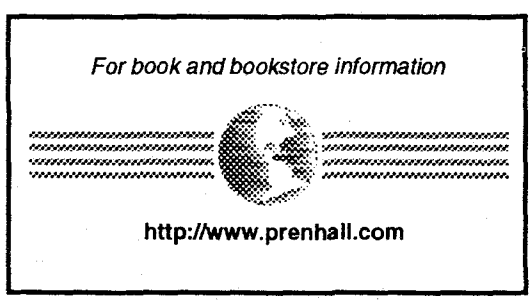

Prentice Hall PTR
Upper Saddle River, New Jersey 07458

Editorial/production manager: *Camille Trentacoste*
Cover design director: *Jerry Votta*
Cover designer: *Anthony Gemmellaro*
Manufacturing manager: *Alexis R. Heydt*
Acquisitions editor: *Karen Gettman*
Editorial assistant: *Barbara Alfieri*

Prentice-Hall, Inc.
A Simon & Schuster Company
Upper Saddle River, New Jersey 07458

The publisher offers discounts on this book when ordered in bulk quantities. For more information, contact Corporate Sales Department, Prentice Hall PTR, One Lake Street, Upper Saddle River, NJ 07458.
Phone: 800-382-3419; FAX: 201- 236-7141.
E-mail: corpsales@prenhall.com

Printed in the United States of America
10 9 8 7 6 5 4

ISBN 0-13-375536-3

Prentice-Hall International (UK) Limited, *London*
Prentice-Hall of Australia Pty. Limited, *Sydney*
Prentice-Hall Canada Inc., *Toronto*
Prentice-Hall Hispanoamericana, S.A., *Mexico*
Prentice-Hall of India Private Limited, *New Delhi*
Prentice-Hall of Japan, Inc., *Tokyo*
Simon & Schuster Asia Pte. Ltd., *Singapore*
Editora Prentice-Hall do Brasil, Ltda., *Rio de Janeiro*

The LORD has blessed me
with a wonderful family
to whom this book is dedicated

To my wife Brenda Marie,
and to our children
Matthew, Natalie, and Jennifer

Contents

CHAPTER 4

Mobile Radio Propagation: Small-Scale Fading and Multipath

Small-scale fading, or simply *fading*, is used to describe the rapid fluctuation of the amplitude of a radio signal over a short period of time or travel distance, so that large-scale path loss effects may be ignored. Fading is caused by interference between two or more versions of the transmitted signal which arrive at the receiver at slightly different times. These waves, called *multipath waves*, combine at the receiver antenna to give a resultant signal which can vary widely in amplitude and phase, depending on the distribution of the intensity and relative propagation time of the waves and the bandwidth of the transmitted signal.

4.1 Small-Scale Multipath Propagation

Multipath in the radio channel creates small-scale fading effects. The three most important effects are:

- Rapid changes in signal strength over a small travel distance or time interval
- Random frequency modulation due to varying Doppler shifts on different multipath signals
- Time dispersion (echoes) caused by multipath propagation delays.

In built-up urban areas, fading occurs because the height of the mobile antennas are well below the height of surrounding structures, so there is no single line-of-sight path to the base station. Even when a line-of-sight exists, multipath still occurs due to reflections from the ground and surrounding structures. The incoming radio waves arrive from different directions with different propagation delays. The signal received by the mobile at any point in space may consist of a large number of plane waves having randomly distributed amplitudes,

phases, and angles of arrival. These multipath components, combine vectorially at the receiver antenna, and can cause the signal received by the mobile to distort or fade. Even when a mobile receiver is stationary, the received signal may fade due to movement of surrounding objects in the radio channel.

If objects in the radio channel are static, and motion is considered to be only due to that of the mobile, then fading is purely a spatial phenomenon. The spatial variations of the resulting signal are seen as temporal variations by the receiver as it moves through the multipath field. Due to the constructive and destructive effects of multipath waves summing at various points in space, a receiver moving at high speed can pass through several fades in a small period of time. In a more serious case, a receiver may stop at a particular location at which the received signal is in a deep fade. Maintaining good communications can then become very difficult, although passing vehicles or people walking in the vicinity of the mobile can often disturb the field pattern, thereby diminishing the likelihood of the received signal remaining in a deep null for a long period of time. Antenna space diversity can prevent deep fading nulls, as shown in Chapter 6. Figure 3.1 shows typical rapid variations in the received signal level due to small-scale fading as a receiver is moved over a distance of a few meters.

Due to the relative motion between the mobile and the base station, each multipath wave experiences an apparent shift in frequency. The shift in received signal frequency due to motion is called the Doppler shift, and is directly proportional to the velocity and direction of motion of the mobile with respect to the direction of arrival of the received multipath wave.

4.1.1 Factors Influencing Small-Scale Fading

Many physical factors in the radio propagation channel influence small-scale fading. These include the following:

- **Multipath propagation** — The presence of reflecting objects and scatterers in the channel creates a constantly changing environment that dissipates the signal energy in amplitude, phase, and time. These effects result in multiple versions of the transmitted signal that arrive at the receiving antenna, displaced with respect to one another in time and spatial orientation. The random phase and amplitudes of the different multipath components cause fluctuations in signal strength, thereby inducing small-scale fading, signal distortion, or both. Multipath propagation often lengthens the time required for the baseband portion of the signal to reach the receiver which can cause signal smearing due to intersymbol interference.
- **Speed of the mobile** — The relative motion between the base station and the mobile results in random frequency modulation due to different Doppler shifts on each of the multipath components. Doppler shift will be positive or negative depending on whether the mobile receiver is moving toward or away from the base station.

- **Speed of surrounding objects** — If objects in the radio channel are in motion, they induce a time varying Doppler shift on multipath components. If the surrounding objects move at a greater rate than the mobile, then this effect dominates the small-scale fading. Otherwise, motion of surrounding objects may be ignored, and only the speed of the mobile need be considered.
- **The transmission bandwidth of the signal** — If the transmitted radio signal bandwidth is greater than the "bandwidth" of the multipath channel, the received signal will be distorted, but the received signal strength will not fade much over a local area (i.e., the small-scale signal fading will not be significant). As will be shown, the bandwidth of the channel can be quantified by the *coherence bandwidth* which is related to the specific multipath structure of the channel. The coherence bandwidth is a measure of the maximum frequency difference for which signals are still strongly correlated in amplitude. If the transmitted signal has a narrow bandwidth as compared to the channel, the amplitude of the signal will change rapidly, but the signal will not be distorted in time. Thus, the statistics of small-scale signal strength and the likelihood of signal smearing appearing over small-scale distances are very much related to the specific amplitudes and delays of the multipath channel, as well as the bandwidth of the transmitted signal.

4.1.2 Doppler Shift

Consider a mobile moving at a constant velocity v, along a path segment having length d between points X and Y, while it receives signals from a remote source S, as illustrated in Figure 4.1. The difference in path lengths traveled by the wave from source S to the mobile at points X and Y is $\Delta = d\cos\theta = v\Delta t\cos\theta$, where Δt is the time required for the mobile to travel from X to Y, and θ is assumed to be the same at points X and Y since the source is assumed to be very far away. The phase change in the received signal due to the difference in path lengths is therefore

$$\Delta\phi = \frac{2\pi\Delta l}{\lambda} = \frac{2\pi v\Delta t}{\lambda}\cos\theta \tag{4.1}$$

and hence the apparent change in frequency, or Doppler shift, is given by f_d, where

$$f_d = \frac{1}{2\pi}\cdot\frac{\Delta\phi}{\Delta t} = \frac{v}{\lambda}\cdot\cos\theta \tag{4.2}$$

Equation (4.2) relates the Doppler shift to the mobile velocity and the spatial angle between the direction of motion of the mobile and the direction of arrival of the wave. It can be seen from equation (4.2) that if the mobile is moving toward the direction of arrival of the wave, the Doppler shift is positive (i.e., the apparent received frequency is increased), and if the mobile is moving away from the direction of arrival of the wave, the Doppler shift is negative (i.e. the

apparent received frequency is decreased). As shown in section 4.7.1, multipath components from a CW signal, which arrive from different directions contribute to Doppler spreading of the received signal, thus increasing the signal bandwidth.

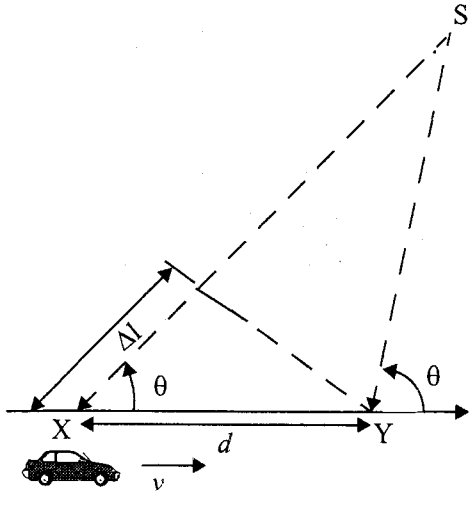

Figure 4.1
Illustration of Doppler effect.

Example 4.1

Consider a transmitter which radiates a sinusoidal carrier frequency of 1850 MHz. For a vehicle moving 60 mph, compute the received carrier frequency if the mobile is moving (a) directly towards the transmitter, (b) directly away from the transmitter, (c) in a direction which is perpendicular to the direction of arrival of the transmitted signal.

Solution to Example 4.1

Given:

Carrier frequency $f_c = 1850$ MHz

Therefore, wavelength $\lambda = c/f_c = \dfrac{3 \times 10^8}{1850 \times 10^6} = 0.162$ m

Vehicle speed $v = 60$ mph $= 26.82$ m/s

(a) The vehicle is moving directly towards the transmitter.
The Doppler shift in this case is positive and the received frequency is given by equation (4.2)

$$f = f_c + f_d = 1850 \times 10^6 + \frac{26.82}{0.162} = 1850.00016 \text{ MHz}$$

(b) The vehicle is moving directly away from the transmitter.
The Doppler shift in this case is negative and hence the received frequency is given by

$$f = f_c - f_d = 1850 \times 10^6 - \frac{26.82}{0.162} = 1849.999834 \text{ MHz}$$

(c) The vehicle is moving perpendicular to the angle of arrival of the transmitted signal.
In this case, $\theta = 90°$, $\cos\theta = 0$, and there is no Doppler shift.
The received signal frequency is the same as the transmitted frequency of 1850 MHz.

4.2 Impulse Response Model of a Multipath Channel

The small-scale variations of a mobile radio signal can be directly related to the impulse response of the mobile radio channel. The impulse response is a wideband channel characterization and contains all information necessary to simulate or analyze any type of radio transmission through the channel. This stems from the fact that a mobile radio channel may be modeled as a linear filter with a time varying impulse response, where the time variation is due to receiver motion in space. The filtering nature of the channel is caused by the summation of amplitudes and delays of the multiple arriving waves at any instant of time. The impulse response is a useful characterization of the channel, since it may be used to predict and compare the performance of many different mobile communication systems and transmission bandwidths for a particular mobile channel condition.

To show that a mobile radio channel may be modeled as a linear filter with a time varying impulse response, consider the case where time variation is due strictly to receiver motion in space. This is shown in Figure 4.2.

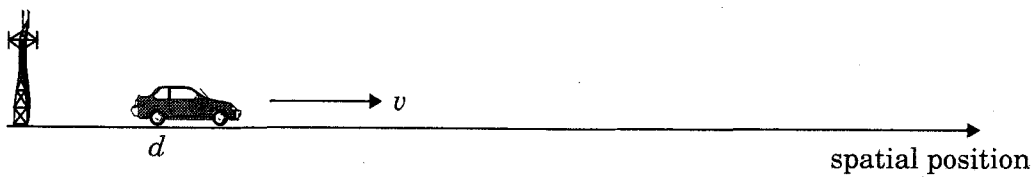

Figure 4.2
The mobile radio channel as a function of time and space.

In Figure 4.2, the receiver moves along the ground at some constant velocity v. For a fixed position d, the channel between the transmitter and the receiver can be modeled as a linear time invariant system. However, due to the different multipath waves which have propagation delays which vary over different spatial locations of the receiver, the impulse response of the linear time invariant channel should be a function of the position of the receiver. That is, the channel impulse response can be expressed as $h(d,t)$. Let $x(t)$ represent the transmitted signal, then the received signal $y(d,t)$ at position d can be expressed as a convolution of $x(t)$ with $h(d,t)$.

$$y(d,t) = x(t) \otimes h(d,t) = \int_{-\infty}^{\infty} x(\tau) h(d, t-\tau)\, d\tau \tag{4.3}$$

For a causal system, $h(d,t) = 0$ for $t<0$, thus equation (4.3) reduces to

$$y(d,t) = \int_{-\infty}^{t} x(\tau) h(d, t-\tau)\, d\tau \tag{4.4}$$

Since the receiver moves along the ground at a constant velocity v, the position of the receiver can by expressed as

$$d = vt \tag{4.5}$$

Substituting (4.5) in (4.4), we obtain

$$y(vt,t) = \int_{-\infty}^{t} x(\tau) h(vt, t-\tau)\, d\tau \tag{4.6}$$

Since v is a constant, $y(vt,t)$ is just a function of t. Therefore, equation (4.6) can be expressed as

$$y(t) = \int_{-\infty}^{t} x(\tau) h(vt, t-\tau)\, d\tau = x(t) \otimes h(vt,t) = x(t) \otimes h(d,t) \tag{4.7}$$

From equation (4.7) it is clear that the mobile radio channel can be modeled as a linear time varying channel, where the channel changes with time and distance.

Since v may be assumed constant over a short time (or distance) interval, we may let $x(t)$ represent the transmitted bandpass waveform, $y(t)$ the received waveform, and $h(t,\tau)$ the impulse response of the time varying multipath radio channel. The impulse response $h(t,\tau)$ completely characterizes the channel and is a function of both t and τ. The variable t represents the time variations due to motion, whereas τ represents the channel multipath delay for a fixed value of t. One may think of τ as being a vernier adjustment of time. The received signal $y(t)$ can be expressed as a convolution of the transmitted signal $x(t)$ with the channel impulse response (see Figure 4.3a).

$$y(t) = \int_{-\infty}^{\infty} x(\tau) h(t,\tau)\, d\tau = x(t) \otimes h(t,\tau) \tag{4.8}$$

If the multipath channel is assumed to be a bandlimited bandpass channel, which is reasonable, then $h(t,\tau)$ may be equivalently described by a complex baseband impulse response $h_b(t,\tau)$ with the input and output being the complex envelope representations of the transmitted and received signals, respectively (see Figure 4.3b). That is,

$$\frac{1}{2} r(t) = \frac{1}{2} c(t) \otimes \frac{1}{2} h_b(t,\tau) \tag{4.9}$$

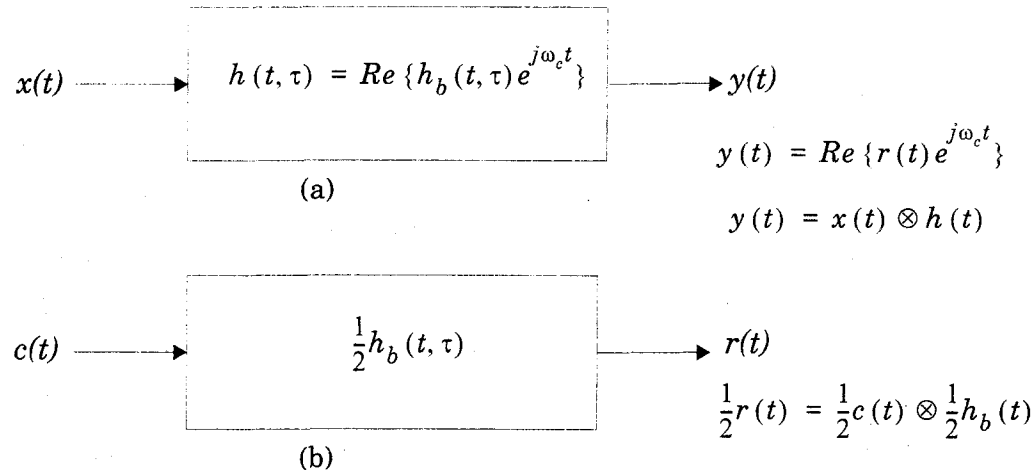

Figure 4.3
(a) Bandpass channel impulse response model.
(b) Baseband equivalent channel impulse response model.

where $c(t)$ and $r(t)$ are related to $x(t)$ and $y(t)$, respectively, through [Cou93]

$$x(t) = Re\{c(t)\exp(j2\pi f_c t)\} \tag{4.10}$$

$$y(t) = Re\{r(t)\exp(j2\pi f_c t)\} \tag{4.11}$$

The factors of $1/2$ in equation (4.9) are due to the properties of the complex envelope, in order to represent the passband radio system at baseband. The low-pass characterization removes the high frequency variations caused by the carrier, making the signal analytically easier to handle. It is shown by Couch [Cou93] that the average power of a bandpass signal $\overline{x^2(t)}$ is equal to $\frac{1}{2}\overline{|c(t)|^2}$, where the overbar denotes ensemble average for a stochastic signal, or time average for a deterministic or ergodic stochastic signal.

It is useful to discretize the multipath delay axis τ of the impulse response into equal time delay segments called *excess delay bins*, where each bin has time a delay width equal to $\tau_{i+1} - \tau_i$, where τ_0 is equal to 0, and represents the first arriving signal at the receiver. Letting i = 0, it is seen that $\tau_1 - \tau_0$ is equal to the time delay bin width given by $\Delta\tau$. For convention, $\tau_0 = 0$, $\tau_1 = \Delta\tau$, and $\tau_i = i\Delta\tau$, for $i = 0$ to $N-1$, where N represents the total number of possible equally-spaced multipath components, including the first arriving component. Any number of multipath signals received within the i th bin are represented by a single resolvable multipath component having delay τ_i. This technique of quantizing the delay bins determines the time delay resolution of the channel model, and the useful frequency span of the model can be shown to be $1/(2\Delta\tau)$. That is, the model may be used to analyze transmitted signals having bandwidths which are less than $1/(2\Delta\tau)$. Note that $\tau_0 = 0$ is the excess time delay

of the first arriving multipath component, and neglects the propagation delay between the transmitter and receiver. *Excess delay* is the relative delay of the i th multipath component as compared to the first arriving component and is given by τ_i. The *maximum excess delay* of the channel is given by $N\Delta\tau$.

Since the received signal in a multipath channel consists of a series of attenuated, time-delayed, phase shifted replicas of the transmitted signal, the baseband impulse response of a multipath channel can be expressed as

$$h_b(t,\tau) = \sum_{i=0}^{N-1} a_i(t,\tau)\exp\left[j2\pi f_c\tau_i(t) + \phi(t,\tau)\right]\delta(\tau-\tau_i(t)) \tag{4.12}$$

where $a_i(t,\tau)$ and $\tau_i(t)$ are the real amplitudes and excess delays, respectively, of i th multipath component at time t. The phase term $2\pi f_c\tau_i(t) + \phi_i(t,\tau)$ in (4.12) represents the phase shift due to free space propagation of the i th multipath component, plus any additional phase shifts which are encountered in the channel. In general, the phase term is simply represented by a single variable $\theta_i(t,\tau)$ which lumps together all the mechanisms for phase shifts of a single multipath component within the ith excess delay bin. Note that some excess delay bins may have no multipath at some time t and delay τ_i, since $a_i(t,\tau)$ may be zero. In equation (4.12), N is the total possible number of multipath components (bins), and $\delta(\bullet)$ is the unit impulse function which determines the specific multipath bins that have components at time t and excess delays τ_i. Figure 4.4 illustrates an example of different snapshots of $h_b(t,\tau)$, where t varies into the page, and the time delay bins are quantized to widths of $\Delta\tau$.

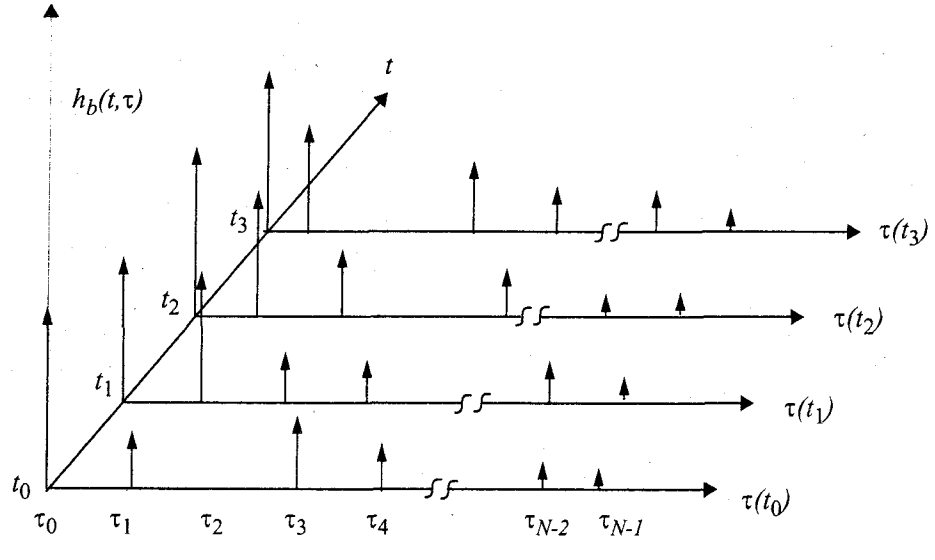

Figure 4.4
An example of the time varying discrete-time impulse response model for a multipath radio channel.

If the channel impulse response is assumed to be time invariant, or is at least wide sense stationary over a small-scale time or distance interval, then the channel impulse response may be simplified as

$$h_b(\tau) = \sum_{i=0}^{N-1} a_i \exp(-j\theta_i)\,\delta(\tau-\tau_i) \tag{4.13}$$

When measuring or predicting $h_b(\tau)$, a probing pulse $p(t)$ which approximates a delta function is used at the transmitter. That is,

$$p(t) \approx \delta(t-\tau) \tag{4.14}$$

is used to sound the channel to determine $h_b(\tau)$.

For small-scale channel modeling, the *power delay profile* of the channel is found by taking the spatial average of $|h_b(t;\tau)|^2$ over a local area. By making several local area measurements of $|h_b(t;\tau)|^2$ in different locations, it is possible to build an ensemble of power delay profiles, each one representing a possible small-scale multipath channel state [Rap91a].

Based on work by Cox [Cox72], [Cox75], if $p(t)$ has a time duration much smaller than the impulse response of the multipath channel, $p(t)$ does not need to be deconvolved from the received signal $r(t)$ in order to determine relative multipath signal strengths. The received power delay profile in a local area is given by

$$P(t;\tau) \approx k|h_b(t;\tau)|^2 \tag{4.15}$$

and many snapshots of $|h_b(t;\tau)|^2$ are typically averaged over a local (small-scale) area to provide a single time-invariant multipath power delay profile $P(\tau)$. The gain k in equation (4.15) relates the transmitted power in the probing pulse $p(t)$ to the total power received in a multipath delay profile.

4.2.1 Relationship Between Bandwidth and Received Power

In actual wireless communication systems, the impulse response of a multipath channel is measured in the field using channel sounding techniques. We now consider two extreme channel sounding cases as a means of demonstrating how the small-scale fading behaves quite differently for two signals with different bandwidths in the identical multipath channel.

Consider a pulsed, transmitted RF signal of the form

$$x(t) = \mathrm{Re}\{p(t)\exp(j2\pi f_c t)\}$$

where $p(t)$ is a repetitive baseband pulse train with very narrow pulse width T_{bb} and repetition period T_{REP} which is much greater than the maximum measured excess delay τ_{max} in the channel. Now let

$$p(t) = 2\sqrt{\tau_{max}/T_{bb}} \text{ for } 0 \le t \le T_{bb}$$

and let $p(t)$ be zero elsewhere for all excess delays of interest. The low pass channel output $r(t)$ closely approximates the impulse response $h_b(t)$ and is given by

$$\begin{aligned} r(t) &= \frac{1}{2}\sum_{i=0}^{N-1} a_i \left(\exp\left(-j\theta_i\right)\right) \cdot p\left(t-\tau_i\right) \\ &= \sum_{i=0}^{N-1} a_i \exp\left(-j\theta_i\right) \cdot \sqrt{\frac{\tau_{max}}{T_{bb}}}\ \text{rect}\left[t-\frac{T_{bb}}{2}-\tau_i\right] \end{aligned} \tag{4.16}$$

To determine the received power at some time t_0, the power $|r(t_0)|^2$ is measured. The quantity $|r(t_0)|^2$ is called the *instantaneous multipath power delay profile* of the channel, and is equal to the energy received over the time duration of the multipath delay divided by τ_{max}. That is, using equation (4.16)

$$\begin{aligned} |r(t_0)|^2 &= \frac{1}{\tau_{max}}\int_0^{\tau_{max}} r(t) \times r^*(t)\, dt \\ &= \frac{1}{\tau_{max}}\int_0^{\tau_{max}} \frac{1}{4}\text{Re}\left\{\sum_{j=0}^{N-1}\sum_{i=0}^{N-1} a_j(t_0)\, a_i(t_0)\, p\left(t-\tau_j\right) p\left(t-\tau_i\right) \exp\left(-j\left(\theta_j-\theta_i\right)\right)\right\} dt \end{aligned} \tag{4.17}$$

Note that if all the multipath components are resolved by the probe *p(t)*, then $|\tau_j-\tau_i| > T_{bb}$ for all $j \neq i$, and

$$\begin{aligned} |r(t_0)|^2 &= \frac{1}{\tau_{max}}\int_0^{\tau_{max}} \frac{1}{4}\left(\sum_{k=0}^{N-1} a_k^2(t_0)\, p^2\left(t-\tau_k\right)\right) dt \\ &= \frac{1}{\tau_{max}}\sum_{k=0}^{N-1} a_k^2(t_0)\int_0^{\tau_{max}} \left\{\sqrt{\frac{\tau_{max}}{T_{bb}}}\ \text{rect}\left[t-\frac{T_{bb}}{2}-\tau_k\right]\right\}^2 dt \\ &= \sum_{k=0}^{N-1} a_k^2(t_0) \end{aligned} \tag{4.18}$$

For a wideband probing signal *p(t)*, T_{bb} is smaller than the delays between multipath components in the channel, and equation (4.18) shows that the total received power is simply related to the sum of the powers in the individual multipath components, and is scaled by the ratio of the probing pulse's width and amplitude, and the maximum observed excess delay of the channel. Assuming that the received power from the multipath components forms a random process where each component has a random amplitude and phase at any time t, the average small-scale received power for the wideband probe is found from equation (4.17) as

$$E_{a,\theta}[P_{WB}] = E_{a,\theta}\left[\sum_{i=0}^{N-1}\left|a_i \exp(j\theta_i)\right|^2\right] \approx \sum_{i=0}^{N-1}\overline{a_i^2} \tag{4.19}$$

In equation (4.19), $E_{a,\theta}[\bullet]$ denotes the ensemble average over all possible values of a_i and θ_i in a local area, and the overbar denotes sample average over a local measurement area which is generally measured using multipath measurement equipment. The striking result of equations (4.18) and (4.19) is that if a transmitted signal is able to resolve the multipaths, then the *small-scale received power is simply the sum of the powers received in each multipath component*. In practice, the amplitudes of individual multipath components do not fluctuate widely in a local area. Thus, the received power of a wideband signal such as $p(t)$ does not fluctuate significantly when a receiver is moved about a local area [Rap89].

Now, instead of a pulse, consider a CW signal which is transmitted into the exact same channel, and let the complex envelope be given by $c(t) = 2$. Then, the instantaneous complex envelope of the received signal is given by the phasor sum

$$r(t) = \sum_{i=0}^{N-1} a_i \exp(j\theta_i(t,\tau)) \tag{4.20}$$

and the instantaneous power is given by

$$|r(t)|^2 = \left|\sum_{i=0}^{N-1} a_i \exp(j\theta_i(t,\tau))\right|^2 \tag{4.21}$$

As the receiver is moved over a local area, the channel changes, and the received signal strength will vary at a rate governed by the fluctuations of a_i and θ_i. As mentioned earlier, a_i varies little over local areas, but θ_i will vary greatly due to changes in propagation distance over space, resulting in large fluctuations of $r(t)$ as the receiver is moved over small distances (on the order of a wavelength). That is, since $r(t)$ is the phasor sum of the individual multipath components, the instantaneous phases of the multipath components cause the large fluctuations which typifies small-scale fading for CW signals. The average received power over a local area is then given by

$$E_{a,\theta}[P_{CW}] = E_{a,\theta}\left[\left|\sum_{i=0}^{N-1} a_i \exp(j\theta_i)\right|^2\right] \tag{4.22}$$

$$E_{a,\theta}[P_{CW}] \approx \overline{\left[\left(a_0 e^{j\theta_0} + a_1 e^{j\theta_1} + \ldots\ldots + a_{N-1} e^{j\theta_{N-1}}\right)\right.} \times \overline{\left.\left(a_0 e^{-j\theta_0} + a_1 e^{-j\theta_1} + \ldots\ldots + a_{N-1} e^{-j\theta_{N-1}}\right)\right]} \tag{4.23}$$

$$E_{a,\theta}[P_{CW}] \approx \sum_{i=0}^{N-1} \overline{a_i^2} + 2\sum_{i=0}^{N-1} \sum_{i,j\neq i}^{N} r_{ij}\, \overline{\cos(\theta_i - \theta_j)} \tag{4.24}$$

where r_{ij} is the path amplitude correlation coefficient defined to be

$$r_{ij} = E_a[a_i a_j] \tag{4.25}$$

and the overbar denotes time average for CW measurements made by a mobile receiver over the local measurement area [Rap89]. Note that when $\overline{\cos(\theta_i - \theta_j)} = 0$ and/or $r_{ij} = 0$, then the average power for a CW signal is equivalent to the average received power for a wideband signal in a small-scale region. This is seen by comparing equation (4.19) and equation (4.24). This can occur when either the multipath phases are identically and independently distributed (i.i.d uniform) over $[0, 2\pi]$ or when the path amplitudes are uncorrelated. The i.i.d uniform distribution of θ is a valid assumption since multipath components traverse differential path lengths that measure hundreds of wavelengths and are likely to arrive with random phases. If for some reason it is believed that the phases are not independent, the average wideband power and average CW power will still be equal if the paths have uncorrelated amplitudes. However, if the phases of the paths are dependent upon each other, then the amplitudes are likely to be correlated, since the same mechanism which affects the path phases is likely to also affect the amplitudes. This situation is highly unlikely at transmission frequencies used in wireless mobile systems.

Thus it is seen that the *received local ensemble average power of wideband and narrowband signals are equivalent*. When the transmitted signal has a bandwidth much greater than the bandwidth of the channel, then the multipath structure is completely resolved by the received signal at any time, and the received power varies very little since the individual multipath amplitudes do not change rapidly over a local area. However, if the transmitted signal has a very narrow bandwidth (e.g., the baseband signal has a duration greater than the excess delay of the channel), then multipath is not resolved by the received signal, and large signal fluctuations (fading) occur at the receiver due to the phase shifts of the many unresolved multipath components.

Figure 4.5 illustrates actual indoor radio channel measurements made simultaneously with a wideband probing pulse having $T_{bb} = 10\,\text{ns}$, and a CW transmitter. The carrier frequency was 4 GHz. It can be seen that the CW signal undergoes rapid fades, whereas the wideband measurements change little over the 5λ measurement track. However, the local average received powers of both signals were measured to be virtually identical [Haw91].

Example 4.2

Assume a discrete channel impulse response is used to model urban radio channels with excess delays as large as $100\ \mu s$ and microcellular channels with excess delays no larger than $4\ \mu s$. If the number of multipath bins is fixed

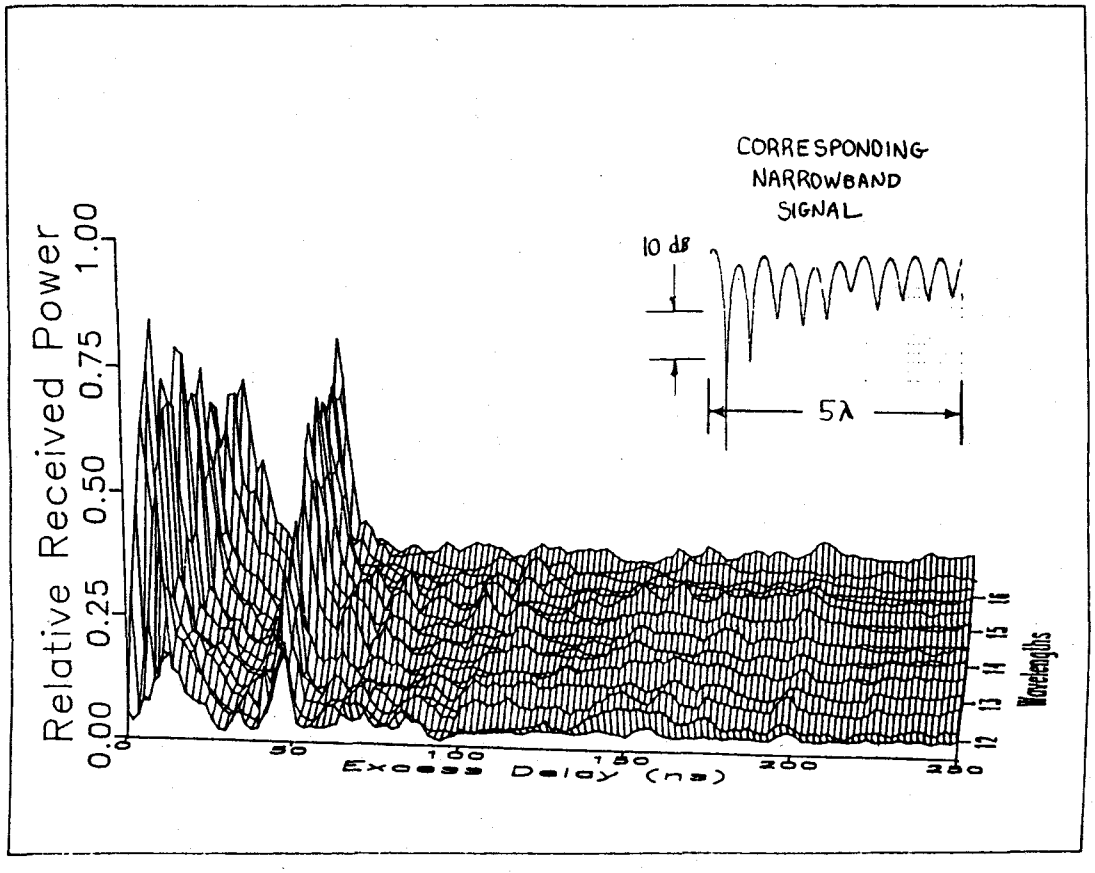

Figure 4.5
Measured wideband and narrowband received signals over a 5λ (0.375 m) measurement track inside a building. Carrier frequency is 4 GHz. Wideband power is computed using equation (4.19), which can be thought of as the area under the power delay profile.

at 64, find (a) $\Delta\tau$, and (b) the maximum bandwidth which the two models can accurately represent. Repeat the exercise for an indoor channel model with excess delays as large as 500 ns. As described in section 4.7.6, SIRCIM and SMRCIM are statistical channel models based on equation (4.12) that use parameters in this example.

Solution to Example 4.2

The maximum excess delay of the channel model is given by $\tau_N = N\Delta\tau$. Therefore, for $\tau_N = 100\mu s$, and $N = 64$ we obtain $\Delta\tau = \tau_N/N = 1.5625\ \mu s$. The maximum bandwidth that the SMRCIM model can accurately represent is equal to

$$1/(2\Delta\tau) = 1/(2(1.5625\mu s)) = 0.32\ \text{MHz}.$$

For the SMRCIM urban microcell model, $\tau_N = 4\mu s$, $\Delta\tau = \tau_N/N = 62.5$ ns. The maximum bandwidth that can be represented is

$$1/(2\Delta\tau) = 1/(2(62.5\ \text{ns})) = 8\ \text{MHz}.$$

Similarly, for indoor channels, $\Delta\tau = \tau_N/N = \dfrac{500 \times 10^{-9}}{64} = 7.8125$ ns.

The maximum bandwidth for the indoor channel model is

$$1/(2\Delta\tau) = 1/(2(7.8125 \text{ ns})) = 64 \text{ MHz}.$$

Example 4.3

Assume a mobile traveling at a velocity of 10 m/s receives two multipath components at a carrier frequency of 1000 MHz. The first component is assumed to arrive at $\tau = 0$ with an initial phase of $0°$ and a power of -70 dBm, and the second component which is 3 dB weaker than the first component is assumed to arrive at $\tau = 1\mu s$, also with an initial phase of $0°$. If the mobile moves directly towards the direction of arrival of the first component and directly away from the direction of arrival of the second component, compute the narrowband instantaneous power at time intervals of 0.1 s from 0 s to 0.5 s. Compute the average narrowband power received over this observation interval. Compare average narrowband and wideband received powers over the interval.

Solution to Example 4.3

Given $v = 10$ m/s, time intervals of 0.1 s correspond to spatial intervals of 1 m. The carrier frequency is given to be 1000 MHz, hence the wavelength of the signal is

$$\lambda = \frac{c}{f} = \frac{3 \times 10^8}{1000 \times 10^6} = 0.3 \text{ m}$$

The narrowband instantaneous power can be computed using equation (4.21). Note -70 dBm = 100 pW. At time $t = 0$, the phases of both multipath components are $0°$, hence the narrowband instantaneous power is equal to

$$|r(t)|^2 = \left| \sum_{i=0}^{N-1} a_i \exp(j\theta_i(t, \tau)) \right|^2$$

$$= \left| \sqrt{100 \text{ pW}} \times \exp(0) + \sqrt{50 \text{ pW}} \times \exp(0) \right|^2 = 291 \text{ pW}$$

Now, as the mobile moves, the phase of the two multipath components changes in opposite directions.

At $t = 0.1$ s, the phase of the first component is

$$\theta_i = \frac{2\pi d}{\lambda} = \frac{2\pi v t}{\lambda} = \frac{2\pi \times 10 \text{ (m/s)} \times 0.1 \text{ s}}{0.3 \text{ m}}$$

$$= 20.94 \text{ rad} = 2.09 \text{ rad} = 120°$$

Since the mobile moves towards the direction of arrival of the first component, and away from the direction of arrival of the second component, θ_1 is positive, and θ_2 is negative.

Therefore, at $t = 0.1$ s, $\theta_1 = 120°$, and $\theta_2 = -120°$, and the instantaneous power is equal to

$$|r(t)|^2 = \left|\sum_{i=0}^{N-1} a_i \exp(j\theta_i(t,\tau))\right|^2$$

$$= \left|\sqrt{100\text{ pW}} \times \exp(j120°) + \sqrt{50\text{ pW}} \times \exp(-j120°)\right|^2 = 78.2\text{ pW}$$

Similarly, at $t = 0.2$ s, $\theta_2 = 240°$, and $\theta_2 = -240°$, and the instantaneous power is equal to

$$|r(t)|^2 = \left|\sum_{i=0}^{N-1} a_i \exp(j\theta_i(t,\tau))\right|^2$$

$$= \left|\sqrt{100\text{ pW}} \times \exp(j240°) + \sqrt{50\text{ pW}} \times \exp(-j240°)\right|^2 = 81.5\text{ pW}$$

Similarly, at $t = 0.3$ s, $\theta_1 = 360° = 0°$, and $\theta_2 = -360° = 0°$, and the instantaneous power is equal to

$$|r(t)|^2 = \left|\sum_{i=0}^{N-1} a_i \exp(j\theta_i(t,\tau))\right|^2$$

$$= \left|\sqrt{100\text{ pW}} \times \exp(j0°) + \sqrt{50\text{ pW}} \times \exp(-j0°)\right|^2 = 291\text{ pW}$$

It follows that at $t = 0.4$ s, $|r(t)|^2 = 78.2$ pW, and at $t = 0.5$ s, $|r(t)|^2 = 81.5$ pW.

The average narrowband received power is equal to

$$\frac{(2)(291) + (2)(78.2) + (2)(81.5)}{6}\text{ pW} = 150.233\text{ pW}$$

Using equation (4.19), the wideband power is given by

$$E_{a,\theta}[P_{W,B}] = E_{a,\theta}\left[\sum_{i=0}^{N-1} |a_i \exp(j\theta_i)|^2\right] \approx \sum_{i=0}^{N-1} \overline{a_i^2}$$

$$E_{a,\theta}[P_{W,B}] = 100\text{ pW} + 50\text{ pW} = 150\text{ pW}$$

As can be seen, the narrowband and wideband received power are virtually identical when averaged over 0.5 s (or 5 m). While the CW signal fades over the observation interval, the wideband signal power remains constant.

4.3 Small-Scale Multipath Measurements

Because of the importance of the multipath structure in determining the small-scale fading effects, a number of wideband channel sounding techniques have been developed. These techniques may be classified as *direct pulse measurements*, *spread spectrum sliding correlator measurements*, and *swept frequency measurements*.

4.3.1 Direct RF Pulse System

A simple channel sounding approach is the direct RF pulse system (see Figure 4.6). This technique allows engineers to determine rapidly the power delay profile of any channel, as demonstrated by Rappaport and Seidel [Rap89], [Rap90]. Essentially a wide band pulsed bistatic radar, this system transmits a repetitive pulse of width τ_{bb} s, and uses a receiver with a wide bandpass filter ($BW = 2/\tau_{bb}$Hz). The signal is then amplified, detected with an envelope detector, and displayed and stored on a high speed oscilloscope. This gives an immediate measurement of the square of the channel impulse response convolved with the probing pulse (see equation (4.17)). If the oscilloscope is set on averaging mode, then this system can provide a local average power delay profile. Another attractive aspect of this system is the lack of complexity, since off-the-shelf equipment may be used.

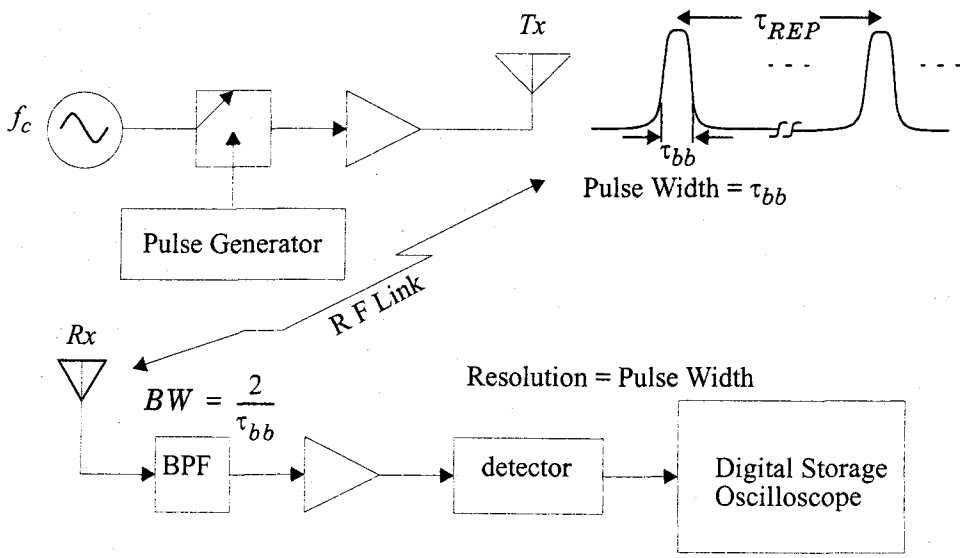

Figure 4.6
Direct RF channel impulse response measurement system.

The minimum resolvable delay between multipath components is equal to the probing pulse width τ_{bb}. The main problem with this system is that it is subject to interference and noise, due to the wide passband filter required for multipath time resolution. Also, the pulse system relies on the ability to trigger the oscilloscope on the first arriving signal. If the first arriving signal is blocked or fades, severe fading occurs, and it is possible the system may not trigger properly. Another disadvantage is that the phases of the individual multipath components are not received, due to the use of an envelope detector. However, use of a coherent detector permits measurement of the multipath phase using this technique.

4.3.2 Spread Spectrum Sliding Correlator Channel Sounding

The basic block diagram of a spread spectrum channel sounding system is shown in Figure 4.7. The advantage of a spread spectrum system is that, while the probing signal may be wideband, it is possible to detect the transmitted signal using a narrowband receiver preceded by a wideband mixer, thus improving the dynamic range of the system as compared to the direct RF pulse system.

In a spread spectrum channel sounder, a carrier signal is "spread" over a large bandwidth by mixing it with a binary pseudo-noise (PN) sequence having a chip duration T_c and a chip rate R_c equal to $1/T_c$ Hz. The power spectrum envelope of the transmitted spread spectrum signal is given by [Dix84] as

$$\left[\frac{\sin(f-f_c)T_c}{(f-f_c)T_c}\right]^2 \tag{4.26}$$

and the null-to-null bandwidth is

$$BW = 2R_c \tag{4.27}$$

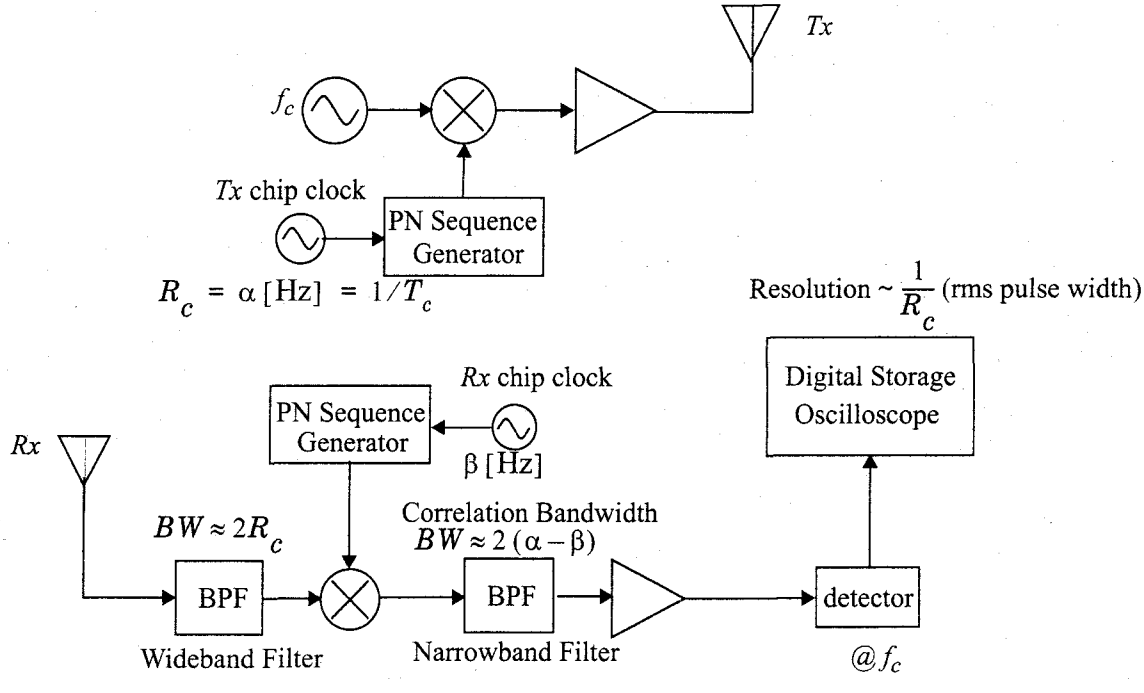

Figure 4.7
Spread spectrum channel impulse response measurement system.

The spread spectrum signal is then received, filtered, and *despread* using a PN sequence generator identical to that used at the transmitter. Although the two PN sequences are identical, the transmitter chip clock is run at a slightly faster rate than the receiver chip clock. Mixing the chip sequences in this fashion implements a *sliding correlator* [Dix84]. When the PN code of the faster chip

clock catches up with the PN code of the slower chip clock, the two chip sequences will be virtually identically aligned, giving maximal correlation. When the two sequences are not maximally correlated, mixing the incoming spread spectrum signal with the unsynchronized receiver chip sequence will spread this signal into a bandwidth at least as large as the receiver's reference PN sequence. In this way, the narrowband filter that follows the correlator can reject almost all of the incoming signal power. This is how *processing gain* is realized in a spread spectrum receiver and how it can reject passband interference, unlike the direct RF pulse sounding system.

Processing gain (PG) is given as

$$PG = \frac{2R_c}{R_{bb}} = \frac{2\tau_{bb}}{T_c} = \frac{(S/N)_{out}}{(S/N)_{in}} \tag{4.28}$$

where $\tau_{bb} = 1/R_{bb}$, is the period of the baseband information. For the case of a sliding correlator channel sounder, the baseband information rate is equal to the frequency offset of the PN sequence clocks at the transmitter and receiver.

When the incoming signal is correlated with the receiver sequence, the signal is collapsed back to the original bandwidth (i.e., "despread"), envelope detected, and displayed on an oscilloscope. Since different incoming multipaths will have different time delays, they will maximally correlate with the receiver PN sequence at different times. The energy of these individual paths will pass through the correlator depending on the time delay. Therefore, after envelope detection, the channel impulse response convolved with the pulse shape of a single chip is displayed on the oscilloscope. Cox [Cox72] first used this method to measure channel impulse responses in outdoor suburban environments at 910 MHz. Devasirvatham [Dev86], [Dev90a] successfully used a direct sequence spread spectrum channel sounder to measure time delay spread of multipath components and signal level measurements in office and residential buildings at 850 MHz. Bultitude [Bul89] used this technique for indoor and microcellular channel sounding work, as did Landron [Lan92].

The time resolution ($\Delta\tau$) of multipath components using a spread spectrum system with sliding correlation is

$$\Delta\tau = 2T_c = \frac{2}{R_c} \tag{4.29}$$

In other words, the system can resolve two multipath components as long as they are equal to or greater than $2T_c$ seconds apart. In actuality, multipath components with interarrival times smaller than $2T_c$ can be resolved since the rms pulse width is smaller than the absolute width of the triangular correlation pulse, and is on the order of T_c.

The sliding correlation process gives *equivalent time* measurements that are updated every time the two sequences are maximally correlated. The time between maximal correlations (T) can be calculated from equation (4.30)

$$\Delta T = T_c \gamma l = \frac{\gamma l}{R_c} \tag{4.30}$$

where T_c = chip period (s)
R_c = chip rate (Hz)
γ = slide factor (dimensionless)
l = sequence length (chips)

The slide factor is defined as the ratio between the transmitter chip clock rate and the difference between the transmitter and receiver chip clock rates [Dev86]. Mathematically, this is expressed as

$$\gamma = \frac{\alpha}{\alpha - \beta} \tag{4.31}$$

where α = transmitter chip clock rate (Hz)
β = receiver chip clock rate (Hz)

For a maximal length PN sequence, the sequence length is

$$l = 2^n - 1 \tag{4.32}$$

where n is the number of shift registers in the sequence generator [Dix84].

Since the incoming spread spectrum signal is mixed with a receiver PN sequence that is slower than the transmitter sequence, the signal is essentially down-converted ("collapsed") to a low-frequency narrowband signal. In other words, the relative rate of the two codes slipping past each other is the rate of information transferred to the oscilloscope. This narrowband signal allows narrowband processing, eliminating much of the passband noise and interference. The processing gain of equation (4.28) is then realized using a narrowband filter ($BW = 2(\alpha - \beta)$).

The equivalent time measurements refer to the relative times of multipath components as they are displayed on the oscilloscope. The observed time scale on the oscilloscope using a sliding correlator is related to the actual propagation time scale by

$$\text{Actual Propagation Time} = \frac{\text{Observed Time}}{\gamma} \tag{4.33}$$

This effect is due to the relative rate of information transfer in the sliding correlator. For example, T_c of equation (4.30) is an observed time measured on an oscilloscope and not actual propagation time. This effect, known as *time dilation*, occurs in the sliding correlator system because the propagation delays are actually expanded in time by the sliding correlator.

Caution must be taken to ensure that the sequence length has a period which is greater than the longest multipath propagation delay. The PN sequence period is

$$\tau_{PNseq} = T_c l \tag{4.34}$$

The sequence period gives an estimate of the maximum unambiguous range of incoming multipath signal components. This range is found by multiplying the speed of light with τ_{PNseq} in equation (4.34).

There are several advantages to the spread spectrum channel sounding system. One of the key spread spectrum modulation characteristics is the ability to reject passband noise, thus improving the coverage range for a given transmitter power. Transmitter and receiver PN sequence synchronization is eliminated by the sliding correlator. Sensitivity is adjustable by changing the sliding factor and the post-correlator filter bandwidth. Also, required transmitter powers can be considerably lower than comparable direct pulse systems due to the inherent "processing gain" of spread spectrum systems.

A disadvantage of the spread spectrum system, as compared to the direct pulse system, is that measurements are not made in real time, but they are compiled as the PN codes slide past one another. Depending on system parameters and measurement objectives, the time required to make power delay profile measurements may be excessive. Another disadvantage of the system described here is that a noncoherent detector is used, so that phases of individual multipath components can not be measured. Even if coherent detection is used, the sweep time of a spread spectrum signal induces delay such that the phases of individual multipath components with different time delays would be measured at substantially different times, during which the channel might change.

4.3.3 Frequency Domain Channel Sounding

Because of the dual relationship between time domain and frequency domain techniques, it is possible to measure the channel impulse response in the frequency domain. Figure 4.8 shows a frequency domain channel sounder used for measuring channel impulse responses. A vector network analyzer controls a synthesized frequency sweeper, and an S-parameter test set is used to monitor the frequency response of the channel. The sweeper scans a particular frequency band (centered on the carrier) by stepping through discrete frequencies. The number and spacings of these frequency steps impact the time resolution of the impulse response measurement. For each frequency step, the S-parameter test set transmits a known signal level at port 1 and monitors the received signal level at port 2. These signal levels allow the analyzer to determine the complex response (i.e., transmissivity $S_{21}(\omega)$) of the channel over the measured frequency range. The transmissivity response is a frequency domain representation of the channel impulse response. This response is then converted to the time domain using inverse discrete Fourier transform (IDFT) processing, giving a band-limited version of the impulse response. In theory, this technique works well and indirectly provides amplitude and phase information in the time domain. However, the system requires careful calibration and hardwired synchronization between the transmitter and receiver, making it useful only for very close mea-

surements (e.g., indoor channel sounding). Another limitation with this system is the non-real-time nature of the measurement. For time varying channels, the channel frequency response can change rapidly, giving an erroneous impulse response measurement. To mitigate this effect, fast sweep times are necessary to keep the total swept frequency response measurement interval as short as possible. A faster sweep time can be accomplished by reducing the number of frequency steps, but this sacrifices time resolution and excess delay range in the time domain. The swept frequency system has been used successfully for indoor propagation studies by Pahlavan [Pah95] and Zaghloul, et.al. [Zag91a], [Zag91b].

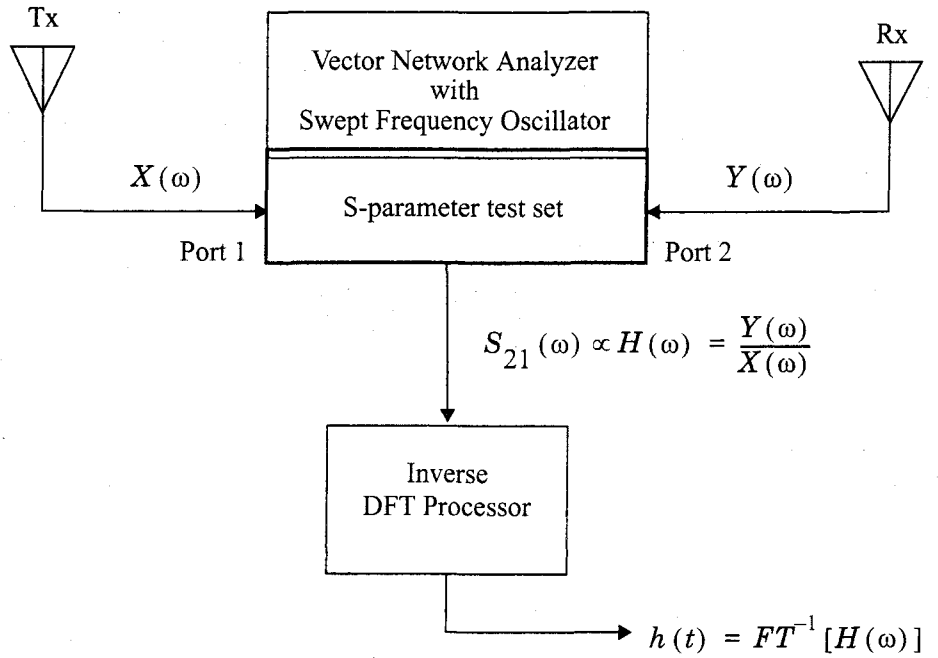

Figure 4.8
Frequency domain channel impulse response measurement system.

4.4 Parameters of Mobile Multipath Channels

Many multipath channel parameters are derived from the power delay profile, given by equation (4.18). Power delay profiles are measured using the techniques discussed in Section 4.4 and are generally represented as plots of relative received power as a function of excess delay with respect to a fixed time delay reference. Power delay profiles are found by averaging instantaneous power delay profile measurements over a local area in order to determine an average small-scale power delay profile. Depending on the time resolution of the probing pulse and the type of multipath channels studied, researchers often choose to sample at spatial separations of a quarter of a wavelength and over receiver movements no greater than 6 m in outdoor channels and no greater than 2 m in indoor channels in the 450 MHz - 6 GHz range. This small-scale sampling avoids

large-scale averaging bias in the resulting small-scale statistics. Figure 4.9 shows typical power delay profile plots from outdoor and indoor channels, determined from a large number of closely sampled instantaneous profiles.

4.4.1 Time Dispersion Parameters

In order to compare different multipath channels and to develop some general design guidelines for wireless systems, parameters which grossly quantify the multipath channel are used. The *mean excess delay, rms delay spread,* and *excess delay spread (X* dB*)* are multipath channel parameters that can be determined from a power delay profile. The time dispersive properties of wide band multipath channels are most commonly quantified by their mean excess delay ($\bar{\tau}$) and rms delay spread (σ_τ). The mean excess delay is the first moment of the power delay profile and is defined to be

$$\bar{\tau} = \frac{\sum_k a_k^2 \tau_k}{\sum_k a_k^2} = \frac{\sum_k P(\tau_k)\,\tau_k}{\sum_k P(\tau_k)} \tag{4.35}$$

The rms delay spread is the square root of the second central moment of the power delay profile and is defined to be

$$\sigma_\tau = \sqrt{\overline{\tau^2} - (\bar{\tau})^2} \tag{4.36}$$

where

$$\overline{\tau^2} = \frac{\sum_k a_k^2 \tau_k^2}{\sum_k a_k^2} = \frac{\sum_k P(\tau_k)\,\tau_k^2}{\sum_k P(\tau_k)} \tag{4.37}$$

These delays are measured relative to the first detectable signal arriving at the receiver at $\tau_0 = 0$. Equations (4.35) - (4.37) do not rely on the absolute power level of $P(\tau)$, but only the relative amplitudes of the multipath components within $P(\tau)$. Typical values of rms delay spread are on the order of microseconds in outdoor mobile radio channels and on the order of nanoseconds in indoor radio channels. Table 4.1 shows the typical measured values of rms delay spread.

It is important to note that the rms delay spread and mean excess delay are defined from a single power delay profile which is the temporal or spatial average of consecutive impulse response measurements collected and averaged over a local area. Typically, many measurements are made at many local areas in order to determine a statistical range of multipath channel parameters for a mobile communication system over a large-scale area [Rap90].

The *maximum excess delay (X* dB*)* of the power delay profile is defined to be the time delay during which multipath energy falls to X dB below the maxi-

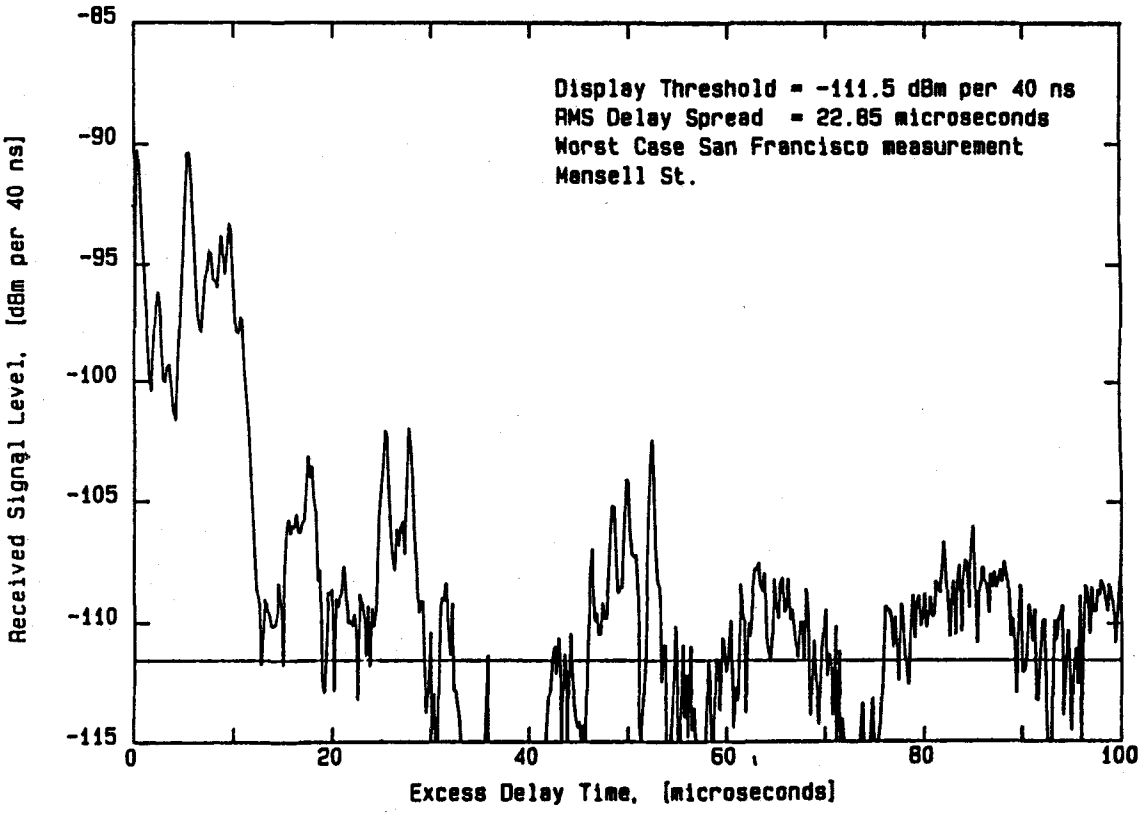

(a)

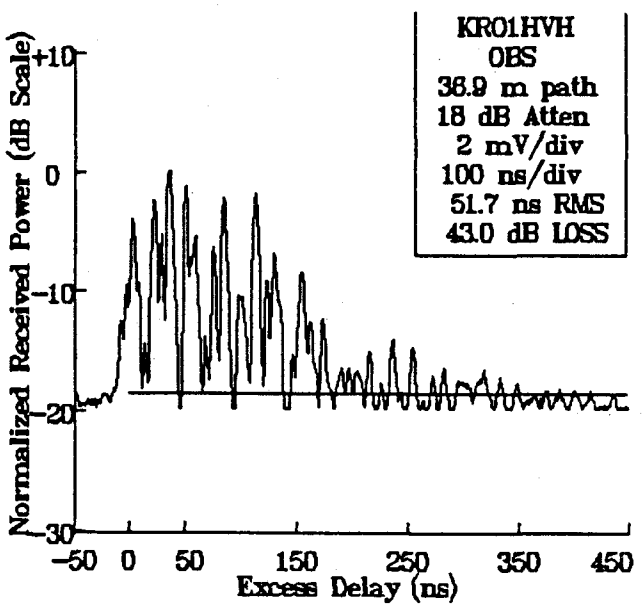

(b)

Figure 4.9
Measured multipath power delay profiles
a) From a 900 MHz cellular system in San Francisco [From [Rap90] © IEEE].
b) Inside a grocery store at 4 GHz [From [Haw91] © IEEE].

Table 4.1 Typical Measured Values of RMS Delay Spread

Environment	Frequency (MHz)	RMS Delay Spread (σ_τ)	Notes	Reference
Urban	910	1300 ns avg. 600 ns st. dev. 3500 ns max.	New York City	[Cox75]
Urban	892	10-25 μs	Worst case San Francisco	[Rap90]
Suburban	910	200-310 ns	Averaged typical case	[Cox72]
Suburban	910	1960-2110 ns	Averaged extreme case	[Cox72]
Indoor	1500	10-50 ns 25 ns median	Office building	[Sal87]
Indoor	850	270 ns max.	Office building	[Dev90a]
Indoor	1900	70-94 ns avg. 1470 ns max.	Three San Francisco buildings	[Sei92a]

mum. In other words, the maximum excess delay is defined as $\tau_X - \tau_0$, where τ_0 is the first arriving signal and τ_X is the maximum delay at which a multipath component is within X dB of the strongest arriving multipath signal (which does not necessarily arrive at τ_0). Figure 4.10 illustrates the computation of the maximum excess delay for multipath components within 10 dB of the maximum. The maximum excess delay (X dB) defines the temporal extent of the multipath that is above a particular threshold. The value of τ_X is sometimes called the *excess delay spread* of a power delay profile, but in all cases must be specified with a threshold that relates the multipath noise floor to the maximum received multipath component.

In practice, values for $\bar{\tau}$, $\overline{\tau^2}$, and σ_τ depend on the choice of noise threshold used to process $P(\tau)$. The noise threshold is used to differentiate between received multipath components and thermal noise. If the noise threshold is set too low, then noise will be processed as multipath, thus giving rise to values of $\bar{\tau}$, $\overline{\tau^2}$, and σ_τ that are artificially high.

It should be noted that the power delay profile and the magnitude frequency response (the spectral response) of a mobile radio channel are related through the Fourier transform. It is therefore possible to obtain an equivalent description of the channel in the frequency domain using its frequency response characteristics. Analogous to the delay spread parameters in the time domain, *coherence bandwidth* is used to characterize the channel in the frequency domain. The rms delay spread and coherence bandwidth are inversely proportional to one another, although their exact relationship is a function of the exact multipath structure.

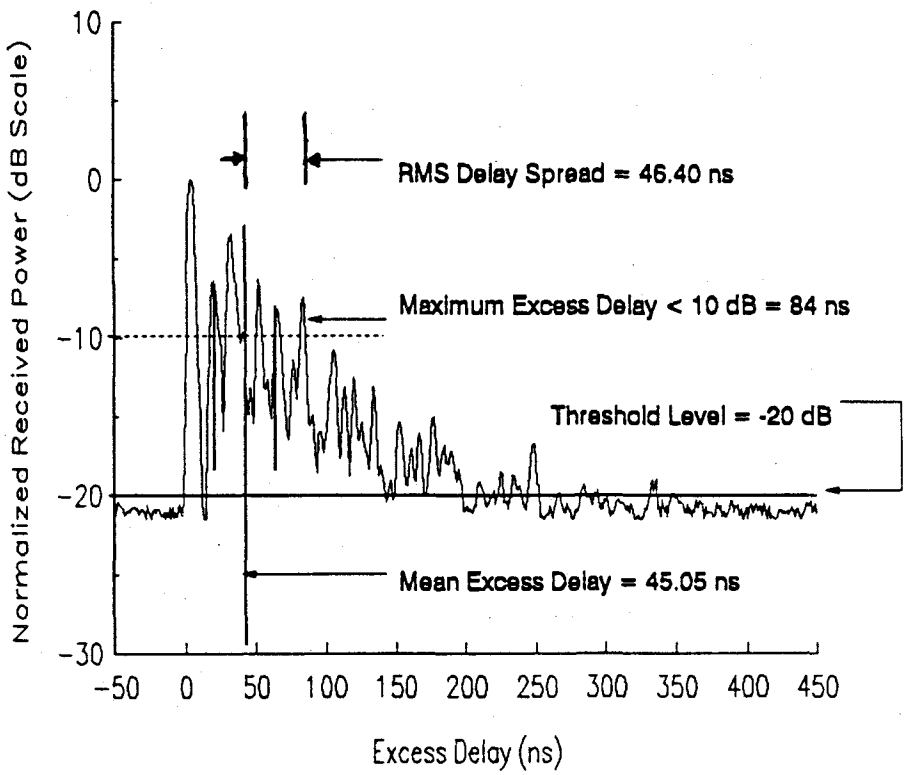

Figure 4.10
Example of an indoor power delay profile; rms delay spread, mean excess delay, maximum excess delay (10 dB), and threshold level are shown.

4.4.2 Coherence Bandwidth

While the delay spread is a natural phenomenon caused by reflected and scattered propagation paths in the radio channel, the coherence bandwidth, B_c, is a defined relation derived from the rms delay spread. Coherence bandwidth is a statistical measure of the range of frequencies over which the channel can be considered "flat" (i.e., a channel which passes all spectral components with approximately equal gain and linear phase). In other words, coherence bandwidth is the range of frequencies over which two frequency components have a strong potential for amplitude correlation. Two sinusoids with frequency separation greater than B_c are affected quite differently by the channel. If the coherence bandwidth is defined as the bandwidth over which the frequency correlation function is above 0.9, then the coherence bandwidth is approximately [Lee89b]

$$B_c \approx \frac{1}{50\sigma_\tau} \tag{4.38}$$

If the definition is relaxed so that the frequency correlation function is above 0.5, then the coherence bandwidth is approximately

$$B_c \approx \frac{1}{5\sigma_\tau} \tag{4.39}$$

It is important to note that an exact relationship between coherence bandwidth and rms delay spread does not exist, and equations (4.38) and (4.39) are "ball park estimates". In general, spectral analysis techniques and simulation are required to determine the exact impact that time varying multipath has on a particular transmitted signal [Chu87], [Fun93], [Ste94]. For this reason, accurate multipath channel models must be used in the design of specific modems for wireless applications [Rap91a], [Woe94].

Example 4.4

Calculate the mean excess delay, rms delay spread, and the maximum excess delay (10 dB) for the multipath profile given in the figure below. Estimate the 50% coherence bandwidth of the channel. Would this channel be suitable for AMPS or GSM service without the use of an equalizer?

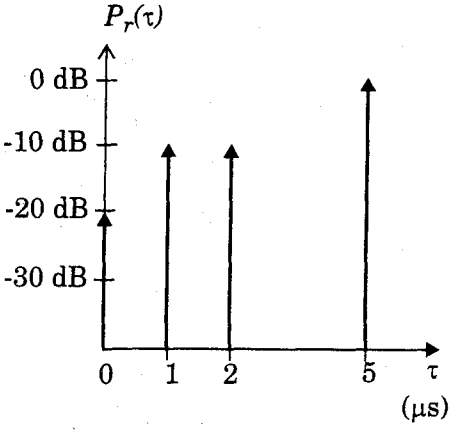

Figure E4.4

Solution to Example 4.4

The rms delay spread for the given multipath profile can be obtained using equations (4.35) — (4.37). The delays of each profile are measured relative to the first detectable signal. The mean excess delay for the given profile

$$\bar{\tau} = \frac{(1)(5) + (0.1)(1) + (0.1)(2) + (0.01)(0)}{[0.01 + 0.1 + 0.1 + 1]} = 4.38\mu s$$

The second moment for the given power delay profile can be calculated as

$$\overline{\tau^2} = \frac{(1)(5)^2 + (0.1)(1)^2 + (0.1)(2)^2 + (0.01)(0)}{1.21} = 21.07\mu s^2$$

Therefore the rms delay spread, $\sigma_\tau = \sqrt{21.07 - (4.38)^2} = 1.37\mu s$

The coherence bandwidth is found from equation (4.39) to be

$$B_c \approx \frac{1}{5\sigma_\tau} = \frac{1}{5(1.37\mu s)} = 146 \text{ kHz}$$

Since B_c is greater than 30 kHz, AMPS will work without an equalizer. However, GSM requires 200 kHz bandwidth which exceeds B_c, thus an equalizer would be needed for this channel.

4.4.3 Doppler Spread and Coherence Time

Delay spread and coherence bandwidth are parameters which describe the time dispersive nature of the channel in a local area. However, they do not offer information about the time varying nature of the channel caused by either relative motion between the mobile and base station, or by movement of objects in the channel. *Doppler spread* and *coherence time* are parameters which describe the time varying nature of the channel in a small-scale region.

Doppler spread B_D is a measure of the spectral broadening caused by the time rate of change of the mobile radio channel and is defined as the range of frequencies over which the received Doppler spectrum is essentially non-zero. When a pure sinusoidal tone of frequency f_c is transmitted, the received signal spectrum, called the Doppler spectrum, will have components in the range $f_c - f_d$ to $f_c + f_d$, where f_d is the Doppler shift. The amount of spectral broadening depends on f_d which is a function of the relative velocity of the mobile, and the angle θ between the direction of motion of the mobile and direction of arrival of the scattered waves. *If the baseband signal bandwidth is much greater than B_D, the effects of Doppler spread are negligible at the receiver.*

Coherence time T_c is the time domain dual of Doppler spread and is used to characterize the time varying nature of the frequency dispersiveness of the channel in the time domain. The Doppler spread and coherence time are inversely proportional to one another. That is,

$$T_C \approx \frac{1}{f_m} \tag{4.40.a}$$

Coherence time is actually a statistical measure of the time duration over which the channel impulse response is essentially invariant, and quantifies the similarity of the channel response at different times. In other words, coherence time is the time duration over which two received signals have a strong potential for amplitude correlation. If the reciprocal bandwidth of the baseband signal is greater than the coherence time of the channel, then the channel will change during the transmission of the baseband message, thus causing distortion at the receiver. If the coherence time is defined as the time over which the time correlation function is above 0.5, then the coherence time is approximately [Ste94]

$$T_C \approx \frac{9}{16\pi f_m} \tag{4.40.b}$$

where f_m is the maximum Doppler shift given by $f_m = v/\lambda$. In practice, (4.40.a) suggests a time duration during which a Rayleigh fading signal may fluctuate

wildly, and (4.40.b) is often too restrictive. A popular rule of thumb for modern digital communications is to define the coherence time as the geometric mean of equations (4.40.a) and (4.40.b). That is,

$$T_C = \sqrt{\frac{9}{16\pi f_m^2}} = \frac{0.423}{f_m} \qquad (4.40.c)$$

The definition of coherence time implies that two signals arriving with a time separation greater than T_C are affected differently by the channel. For example, for a vehicle traveling 60 mph using a 900 MHz carrier, a conservative value of T_C can be shown to be 2.22 ms from (4.40.b). If a digital transmission system is used, then as long as the symbol rate is greater than $1/T_C = 454$ bps, the channel will not cause distortion due to motion (however, distortion could result from multipath time delay spread, depending on the channel impulse response). Using the practical formula of (4.40.c), $T_C = 6.77$ ms and the symbol rate must exceed 150 bits/s in order to avoid distortion due to frequency dispersion.

Example 4.5

Determine the proper spatial sampling interval required to make small-scale propagation measurements which assume that consecutive samples are highly correlated in time. How many samples will be required over 10 m travel distance if $f_c = 1900$ MHz and $v = 50$ m/s. How long would it take to make these measurements, assuming they could be made in real time from a moving vehicle? What is the Doppler spread B_D for the channel?

Solution to Example 4.5

For correlation, ensure that the time between samples is equal to $T_C/2$, and use the smallest value of T_C for conservative design.
Using equation (4.40.b)

$$T_C \approx \frac{9}{16\pi f_m} = \frac{9\lambda}{16\pi v} = \frac{9c}{16\pi v f_c} = \frac{9 \times 3 \times 10^8}{16 \times 3.14 \times 50 \times 1900 \times 10^6}$$

$$T_C = 565\mu s$$

Taking time samples at less than half T_C, at $282.5\mu s$ corresponds to a spatial sampling interval of

$$\Delta x = \frac{vT_C}{2} = \frac{50 \times 565\mu s}{2} = 0.014125 \text{ m} = 1.41 \text{ cm}$$

Therefore, the number of samples required over a 10 m travel distance is

$$N_x = \frac{10}{\Delta x} = \frac{10}{0.014125} = 708 \text{ samples}$$

The time taken to make this measurement is equal to $\frac{10\text{m}}{50 \text{ m/s}} = 0.2$ s
The Doppler spread is

$$B_D = f_m = \frac{vf_c}{c} = \frac{50 \times 1900 \times 10^6}{3 \times 10^8} = 316.66 \text{ Hz}$$

4.5 Types of Small-Scale Fading

Section 4.3 demonstrated that the type of fading experienced by a signal propagating through a mobile radio channel depends on the nature of the transmitted signal with respect to the characteristics of the channel. Depending on the relation between the signal parameters (such as bandwidth, symbol period, etc.) and the channel parameters (such as rms delay spread and Doppler spread), different transmitted signals will undergo different types of fading. The time dispersion and frequency dispersion mechanisms in a mobile radio channel lead to four possible distinct effects, which are manifested depending on the nature of the transmitted signal, the channel, and the velocity. While multipath delay spread leads to *time dispersion* and *frequency selective fading*, Doppler spread leads to *frequency dispersion* and *time selective fading*. The two propagation mechanisms are independent of one another. Figure 4.11 shows a tree of the four different types of fading.

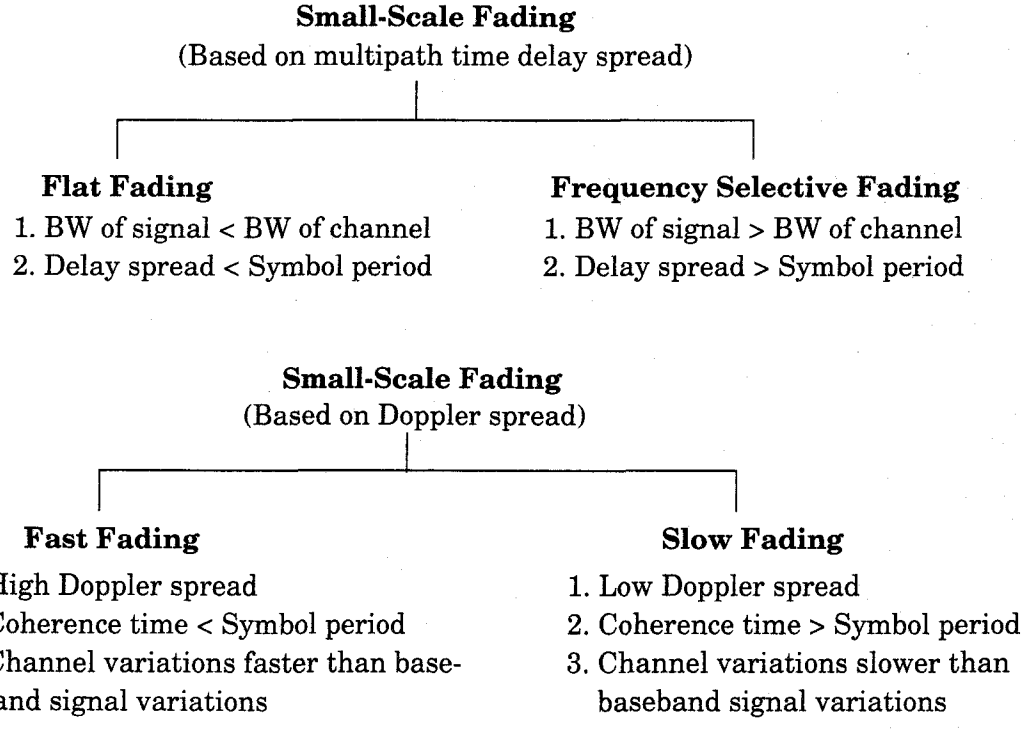

Figure 4.11
Types of small-scale fading.

4.5.1 Fading Effects Due to Multipath Time Delay Spread

Time dispersion due to multipath causes the transmitted signal to undergo either flat or frequency selective fading.

4.5.1.1 Flat fading

If the mobile radio channel has a constant gain and linear phase response over a bandwidth which is greater than the bandwidth of the transmitted signal, then the received signal will undergo *flat fading*. This type of fading is historically the most common type of fading described in the technical literature. In flat fading, the multipath structure of the channel is such that the spectral characteristics of the transmitted signal are preserved at the receiver. However the strength of the received signal changes with time, due to fluctuations in the gain of the channel caused by multipath. The characteristics of a flat fading channel are illustrated in Figure 4.12.

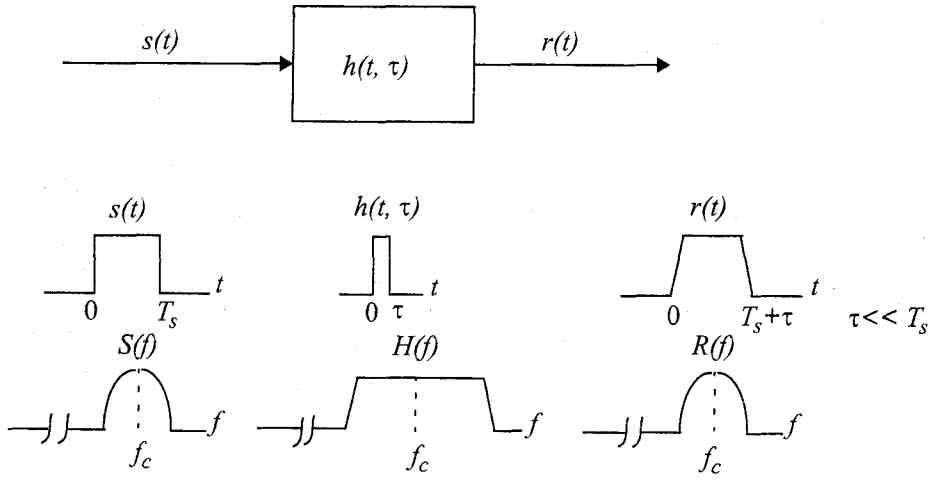

Figure 4.12
Flat fading channel characteristics.

It can be seen from Figure 4.12 that if the channel gain changes over time, a change of amplitude occurs in the received signal. Over time, the received signal $r(t)$ varies in gain, but the spectrum of the transmission is preserved. In a flat fading channel, the reciprocal bandwidth of the transmitted signal is much larger than the multipath time delay spread of the channel, and $h_b(t, \tau)$ can be approximated as having no excess delay (i.e., a single delta function with $\tau = 0$). Flat fading channels are also known as *amplitude varying channels* and are sometimes referred to as *narrowband channels*, since the bandwidth of the applied signal is *narrow* as compared to the channel flat fading bandwidth. Typical flat fading channels cause deep fades, and thus may require 20 or 30 dB more transmitter power to achieve low bit error rates during times of deep fades as

compared to systems operating over non-fading channels. The distribution of the instantaneous gain of flat fading channels is important for designing radio links, and the most common amplitude distribution is the Rayleigh distribution. The Rayleigh flat fading channel model assumes that the channel induces an amplitude which varies in time according to the Rayleigh distribution.

To summarize, a signal undergoes flat fading if

$$B_S \ll B_C \tag{4.41}$$

and

$$T_S \gg \sigma_\tau \tag{4.42}$$

where T_S is the reciprocal bandwidth (e.g., symbol period) and B_S is the bandwidth, respectively, of the transmitted modulation, and σ_τ and B_C are the rms delay spread and coherence bandwidth, respectively, of the channel.

4.5.1.2 Frequency Selective Fading

If the channel possesses a constant-gain and linear phase response over a bandwidth that is smaller than the bandwidth of transmitted signal, then the channel creates *frequency selective fading* on the received signal. Under such conditions the channel impulse response has a multipath delay spread which is greater than the reciprocal bandwidth of the transmitted message waveform. When this occurs, the received signal includes multiple versions of the transmitted waveform which are attenuated (faded) and delayed in time, and hence the received signal is distorted. Frequency selective fading is due to time dispersion of the transmitted symbols within the channel. Thus the channel induces *intersymbol interference* (ISI). Viewed in the frequency domain, certain frequency components in the received signal spectrum have greater gains than others.

Frequency selective fading channels are much more difficult to model than flat fading channels since each multipath signal must be modeled and the channel must be considered to be a linear filter. It is for this reason that wideband multipath measurements are made, and models are developed from these measurements. When analyzing mobile communication systems, statistical impulse response models such as the 2-ray Rayleigh fading model (which considers the impulse response to be made up of two delta functions which independently fade and have sufficient time delay between them to induce frequency selective fading upon the applied signal), or computer generated or measured impulse responses, are generally used for analyzing frequency selective small-scale fading. Figure 4.13 illustrates the characteristics of a frequency selective fading channel.

For frequency selective fading, the spectrum $S(f)$ of the transmitted signal has a bandwidth which is greater than the coherence bandwidth B_C of the channel. Viewed in the frequency domain, the channel becomes frequency selective, where the gain is different for different frequency components. Frequency selec-

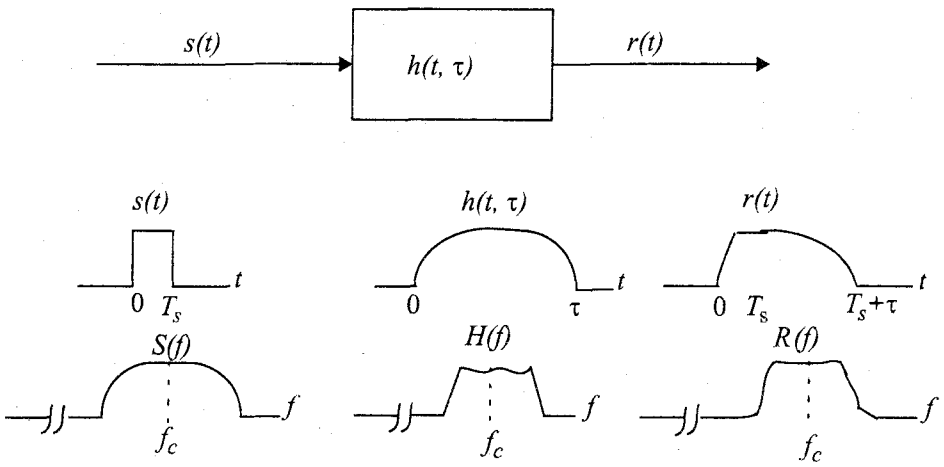

Figure 4.13
Frequency selective fading channel characteristics.

tive fading is caused by multipath delays which approach or exceed the symbol period of the transmitted symbol. Frequency selective fading channels are also known as *wideband channels* since the bandwidth of the signal $s(t)$ is wider than the bandwidth of the channel impulse response. As time varies, the channel varies in gain and phase across the spectrum of *s(t)*, resulting in time varying distortion in the received signal *r(t)*. To summarize, a signal undergoes frequency selective fading if

$$B_S > B_C \tag{4.43}$$

and

$$T_S < \sigma_\tau \tag{4.44}$$

A common rule of thumb is that a channel is frequency selective if $\sigma_\tau > 0.1T_s$, although this is dependent on the specific type of modulation used. Chapter 5 presents simulation results which illustrate the impact of time delay spread on bit error rate (BER).

4.5.2 Fading Effects Due to Doppler Spread

4.5.2.1 Fast Fading

Depending on how rapidly the transmitted baseband signal changes as compared to the rate of change of the channel, a channel may be classified either as a *fast fading* or *slow fading* channel. In a *fast fading channel*, the channel impulse response changes rapidly within the symbol duration. That is, the coherence time of the channel is smaller than the symbol period of the transmitted signal. This causes frequency dispersion (also called time selective fading) due to Doppler spreading, which leads to signal distortion. Viewed in the frequency domain, signal distortion due to fast fading increases with increasing Doppler

spread relative to the bandwidth of the transmitted signal. Therefore, a signal undergoes fast fading if

$$T_S > T_C \tag{4.45}$$

and

$$B_S < B_D \tag{4.46}$$

It should be noted that when a channel is specified as a fast or slow fading channel, it does not specify whether the channel is flat fading or frequency selective in nature. Fast fading only deals with the rate of change of the channel due to motion. In the case of the flat fading channel, we can approximate the impulse response to be simply a delta function (no time delay). Hence, a *flat fading, fast fading* channel is a channel in which the amplitude of the delta function varies faster than the rate of change of the transmitted baseband signal. In the case of a *frequency selective, fast fading* channel, the amplitudes, phases, and time delays of any one of the multipath components vary faster than the rate of change of the transmitted signal. In practice, fast fading only occurs for very low data rates.

4.5.2.2 Slow Fading

In a *slow fading channel*, the channel impulse response changes at a rate much slower than the transmitted baseband signal *s(t)*. In this case, the channel may be assumed to be static over one or several reciprocal bandwidth intervals. In the frequency domain, this implies that the Doppler spread of the channel is much less than the bandwidth of the baseband signal. Therefore, a signal undergoes slow fading if

$$T_S \ll T_C \tag{4.47}$$

and

$$B_S \gg B_D \tag{4.48}$$

It should be clear that the velocity of the mobile (or velocity of objects in the channel) and the baseband signaling determines whether a signal undergoes fast fading or slow fading.

The relation between the various multipath parameters and the type of fading experienced by the signal are summarized in Figure 4.14. Over the years, some authors have confused the terms fast and slow fading with the terms large-scale and small-scale fading. It should be emphasized that fast and slow fading deal with the relationship between the time rate of change in the channel and the transmitted signal, and not with propagation path loss models.

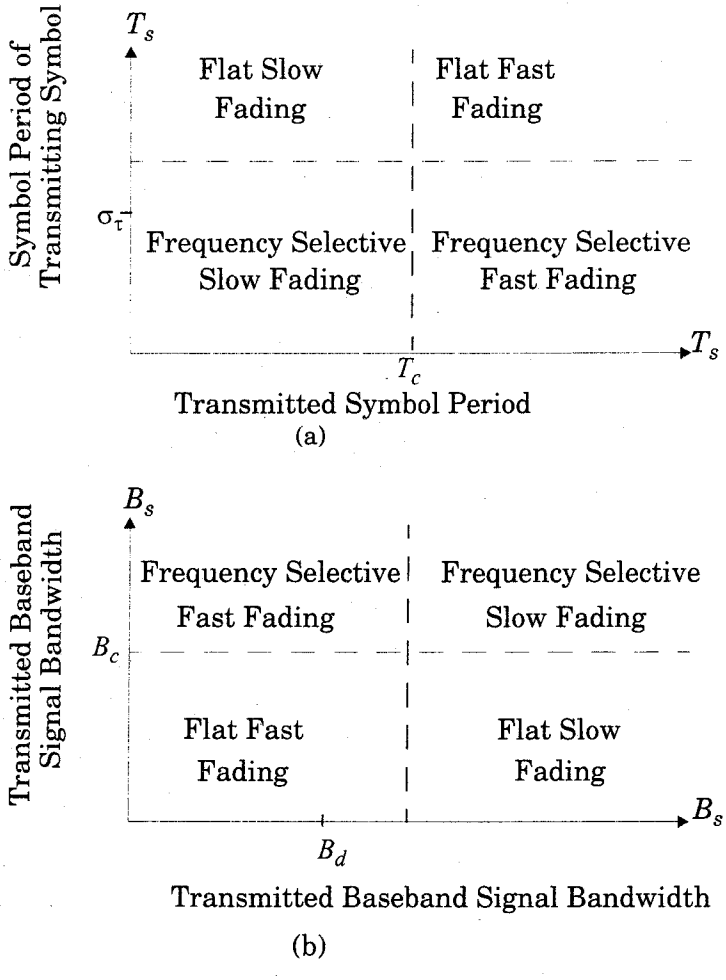

Figure 4.14
Matrix illustrating type of fading experienced by a signal as a function of
(a) symbol period
(b) baseband signal bandwidth.

4.6 Rayleigh and Ricean Distributions

4.6.1 Rayleigh Fading Distribution

In mobile radio channels, the Rayleigh distribution is commonly used to describe the statistical time varying nature of the received envelope of a flat fading signal, or the envelope of an individual multipath component. It is well known that the envelope of the sum of two quadrature Gaussian noise signals obeys a Rayleigh distribution. Figure 4.15 shows a Rayleigh distributed signal envelope as a function of time. The Rayleigh distribution has a probability density function (pdf) given by

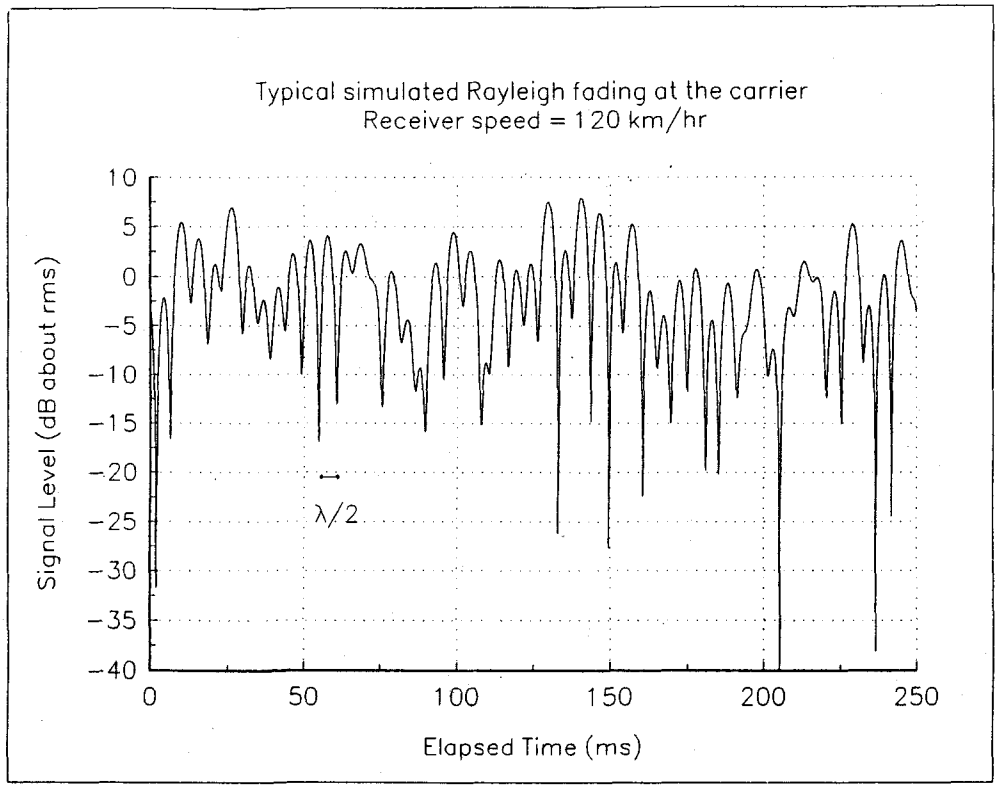

Figure 4.15
A typical Rayleigh fading envelope at 900 MHz [From [Fun93] © IEEE].

$$p(r) = \begin{cases} \dfrac{r}{\sigma^2}\exp\left(-\dfrac{r^2}{2\sigma^2}\right) & (0 \le r \le \infty) \\ 0 & (r < 0) \end{cases} \tag{4.49}$$

where σ is the rms value of the received voltage signal before *envelope detection*, and σ^2 is the time-average power of the received signal *before* envelope detection. The probability that the envelope of the received signal does not exceed a specified value R is given by the corresponding cumulative distribution function (CDF)

$$P(R) = Pr(r \le R) = \int_0^R p(r)\,dr = 1 - \exp\left(-\frac{R^2}{2\sigma^2}\right) \tag{4.50}$$

The mean value r_{mean} of the Rayleigh distribution is given by

$$r_{mean} = E[r] = \int_0^\infty rp(r)\,dr = \sigma\sqrt{\frac{\pi}{2}} = 1.2533\sigma \tag{4.51}$$

and the variance of the Rayleigh distribution is given by σ_r^2, which represents the ac power in the signal envelope

$$\sigma_r^2 = E[r^2] - E^2[r] = \int_0^\infty r^2 p(r)\,dr - \frac{\sigma^2\pi}{2} \tag{4.52}$$

$$= \sigma^2\left(2 - \frac{\pi}{2}\right) = 0.4292\sigma^2$$

The rms value of the envelope is the square root of the mean square, or $\sqrt{2}\sigma$.

The median value of r is found by solving

$$\frac{1}{2} = \int_0^{r_{median}} p(r)\,dr \tag{4.53}$$

and is

$$r_{median} = 1.177\sigma \tag{4.54}$$

Thus the mean and the median differ by only 0.55 dB in a Rayleigh fading signal. Note that the median is often used in practice, since fading data are usually measured in the field and a particular distribution cannot be assumed. By using median values instead of mean values it is easy to compare different fading distributions which may have widely varying means. Figure 4.16 illustrates the Rayleigh pdf. The corresponding Rayleigh cumulative distribution function (CDF) is shown in Figure 4.17.

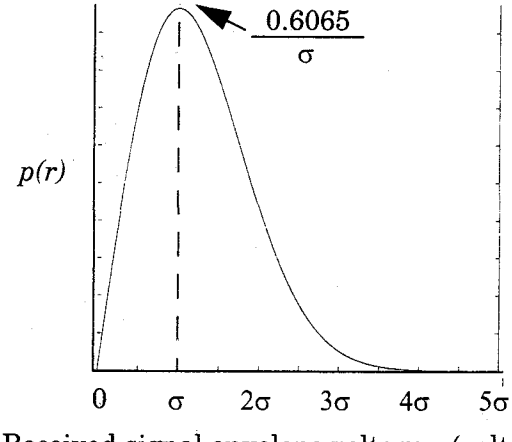

Figure 4.16
Rayleigh probability density function (pdf).

4.6.2 Ricean Fading Distribution

When there is a dominant stationary (nonfading) signal component present, such as a line-of-sight propagation path, the small-scale fading envelope

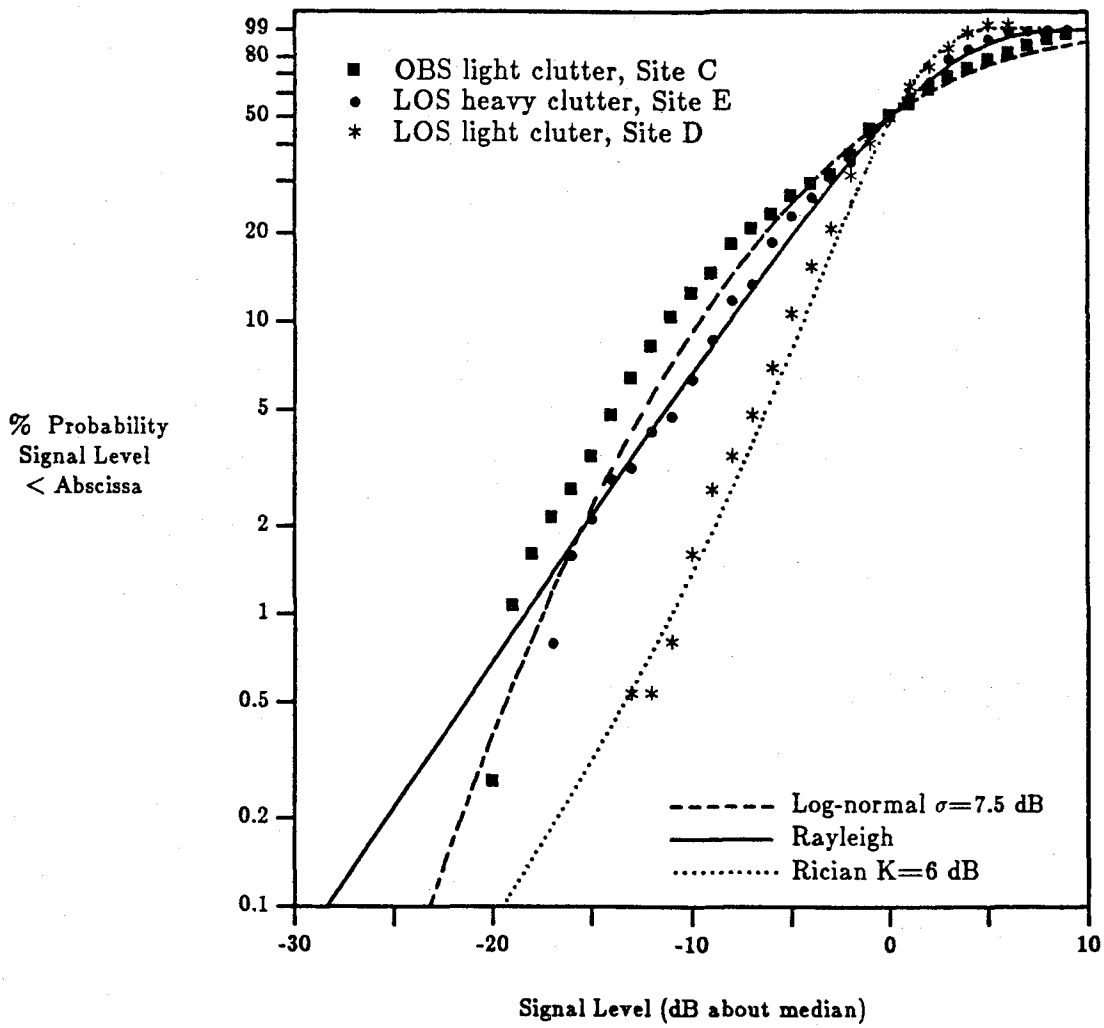

Figure 4.17
Cumulative distribution for three small-scale fading measurements and their fit to Rayleigh, Ricean, and log-normal distributions [From [Rap89] © IEEE].

distribution is Ricean. In such a situation, random multipath components arriving at different angles are superimposed on a stationary dominant signal. At the output of an envelope detector, this has the effect of adding a dc component to the random multipath.

Just as for the case of detection of a sine wave in thermal noise [Ric48], the effect of a dominant signal arriving with many weaker multipath signals gives rise to the Ricean distribution. As the dominant signal becomes weaker, the composite signal resembles a noise signal which has an envelope that is Rayleigh. Thus, the Ricean distribution degenerates to a Rayleigh distribution when the dominant component fades away.

The Ricean distribution is given by

$$p(r) = \begin{cases} \frac{r}{\sigma^2} e^{-\frac{(r^2+A^2)}{2\sigma^2}} I_0\left(\frac{Ar}{\sigma^2}\right) & \text{for } (A \geq 0, r \geq 0) \\ 0 & \text{for } (r < 0) \end{cases} \tag{4.55}$$

The parameter A denotes the peak amplitude of the dominant signal and $I_0(\bullet)$ is the modified Bessel function of the first kind and zero-order. The Ricean distribution is often described in terms of a parameter K which is defined as the ratio between the deterministic signal power and the variance of the multipath. It is given by $K = A^2/(2\sigma^2)$ or, in terms of dB

$$K(\text{dB}) = 10\log\frac{A^2}{2\sigma^2} \text{ dB} \tag{4.56}$$

The parameter K is known as the Ricean factor and completely specifies the Ricean distribution. As $A \to 0, K \to -\infty$ dB, and as the dominant path decreases in amplitude, the Ricean distribution degenerates to a Rayleigh distribution. Figure 4.18 shows the Ricean pdf. The Ricean CDF is compared with the Rayleigh CDF in Figure 4.17.

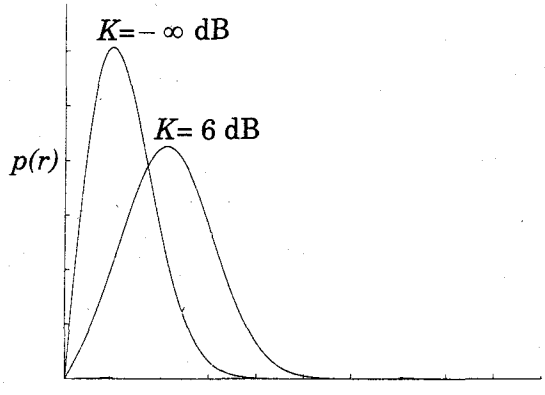

Figure 4.18
Probability density function of Ricean distributions: $K = -\infty$ dB (Rayleigh) and $K = 6$ dB. For K>>1, the Ricean pdf is approximately Gaussian about the mean.

4.7 Statistical Models for Multipath Fading Channels

Several multipath models have been suggested to explain the observed statistical nature of a mobile channel. The first model presented by Ossana [Oss64] was based on interference of waves incident and reflected from the flat sides of randomly located buildings. Although Ossana's model [Oss64] predicts flat fading power spectra that were in agreement with measurements in suburban

areas, it assumes the existence of a direct path between the transmitter and receiver, and is limited to a restricted range of reflection angles. Ossana's model is therefore rather inflexible and inappropriate for urban areas where the direct path is almost always blocked by buildings or other obstacles. Clarke's model [Cla68] is based on scattering and is widely used.

4.7.1 Clarke's Model for Flat Fading

Clarke [Cla68] developed a model where the statistical characteristics of the electromagnetic fields of the received signal at the mobile are deduced from scattering. The model assumes a fixed transmitter with a vertically polarized antenna. The field incident on the mobile antenna is assumed to comprise of N azimuthal plane waves with arbitrary carrier phases, arbitrary azimuthal angles of arrival, and each wave having equal average amplitude. It should be noted that the equal average amplitude assumption is based on the fact that in the absence of a direct line-of-sight path, the scattered components arriving at a receiver will experience similar attenuation over small-scale distances.

Figure 4.19 shows a diagram of plane waves incident on a mobile traveling at a velocity v, in the x-direction. The angle of arrival is measured in the x-y plane with respect to the direction of motion. Every wave that is incident on the mobile undergoes a Doppler shift due to the motion of the receiver and arrives at the receiver at the same time. That is, no excess delay due to multipath is assumed for any of the waves (flat fading assumption). For the n th wave arriving at an angle α_n to the x-axis, the Doppler shift in Hertz is given by

$$f_n = \frac{v}{\lambda}\cos\alpha_n \tag{4.57}$$

where λ is the wavelength of the incident wave.

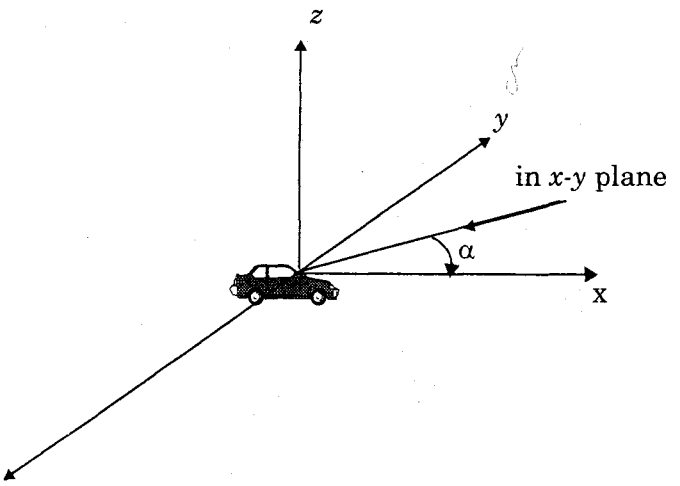

Figure 4.19
Illustrating plane waves arriving at random angles.

The vertically polarized plane waves arriving at the mobile have E and H field components given by

$$E_z = E_o \sum_{n=1}^{N} C_n \cos(2\pi f_c t + \theta_n) \tag{4.58}$$

$$H_x = -\frac{E_o}{\eta} \sum_{n=1}^{N} C_n \sin\alpha_n \cos(2\pi f_c t + \theta_n) \tag{4.59}$$

$$H_y = -\frac{E_o}{\eta} \sum_{n=1}^{N} C_n \cos\alpha_n \cos(2\pi f_c t + \theta_n) \tag{4.60}$$

where E_0 is the real amplitude of local average E-field (assumed constant), C_n is a real random variable representing the amplitude of individual waves, η is the intrinsic impedance of free space (377Ω), and f_c is the carrier frequency. The random phase of the n th arriving component θ_n is given by

$$\theta_n = 2\pi f_n t + \phi_n \tag{4.61}$$

The amplitudes of the E-and H-field are normalized such that the ensemble average of the C_n's is given by

$$\sum_{n=1}^{N} \overline{C_n^2} = 1 \tag{4.62}$$

Since the Doppler shift is very small when compared to the carrier frequency, the three field components may be modeled as narrow band random processes. The three components E_z, H_x, and H_y can be approximated as Gaussian random variables if N is sufficiently large. The phase angles are assumed to have a uniform probability density function (pdf) on the interval $(0,2\sigma]$. Based on the analysis by Rice [Ric48] the E-field can be expressed in an in-phase and quadrature form

$$E_z = T_c(t)\cos(2\pi f_c t) - T_s(t)\sin(2\pi f_c t) \tag{4.63}$$

where

$$T_c(t) = E_0 \sum_{n=1}^{N} C_n \cos(2\pi f_n t + \phi_n) \tag{4.64}$$

and

$$T_s(t) = E_0 \sum_{n=1}^{N} C_n \sin(2\pi f_n t + \phi_n) \tag{4.65}$$

Both $T_c(t)$ and $T_s(t)$ are Gaussian random processes which are denoted as T_c and T_s, respectively, at any time t. T_c and T_s are uncorrelated zero-mean Gaussian random variables with an equal variance given by

$$\overline{T_c^2} = \overline{T_s^2} = \overline{|E_z|^2} = E_0^2/2 \tag{4.66}$$

where the overbar denotes the ensemble average.

The envelope of the received E-field, $E_z(t)$, is given by

$$|E_z(t)| = \sqrt{T_c^2(t) + T_s^2(t)} = r(t) \tag{4.67}$$

Since T_c and T_s are Gaussian random variables, it can be shown through a Jacobean transformation [Pap91] that the random received signal envelope r has a Rayleigh distribution given by

$$p(r) = \begin{cases} \dfrac{r}{\sigma^2}\exp\left(-\dfrac{r^2}{2\sigma^2}\right) & 0 \le r \le \infty \\ 0 & r < 0 \end{cases} \tag{4.68}$$

where $\sigma^2 = E_0^2/2$

4.7.1.1 Spectral Shape Due to Doppler Spread in Clarke's Model

Gans [Gan72] developed a spectrum analysis for Clarke's model. Let $p(\alpha)\,d\alpha$ denote the fraction of the total incoming power within $d\alpha$ of the angle α, and let A denote the average received power with respect to an isotropic antenna. As $N \to \infty$, $p(\alpha)\,d\alpha$ approaches a continuous, rather than a discrete, distribution. If $G(\alpha)$ is the azimuthal gain pattern of the mobile antenna as a function of the angle of arrival, the total received power can be expressed as

$$P_r = \int_0^{2\pi} AG(\alpha)p(\alpha)\,d\alpha \tag{4.69}$$

where $AG(\alpha)p(\alpha)\,d\alpha$ is the differential variation of received power with angle. If the scattered signal is a CW signal of frequency f_c, then the instantaneous frequency of the received signal component arriving at an angle α is obtained using equation (4.57)

$$f(\alpha) = f = \frac{v}{\lambda}\cos(\alpha) + f_c = f_m \cos\alpha + f_c \tag{4.70}$$

where f_m is the maximum Doppler shift. It should be noted that $f(\alpha)$ is an even function of α, (i.e., $f(\alpha) = f(-\alpha)$).

If $S(f)$ is the power spectrum of the received signal, the differential variation of received power with frequency is given by

$$S(f)\,|df| \tag{4.71}$$

Equating the differential variation of received power with frequency to the differential variation in received power with angle, we have

$$S(f)|df| = A[p(\alpha)G(\alpha) + p(-\alpha)G(-\alpha)]|d\alpha| \tag{4.72}$$

Differentiating equation (4.70), and rearranging the terms, we have

$$|df| = |d\alpha||-\sin\alpha|f_m \tag{4.73}$$

Using equation (4.70), α can be expressed as a function of f as

$$\alpha = \cos^{-1}\left[\frac{f-f_c}{f_m}\right] \tag{4.74}$$

This implies that

$$\sin\alpha = \sqrt{1-\left(\frac{f-f_c}{f_m}\right)^2} \tag{4.75}$$

Substituting equation (4.73) and (4.75) into both sides of (4.72), the power spectral density $S(f)$ can be expressed as

$$S(f) = \frac{A[p(\alpha)G(\alpha) + p(-\alpha)G(-\alpha)]}{f_m\sqrt{1-\left(\frac{f-f_c}{f_m}\right)^2}} \tag{4.76}$$

where

$$S(f) = 0, \qquad |f-f_c| > f_m \tag{4.77}$$

The spectrum is centered on the carrier frequency and is zero outside the limits of $f_c \pm f_m$. Each of the arriving waves has its own carrier frequency (due to its direction of arrival) which is slightly offset from the center frequency. For the case of a vertical $\lambda/4$ antenna ($G(\alpha) = 1.5$), and a uniform distribution $p(\alpha) = 1/2\pi$ over 0 to 2π, the output spectrum is given by (4.76) as

$$S_{E_z}(f) = \frac{1.5}{\pi f_m\sqrt{1-\left(\frac{f-f_c}{f_m}\right)^2}} \tag{4.78}$$

In equation (4.78) the power spectral density at $f = f_c \pm f_m$ is infinite, i.e., Doppler components arriving at exactly 0° and 180° have an infinite power spectral density. This is not a problem since α is continuously distributed and the probability of components arriving at exactly these angles is zero.

Figure 4.20 shows the power spectral density of the resulting RF signal due to Doppler fading. Smith [Smi75] demonstrated an easy way to simulate Clarke's model using a computer simulation as described Section 4.7.2.

After envelope detection of the Doppler-shifted signal, the resulting baseband spectrum has a maximum frequency of $2f_m$. It can be shown [Jak74] that the electric field produces a baseband power spectral density given by

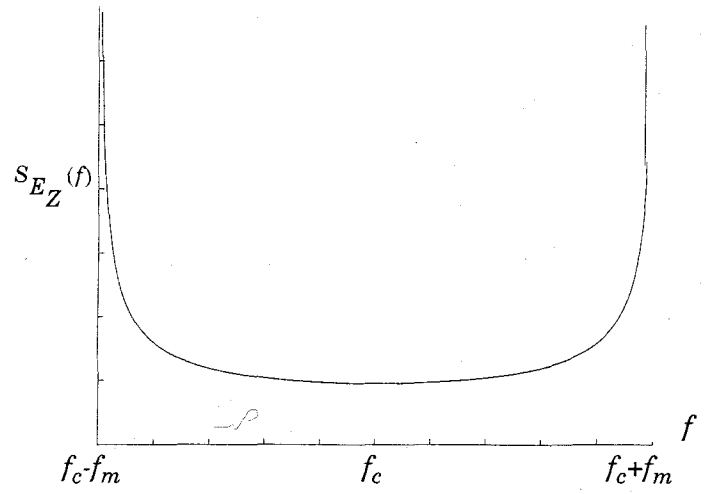

Figure 4.20
Doppler power spectrum for an unmodulated CW carrier [From [Gan72]] © IEEE].

$$S_{bbE_z}(f) = \frac{1}{8\pi f_m} K\left[\sqrt{1-\left(\frac{f}{2f_m}\right)^2}\right] \tag{4.79}$$

where $K[\bullet]$ is the complete elliptical integral of the first kind. Equation (4.79) is not intuitive and is a result of the temporal correlation of the received signal when passed through a nonlinear envelope detector. Figure 4.21 illustrates the baseband spectrum of the received signal after envelope detection.

The spectral shape of the Doppler spread determines the time domain fading waveform and dictates the temporal correlation and fade slope behaviors. Rayleigh fading simulators must use a fading spectrum such as equation (4.78) in order to produce realistic fading waveforms that have proper time correlation.

4.7.2 Simulation of Clarke and Gans Fading Model

It is often useful to simulate multipath fading channels in hardware or software. A popular simulation method uses the concept of in-phase and quadrature modulation paths to produce a simulated signal with spectral and temporal characteristics very close to measured data.

As shown in Figure 4.22, two independent Gaussian low pass noise sources are used to produce in-phase and quadrature fading branches. Each Gaussian source may be formed by summing two independent Gaussian random variables which are orthogonal (i.e., $g = a + jb$, where a and b are real Gaussian random variables and g is complex Gaussian). By using the spectral filter defined by equation (4.78) to shape the random signals in the frequency domain, accurate time domain waveforms of Doppler fading can be produced by using an inverse fast Fourier transform (IFFT) at the last stage of the simulator.

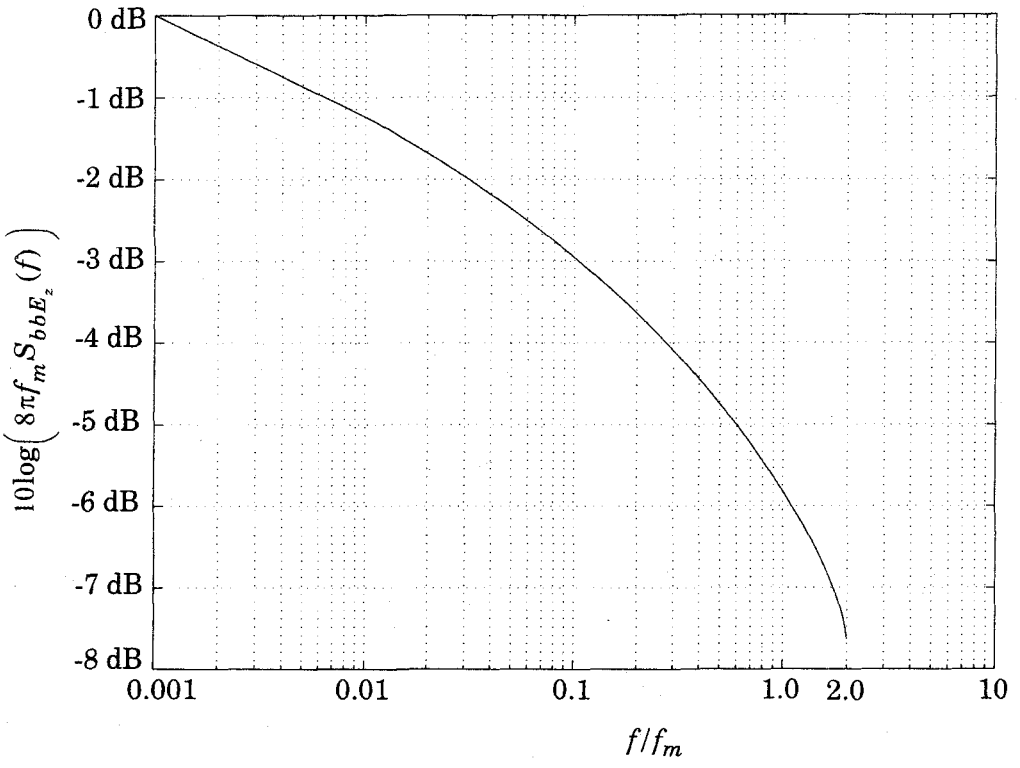

Figure 4.21
Baseband power spectral density of a CW Doppler signal after envelope detection.

Smith [Smi75] demonstrated a simple computer program that implements Figure 4.22(b). His method uses a complex Gaussian random number generator (noise source) to produce a baseband line spectrum with complex weights in the positive frequency band. The maximum frequency component of the line spectrum is f_m. Using the property of real signals, the negative frequency components are constructed by simply conjugating the complex Gaussian values obtained for the positive frequencies. Note that the IFFT of this signal is a purely real Gaussian random process in the time domain which is used in one of the quadrature arms shown in Figure 4.22. The random valued line spectrum is then multiplied with a discrete frequency representation of $\sqrt{S_{E_z}(f)}$ having the same number of points as the noise source. To handle the case where equation (4.78) approaches infinity at the passband edge, Smith truncated the value of $S_{E_z}(f_m)$ by computing the slope of the function at the sample frequency just prior to the passband edge and extended the slope to the passband edge. Simulations using the architecture in Figure 4.22 are usually implemented in the frequency domain using complex Gaussian line spectra to take advantage of easy implementation of equation (4.78). This, in turn, implies that the low pass Gaus-

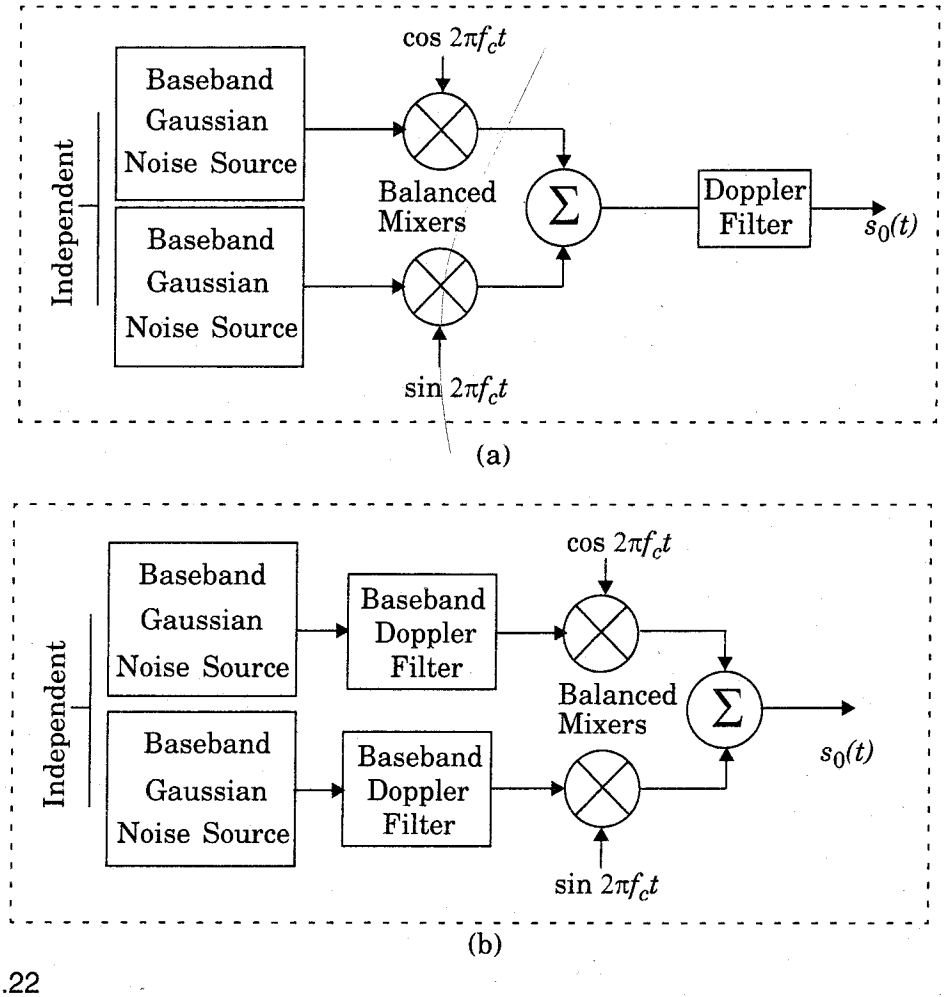

Figure 4.22
Simulator using quadrature amplitude modulation with (a) RF Doppler filter and (b) baseband Doppler filter.

sian noise components are actually a series of frequency components (line spectrum from $-f_m$ to f_m), which are equally spaced and each have a complex Gaussian weight. Smith's simulation methodology is shown in Figure 4.23.

To implement the simulator shown in Figure 4.23, the following steps are used:

(1) Specify the number of frequency domain points (N) used to represent $\sqrt{S_{E_z}(f)}$ and the maximum Doppler frequency shift (f_m). The value used for N is usually a power of 2.

(2) Compute the frequency spacing between adjacent spectral lines as $\Delta f = 2f_m/(N-1)$. This defines the time duration of a fading waveform, $T = 1/\Delta f$.

(3) Generate complex Gaussian random variables for each of the $N/2$ positive frequency components of the noise source.

(4) Construct the negative frequency components of the noise source by conju-

gating positive frequency values and assigning these at negative frequency values.

(5) Multiply the in-phase and quadrature noise sources by the fading spectrum $\sqrt{S_{E_z}(f)}$.

(6) Perform an IFFT on the resulting frequency domain signal from the in-phase and quadrature arms, and compute the sum of the squares of each signal.

(7) Take the square root of the sum obtained in step 6 to obtain an N point time series of a simulated Rayleigh fading signal with the proper Doppler spread and time correlation.

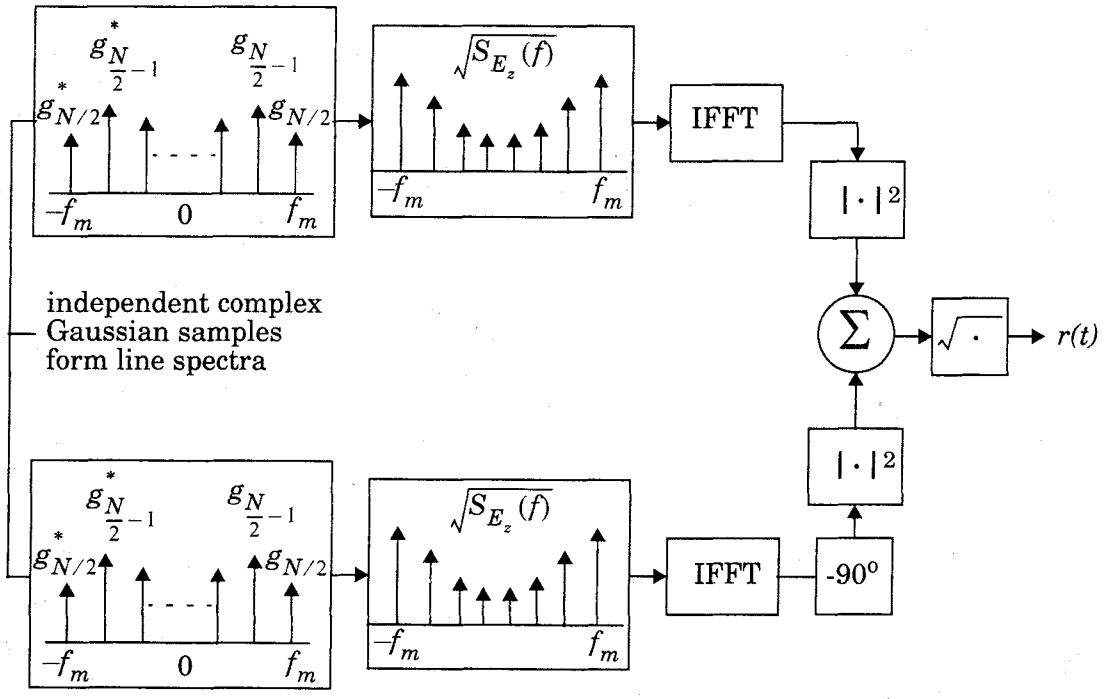

Figure 4.23
Frequency domain implementation of a Rayleigh fading simulator at baseband

Several Rayleigh fading simulators may be used in conjunction with variable gains and time delays to produce frequency selective fading effects. This is shown in Figure 4.24.

By making a single frequency component dominant in amplitude within $\sqrt{S_{E_z}(f)}$, the fading is changed from Rayleigh to Ricean. This can be used to alter the probability distributions of the individual multipath components in the simulator of Figure 4.24.

To determine the impact of flat fading on an applied signal $s(t)$, one merely needs to multiply the applied signal by $r(t)$, the output of the fading simulator. To determine the impact of more than one multipath component, a convolution must be performed as shown in Figure 4.24.

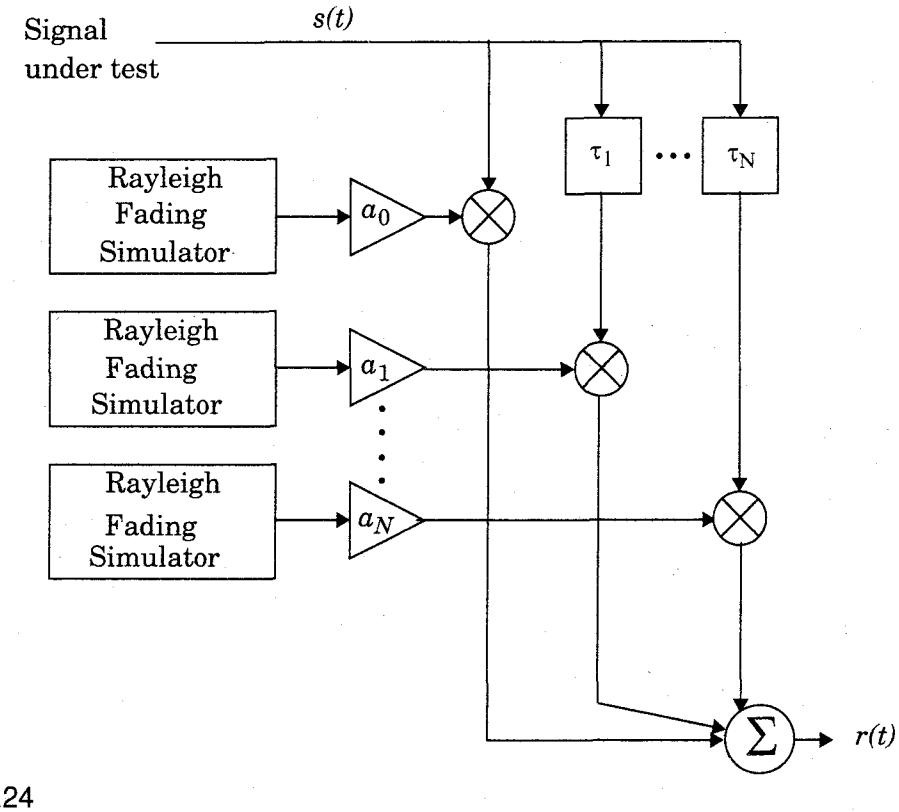

Figure 4.24
A signal may be applied to a Rayleigh fading simulator to determine performance in a wide range of channel conditions. Both flat and frequency selective fading conditions may be simulated, depending on gain and time delay settings.

4.7.3 Level Crossing and Fading Statistics

Rice computed joint statistics for a mathematical problem which is similar to Clarke's fading model [Cla68], and thereby provided simple expressions for computing the average number of level crossing and the duration of fades. The *level crossing rate* (LCR) and *average fade duration* of a Rayleigh fading signal are two important statistics which are useful for designing error control codes and diversity schemes to be used in mobile communication systems, since it becomes possible to relate the time rate of change of the received signal to the signal level and velocity of the mobile.

The *level crossing rate* (LCR) is defined as the expected rate at which the Rayleigh fading envelope, normalized to the local rms signal level, crosses a specified level in a positive-going direction. The number of level crossings per second is given by

$$N_R = \int_0^\infty \dot{r}\, p(R, \dot{r})\, d\dot{r} = \sqrt{2\pi} f_m \rho e^{-\rho^2} \tag{4.80}$$

where $\dot{r}$ is the time derivative of $r(t)$ (i.e., the slope), $p(R, \dot{r})$ is the joint density function of r and $\dot{r}$ at $r = R$, f_m is the maximum Doppler frequency and $\rho = R/R_{rms}$ is the value of the specified level R, normalized to the local rms amplitude of the fading envelope [Jak74]. Equation (4.80) gives the value of N_R, the average number of level crossings per second at specified R. The level crossing rate is a function of the mobile speed as is apparent from the presence of f_m in equation (4.80). There are few crossings at both high and low levels, with the maximum rate occurring at $\rho = 1/\sqrt{2}$, (i.e., at a level 3 dB below the rms level). The signal envelope experiences very deep fades only occasionally, but shallow fades are frequent.

Example 4.6

For a Rayleigh fading signal, compute the positive-going level crossing rate for $\rho = 1$, when the maximum Doppler frequency (f_m) is 20 Hz. What is the maximum velocity of the mobile for this Doppler frequency if the carrier frequency is 900 MHz?

Solution to Example 4.6

Using equation (4.80), the number of zero level crossings is

$$N_R = \sqrt{2\pi}(20)(1)e^{-1} = 18.44 \text{ crossings per second}$$

The maximum velocity of the mobile can be obtained using the Doppler relation, $f_{d,max} = v/\lambda$.

Therefore velocity of the mobile at $f_m = 20$ Hz is

$$v = f_d\lambda = 20 \text{ Hz}(1/3 \text{ m}) = 6.66 \text{ m/s} = 24 \text{ km/hr}$$

The *average fade duration* is defined as the average period of time for which the received signal is below a specified level R. For a Rayleigh fading signal, this is given by

$$\bar{\tau} = \frac{1}{N_R} Pr[r \le R] \tag{4.81}$$

where $Pr[r \le R]$ is the probability that the received signal r is less than R and is given by

$$Pr[r \le R] = \frac{1}{T}\sum_i \tau_i \tag{4.82}$$

where τ_i is the duration of the fade and T is the observation interval of the fading signal. The probability that the received signal r is less than the threshold R is found from the Rayleigh distribution as

$$P_r[r \le R] = \int_0^R p(r)\,dr = 1 - \exp(-\rho^2) \tag{4.83}$$

where $p(r)$ is the pdf of a Rayleigh distribution. Thus, using equations (4.80), (4.81), and (4.83), the average fade duration as a function of ρ and f_m can be expressed as

$$\bar{\tau} = \frac{e^{\rho^2} - 1}{\rho f_m \sqrt{2\pi}} \tag{4.84}$$

The average duration of a signal fade helps determine the most likely number of signaling bits that may be lost during a fade. Average fade duration primarily depends upon the speed of the mobile, and decreases as the maximum Doppler frequency f_m becomes large. If there is a particular fade margin built into the mobile communication system, it is appropriate to evaluate the receiver performance by determining the rate at which the input signal falls below a given level R, and how long it remains below the level, on average. This is useful for relating SNR during a fade to the instantaneous BER which results.

Example 4.7

Find the average fade duration for threshold levels $\rho = 0.01, \rho = 0.1$, and $\rho = 1$, when the Doppler frequency is 200 Hz.

Solution to Example 4.7

Average fade duration can be found by substituting the given values in equation (4.75)

For $\rho = 0.01$

$$\bar{\tau} = \frac{e^{0.01^2} - 1}{(0.01)\,200\sqrt{2\pi}} = 19.9\mu s$$

For $\rho = 0.1$

$$\bar{\tau} = \frac{e^{0.1^2} - 1}{(0.1)\,200\sqrt{2\pi}} = 200\mu s$$

For $\rho = 1$

$$\bar{\tau} = \frac{e^{1^2} - 1}{(1)\,200\sqrt{2\pi}} = 3.43 \text{ ms}$$

Example 4.8

Find the average fade duration for a threshold level of $\rho = 0.707$ when the Doppler frequency is 20 Hz. For a binary digital modulation with bit duration of 50 bps, is the Rayleigh fading slow or fast? What is the average number of bit errors per second for the given data rate. Assume that a bit error occurs whenever any portion of a bit encounters a fade for which $\rho < 0.1$.

Solution to Example 4.8

The average fade duration can be obtained using equation (4.84).

$$\bar{\tau} = \frac{e^{0.707^2} - 1}{(0.707)\,20\sqrt{2\pi}} = 18.3 \text{ ms}$$

For a data rate of 50 bps, the bit period is 20 ms. Since the bit period is greater than the average fade duration, for the given data rate the signal undergoes fast Rayleigh fading. Using equation (4.84), the average fade duration for $\rho = 0.1$ is equal to 0.002 s. This is less than the duration of one bit. Therefore, only one bit on average will be lost during a fade. Using equation (4.80), the number of level crossings for $\rho = 0.1$ is $N_r = 4.96$ crossings per seconds. Since a bit error is assumed to occur whenever a portion of a bit encounters a fade, and since average fade duration spans only a fraction of a bit duration, the total number of bits in error is 5 per second, resulting in a BER = (5/50) = 0.1.

4.7.4 Two-ray Rayleigh Fading Model

Clarke's model and the statistics for Rayleigh fading are for flat fading conditions and do not consider multipath time delay. In modern mobile communication systems with high data rates, it has become necessary to model the effects of multipath delay spread as well as fading. A commonly used multipath model is an independent Rayleigh fading 2-ray model (which is a specific implementation of the generic fading simulator shown in Figure 4.24). Figure 4.25 shows a block diagram of the 2-ray independent Rayleigh fading channel model. The impulse response of the model is represented as

$$h_b(t) = \alpha_1 \exp(j\phi_1)\,\delta(t) + \alpha_2 \exp(j\phi_2)\,\delta(t-\tau) \tag{4.85}$$

where α_1 and α_2 are independent and Rayleigh distributed, ϕ_1 and ϕ_2 are independent and uniformly distributed over $[0, 2\pi]$, and τ is the time delay between the two rays. By setting α_2 equal to zero, the special case of a flat Rayleigh fading channel is obtained as

$$h_b(t) = \alpha_1 \exp(j\phi_1)\,\delta(t) \tag{4.86}$$

By varying τ, it is possible to create a wide range of frequency selective fading effects. The proper time correlation properties of the Rayleigh random variables α_1 and α_2 are guaranteed by generating two independent waveforms, each produced from the inverse Fourier transform of the spectrum described in Section 4.7.2.

4.7.5 Saleh and Valenzuela Indoor Statistical Model

Saleh and Valenzuela [Sal87] reported the results of indoor propagation measurements between two vertically polarized omni-directional antennas located on the same floor of a medium sized office building. Measurements were made using 10 ns, 1.5 GHz, radar-like pulses. The method involved averaging the square law detected pulse response while sweeping the frequency of the

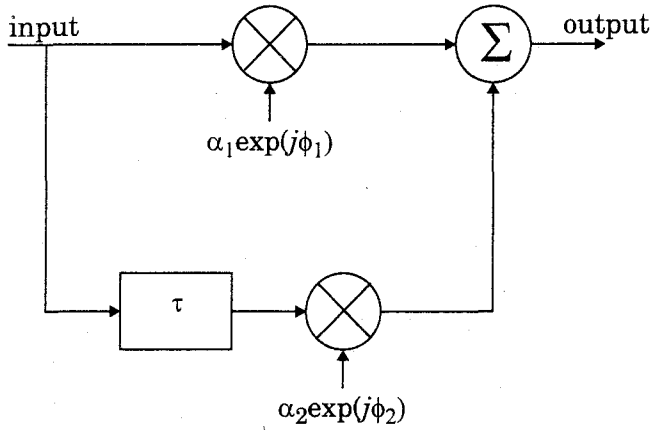

Figure 4.25
Two-ray Rayleigh fading model.

transmitted pulse. Using this method, multipath components within 5 ns were resolvable.

The results obtained by Saleh and Valenzula show that: (a) the indoor channel is quasi-static or very slowly time varying, and (b) the statistics of the channel impulse response are independent of transmitting and receiving antenna polarization, if there is no line-of-sight path between them. They reported a maximum multipath delay spread of 100 ns to 200 ns within the rooms of a building, and 300 ns in hallways. The measured rms delay spread within rooms had a median of 25 ns and a maximum of 50 ns. The large-scale path loss with no line-of-sight path was found to vary over a 60 dB range and obey a log-distance power law (see equation (3.68)) with an exponent between 3 and 4.

Saleh and Valenzuela developed a simple multipath model for indoor channels based on measurement results. The model assumes that the multipath components arrive in clusters. The amplitudes of the received components are independent Rayleigh random variables with variances that decay exponentially with cluster delay as well as excess delay within a cluster. The corresponding phase angles are independent uniform random variables over $[0,2\pi]$. The clusters and multipath components within a cluster form Poisson arrival processes with different rates. The clusters and multipath components within a cluster have exponentially distributed interarrival times. The formation of the clusters is related to the building structure, while the components within the cluster are formed by multiple reflections from objects in the vicinity of the transmitter and the receiver.

4.7.6 SIRCIM and SMRCIM Indoor and Outdoor Statistical Models

Rappaport and Seidel [Rap91a] reported measurements at 1300 MHz in five factory buildings and carried out subsequent measurements in other types of

buildings. The authors developed an elaborate, empirically derived statistical model based on the discrete impulse response channel model and wrote a computer program called SIRCIM (Simulation of Indoor Radio Channel Impulse-response Models). SIRCIM generates realistic samples of small-scale indoor channel impulse response measurements [Rap91a]. Subsequent work by Huang produced SMRCIM (Simulation of Mobile Radio Channel Impulse-response Models), a similar program that generates small-scale urban cellular and microcellular channel impulse responses [Rap93a]. These programs are currently in use at over 100 institutions throughout the world.

By recording power delay profile impulse responses at $\lambda/4$ intervals on a 1 m track at many indoor measurement locations, the authors were able to characterize local small-scale fading of individual multipath components, and the small-scale variation in the number and arrival times of multipath components within a local area. Thus, the resulting statistical models are functions of multipath time delay bin τ_i, the small-scale receiver spacing, X_l, within a 1 m local area, the topography S_m which is either line-of-sight (LOS) or obstructed, the large-scale T-R separation distance D_n, and the particular measurement location P_n. Therefore, each individual baseband power delay profile is expressed in a manner similar to equation (4.13), except the random amplitudes and time delays are random variables which depend on the surrounding environment. Phases are synthesized using a pseudo-deterministic model which provides realistic results, so that a complete time varying complex baseband channel impulse response $h_b(t;\tau_i)$ may be obtained over a local area through simulation.

$$h_b(t, X_l, S_m, D_n, P_n) = \sum_i A_i(\tau_i, X_l, S_m, D_n, P_n)\, e^{j\theta_i[\tau_i, X_l, S_m, D_n, P_n]} \delta(t - \tau_i(X_l, S_m, D_n, P_n)) \tag{4.87}$$

In equation (4.87), A_i^2 is the average multipath receiver power within a discrete excess delay interval of 7.8125 ns.

The measured multipath delays inside open-plan buildings ranged from 40 ns to 800 ns. Mean multipath delay and rms delay spread values ranged from 30 ns to 300 ns, with median values of 96 ns in LOS paths and 105 ns in obstructed paths. Delay spreads were found to be uncorrelated with T-R separation but were affected by factory inventory, building construction materials, building age, wall locations, and ceiling heights. Measurements in a food processing factory that manufactures dry-goods and has considerably less metal inventory than other factories had an rms delay spread that was half of those observed in factories producing metal products. Newer factories which incorporate steel beams and steel reinforced concrete in the building structure have stronger multipath signals and less attenuation than older factories which used wood and brick for perimeter walls. The data suggested that radio propagation in buildings may be described by a hybrid geometric/statistical model that accounts for both reflec-

tions from walls and ceilings and random scattering from inventory and equipment.

By analyzing the measurements from fifty local areas in many buildings, it was found that the number of multipath components, N_p, arriving at a certain location is a function of X, S_m, and P_n, and almost always has a Gaussian distribution. The average number of multipath components ranges between 9 and 36, and is generated based on an empirical fit to measurements. The probability that a multipath component will arrive at a receiver at a particular excess delay T_i in a particular environment S_m is denoted as $P_R(T_i, S_m)$. This was found from measurements by counting the total number of detected multipath components at a particular discrete excess delay time, and dividing by the total number of possible multipath components for each excess delay interval. The probabilities for multipath arriving at a particular excess delay values may be modeled as piecewise functions of excess delay, and are given by

$$P_R(T_i, S_1)\ \text{for LOS} = \begin{cases} 1 - \dfrac{T_i}{367} & (T_i < 110\ \text{ns}) \\ 0.65 - \dfrac{(T_i - 110)}{360} & (110\ \text{ns} < T_i < 200\ \text{ns}) \\ 0.22 - \dfrac{(T_i - 200)}{1360} & (200\ \text{ns} < T_i < 500\ \text{ns}) \end{cases} \tag{4.88}$$

$$P_R(T_i, S_2)\ \text{for OBS} = \begin{cases} 0.55 + \dfrac{T_i}{667} & (T_i < 100\ \text{ns}) \\ 0.08 + 0.62 \exp\left(-\dfrac{(T_i - 100)}{75}\right) & (100\ \text{ns} < T_i < 500\ \text{ns}) \end{cases} \tag{4.89}$$

where S_1 corresponds to the LOS topography, and S_2 corresponds to obstructed topography. SIRCIM uses the probability of arrival distributions described by equation (4.88) or (4.89) along with the probability distribution of the number of multipath components, $N_P(X, S_m, P_n)$, to simulate power delay profiles over small-scale distances. A recursive algorithm repeatedly compares equation (4.88) or (4.89) with a uniformly distributed random variable until the proper N_P is generated for each profile [Hua91], [Rap91a].

Figure 4.26 shows an example of measured power delay profiles at 19 discrete receiver locations along a 1 m track, and illustrates accompanying narrowband information which SIRCIM computes based on synthesized phases for each multipath component [Rap91a]. Measurements reported in the literature provide excellent agreement with impulse responses predicted by SIRCIM.

Using similar statistical modeling techniques, urban cellular and microcellular multipath measurement data from [Rap90], [Sei91], [Sei92a] were used to develop SMRCIM. Both large cell and microcell models were developed. Figure

4.27 shows an example of SMRCIM output for an outdoor microcell environment [Rap93a].

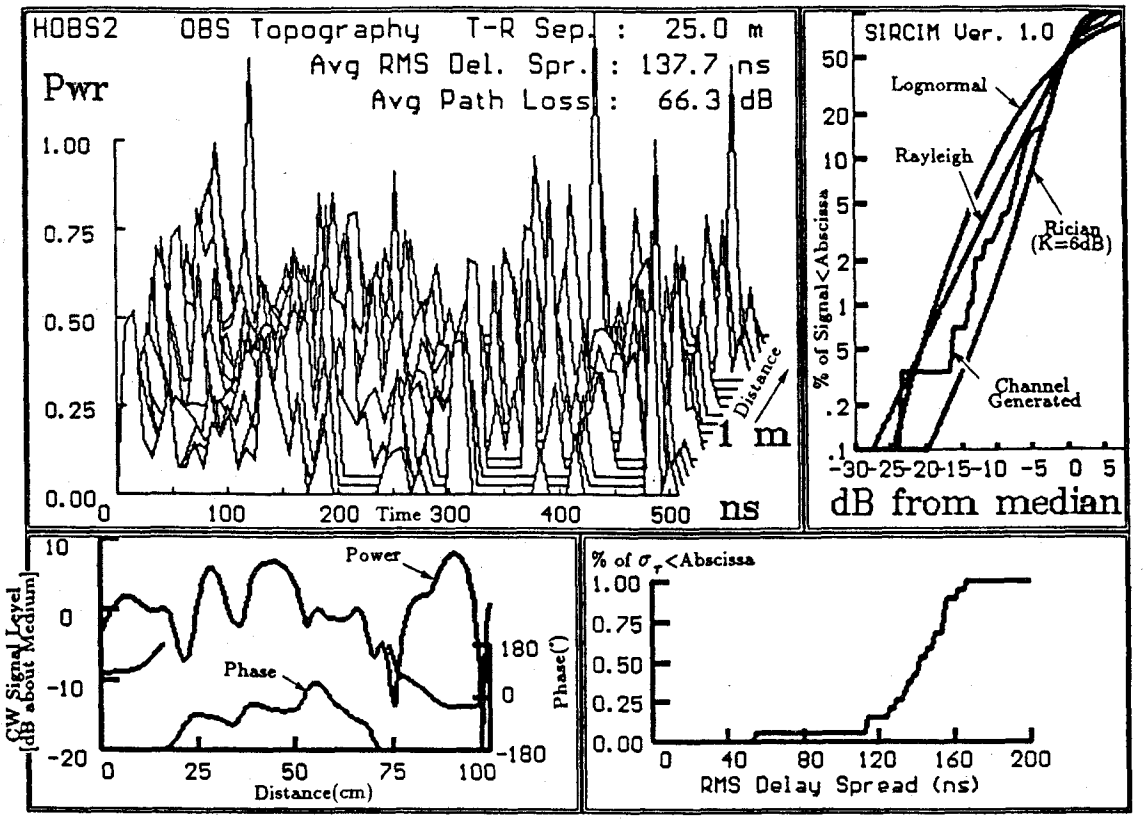

Figure 4.26
Indoor wide band impulse responses simulated by SIRCIM at 1.3 GHz. Also shown are the distributions of the rms delay spread and the narrowband signal power distribution. The channel is simulated as being obstructed in an open-plan building, T-R separation is 25 m. The rms delay spread is 137.7 ns. All multipath components and parameters are stored on disk [From [Rap93a] © IEEE].

4.8 Problems

4.1 Draw a block diagram of a binary spread spectrum sliding correlator multipath measurement system. Explain in words how it is used to measure power delay profiles.

(a) If the transmitter chip period is 10 ns, the PN sequence has length 1023, and a 6 GHz carrier is used at the transmitter, find the time between maximal correlation and the slide factor if the receiver uses a PN sequence clock that is 30 kHz slower than the transmitter.

(b) If an oscilloscope is used to display one complete cycle of the PN sequence (that is, if two successive maximal correlation peaks are to be displayed on the oscilloscope), and if 10 divisions are provided on the oscilloscope time axis, what is the most appropriate sweep setting (in seconds/divi-

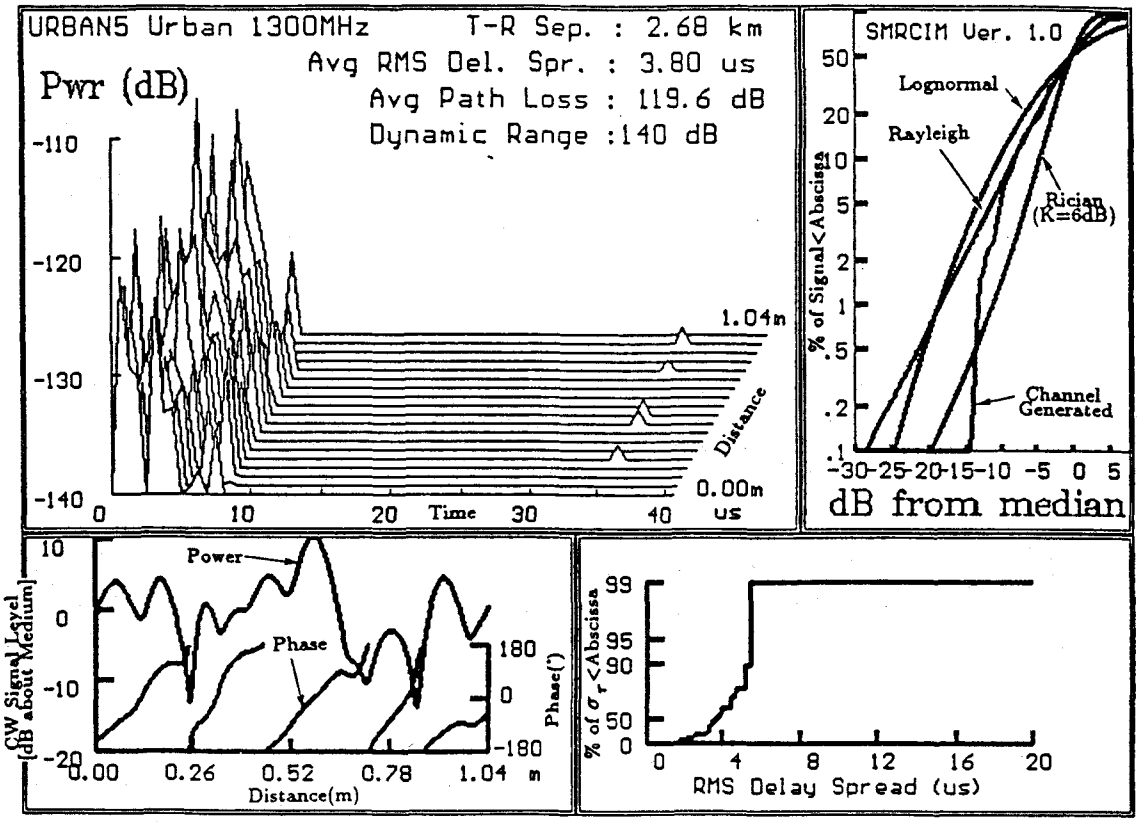

Figure 4.27
Urban wideband impulse responses simulated by SMRCIM at 1.3 GHz. Also shown are the distributions of the rms delay spread and the narrowband fading. T-R separation is 2.68 km. The rms delay spread is 3.8 μs. All multipath components and parameters are saved on disk. [From [Rap93a] © IEEE].

sion) to be used?

(c) What is the required IF passband bandwidth for this system? How is this much better than a direct pulse system with similar time resolution?

4.2 If a particular modulation provides suitable BER performance whenever $\sigma/T_s \leq 0.1$, determine the smallest symbol period T_s (and thus the greatest symbol rate) that may be sent through RF channels shown in Figure P4.2.

4.3 For the power delay profiles in Figure P4.2, estimate the 90% correlation and 50% correlation coherence bandwidths.

4.4 Approximately how large can the rms delay spread be in order for a binary modulated signal with a bit rate of 25 kbps to operate without an equalizer? What about an 8-PSK system with a bit rate of 75 kbps?

4.5 Given that the probability density function of a Rayleigh distributed envelope is given by $p(r) = \frac{r}{\sigma^2}\exp\left(\frac{-r^2}{2\sigma^2}\right)$, where σ^2 is the variance, show that the

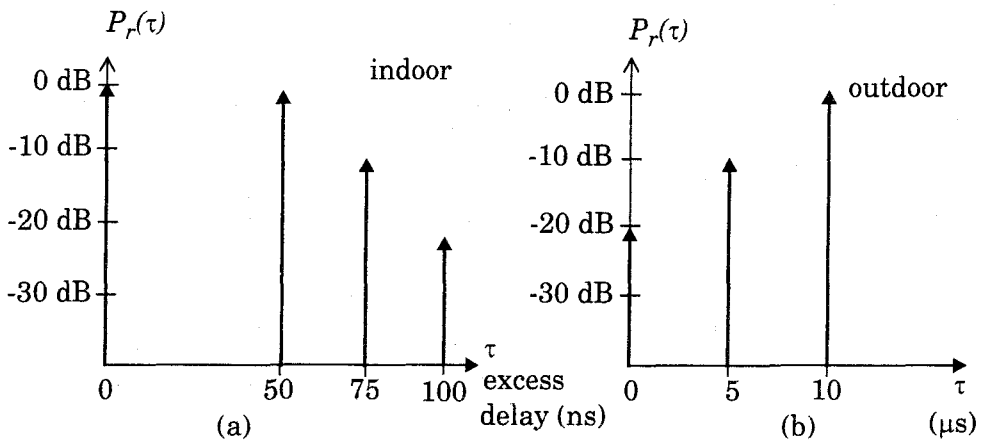

Figure P4.2: Two channel responses for Problem 4.2

cumulative distribution function is given as $p(r<R) = 1-\exp\left(\frac{-R^2}{2\sigma^2}\right)$. Find the percentage of time that a signal is 10 dB or more below the rms value for a Rayleigh fading signal.

4.6 The fading characteristics of a CW carrier in an urban area are to be measured. The following assumptions are made:
(1) The mobile receiver uses a simple vertical monopole
(2) Large-scale fading due to path loss is ignored.
(3) The mobile has no line-of-sight path to the base station.
(4) The pdf of the received signal follows a Rayleigh distribution.
(a) Derive the ratio of the desired signal level to the rms signal level that maximizes the level crossing rate. Express your answer in dB.
(b) Assuming the maximum velocity of the mobile is 50 km/hr, and the carrier frequency is 900 MHz, determine the maximum number of times the signal envelope will fade below the level found in (a) during a 1 minute test.
(c) How long, on average, will each fade in (b) last?

4.7 A vehicle receives a 900 MHz transmission while traveling at a constant velocity for 10 s. The average fade duration for a signal level 10 dB below the rms level is 1 ms. How far does the vehicle travel during the 10 s interval? How many fades does the signal undergo at the rms threshold level during a 10 s interval? Assume that the local mean remains constant during travel.

4.8 An automobile moves with velocity $v(t)$ shown in Figure P4.8. The received mobile signal experiences multipath Rayleigh fading on a 900 MHz CW carrier. What is the average crossing rate and fade duration over the 100 s interval? Assume $\rho = 0.1$ and ignore large-scale fading effects.

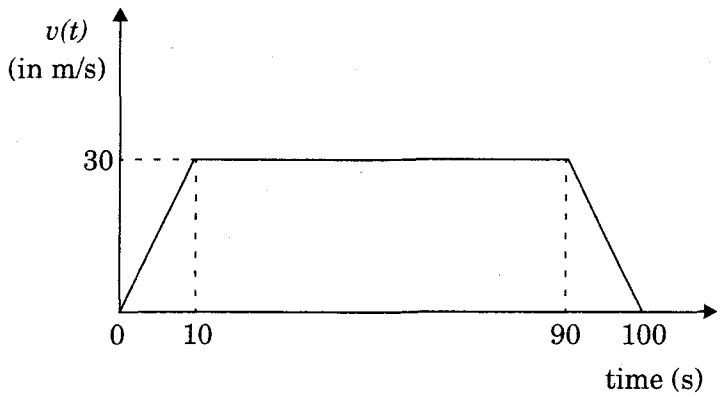

Figure P4.8 Graph of velocity of mobile.

4.9 For a mobile receiver operating at frequency of 860 MHz and moving at 100 km/hr
(a) sketch the Doppler spectrum if a CW signal is transmitted and indicate the maximum and minium frequencies
(b) calculate the level crossing rate and average fade duration if $\rho = -20$ dB.

4.10 For the following digital wireless systems, estimate the maximum rms delay spread for which no equalizer is required at the receiver (neglect channel coding, antenna diversity, or use of extremely low power levels).

System	RF Data Rate	Modulation
USDC	48.6 kbps	π/4DQPSK
GSM	270.833 kbps	GMSK
DECT	1152 kbps	GMSK

4.11 Derive the RF Doppler spectrum for a 5/8λ vertical monopole receiving a CW signal using the models by Clarke and Gans. Plot the RF Doppler spectrum and the corresponding baseband spectrum out of an envelope detector. Assume isotropic scattering and unit average received power.

4.12 Show that the magnitude (envelope) of the sum of two independent identically distributed complex (quadrature) Gaussian sources is Rayleigh distributed. Assume that the Gaussian sources are zero mean and have unit variance.

4.13 Using the method described in Chapter 4, generate a time sequence of 8192 sample values of a Rayleigh fading signal for
(a) $f_d = 20$ Hz and (b) $f_d = 200$ Hz.

4.14 Generate 100 sample functions of fading data described in Problem 4.13, and compare the simulated and theoretical values of R_{RMS}, N_R, and $\bar{\tau}$ for $\rho = 1$, 0.1, and 0.01. Do your simulations agree with theory?

4.15 Recreate the plots of the CDFs shown in Figure 4.17, starting with the pdfs for Rayleigh, Ricean, and log-normal distributions.

4.16 Plot the probability density function and the CDF for a Ricean distribution having (a) $K = 10$ dB and (b) $K = 3$ dB. The abscissa of the CDF plot should be labeled in dB relative to the median signal level for both plots. Note that the median value for a Ricean distribution changes as K changes.

4.17 Based on your answer in Problem 4.16, if the median SNR is -70 dBm, what is the likelihood that a signal greater than -80 dBm will be received in a Ricean fading channel having (a) K = 10 dB, and (b) K = 3 dB?

4.18 A local spatial average of a power delay profile is shown in Figure P4.18.

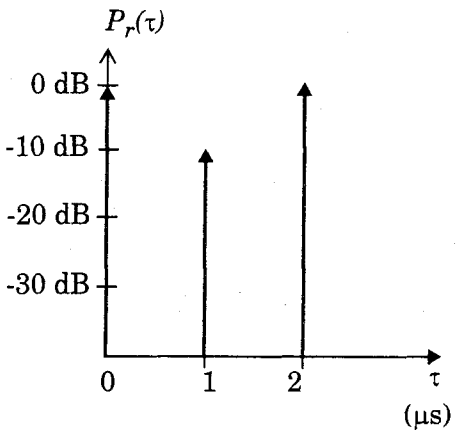

Figure P4.18. Power delay profile.

(a) Determine the rms delay spread and mean excess delay for the channel.
(b) Determine the maximum excess delay (20 dB).
(c) If the channel is to be used with a modulation that requires an equalizer whenever the symbol duration T is less than $10\sigma_\tau$, determine the maximum RF symbol rate that can be supported without requiring an equalizer.
(d) If a mobile traveling at 30 km/hr receives a signal through the channel, determine the time over which the channel appears stationary (or at least highly correlated).

4.19 A flat Rayleigh fading signal at 6 GHz is received by a mobile traveling at 80 km/hr.
(a) Determine the number of positive-going zero crossings about the rms value that occur over a 5 s interval.
(b) Determine the average duration of a fade below the rms level.
(c) Determine the average duration of a fade at a level of 20 dB below the rms value.

4.20 Using computer simulation, create a Rayleigh fading simulator that has 3 independent Rayleigh fading multipath components, each having variable multipath time delay and average power. Then convolve a random binary bit stream through your simulator and observe the time waveforms of the output stream. You may wish to use several samples for each bit (7 is a good number). Observe the effects of multipath spread as you vary the bit period and time delay of the channel.

4.21 Based on concepts taught in this chapter, propose methods that could be used by a base station to determine the vehicular speed of a mobile user. Such methods are useful for handoff algorithms.

CHAPTER 6

Equalization, Diversity, and Channel Coding

Mobile communication systems require signal processing techniques that improve the link performance in hostile mobile radio environments. As seen in Chapters 3 and 4, the mobile radio channel is particularly dynamic due to multipath fading and Doppler spread, and as shown in the latter part of Chapter 5, these effects have a strong negative impact on the bit error rate of any modulation technique. Mobile radio channel impairments cause the signal at the receiver to distort or fade significantly as compared to AWGN channels.

6.1 Introduction

Equalization, diversity, and channel coding are three techniques which can be used independently or in tandem to improve received signal quality.

Equalization compensates for *intersymbol interference* (ISI) created by multipath within time dispersive channels. As shown in Chapters 4 and 5, if the modulation bandwidth exceeds the coherence bandwidth of the radio channel, ISI occurs and modulation pulses are spread in time. An equalizer within a receiver compensates for the average range of expected channel amplitude and delay characteristics. Equalizers must be adaptive since the channel is generally unknown and time varying.

Diversity is another technique used to compensate for fading channel impairments, and is usually implemented by using two or more receiving antennas. As with an equalizer, the quality of a mobile communications link is improved without increasing the transmitted power or bandwidth. However, while equalization is used to counter the effects of time dispersion (ISI), diversity is usually employed to reduce the depth and duration of the fades experienced by

a receiver in a flat fading (narrowband) channel. Diversity techniques can be employed at both base station and mobile receivers. The most common diversity technique is called *spatial diversity,* whereby multiple antennas are strategically spaced and connected to a common receiving system. While one antenna sees a signal null, one of the other antennas may see a signal peak, and the receiver is able to select the antenna with the best signal at any time. Other diversity techniques include antenna polarization diversity, frequency diversity, and time diversity. CDMA systems often use a RAKE receiver, which provides link improvement through time diversity.

Channel coding improves mobile communication link performance by adding redundant data bits in the transmitted message. At the baseband portion of the transmitter, a channel coder maps a digital message sequence into another specific code sequence containing a greater number of bits than originally contained in the message. The coded message is then modulated for transmission in the wireless channel.

Channel coding is used by the receiver to detect or correct some (or all) of the errors introduced by the channel in a particular sequence of message bits. Because decoding is performed after the demodulation portion of the receiver, coding can be considered to be a post detection technique. The added coding bits lowers the raw data transmission rate through the channel (expands the occupied bandwidth for a particular message data rate). There are two general types of channel codes: *block codes* and *convolutional codes*. Channel coding is generally treated independently from the type of modulation used, although this has changed recently with the use of trellis coded modulation schemes that combine coding and modulation to achieve large coding gains without any bandwidth expansion.

The three techniques of equalization, diversity, and channel coding are used to improve radio link performance (i.e. to minimize the instantaneous bit error rate), but the approach, cost, complexity, and effectiveness of each technique varies widely in practical wireless communication systems.

6.2 Fundamentals of Equalization

Intersymbol interference (ISI) caused by multipath in bandlimited (frequency selective) time dispersive channels distorts the transmitted signal, causing bit errors at the receiver. ISI has been recognized as the major obstacle to high speed data transmission over mobile radio channels. Equalization is a technique used to combat intersymbol interference.

In a broad sense, the term *equalization* can be used to describe any signal processing operation that minimizes ISI [Qur85]. In radio channels, a variety of adaptive equalizers can be used to cancel interference while providing diversity [Bra70], [Mon84]. Since the mobile fading channel is random and time varying,

equalizers must track the time varying characteristics of the mobile channel, and thus are called *adaptive equalizers.*

The general operating modes of an adaptive equalizer include training and tracking. First, a known, fixed-length training sequence is sent by the transmitter so that the receiver's equalizer may average to a proper setting. The training sequence is typically a pseudorandom binary signal or a fixed, prescribed bit pattern. Immediately following this training sequence, the user data (which may or may not include coding bits) is sent, and the adaptive equalizer at the receiver utilizes a recursive algorithm to evaluate the channel and estimate filter coefficients to compensate for the channel. The training sequence is designed to permit an equalizer at the receiver to acquire the proper filter coefficients in the worst possible channel conditions so that when the training sequence is finished, the filter coefficients are near the optimal values for reception of user data. As user data are received, the adaptive algorithm of the equalizer tracks the changing channel [Hay86]. As a consequence, the adaptive equalizer is continually changing its filter characteristics over time.

The time span over which an equalizer converges is a function of the equalizer algorithm, the equalizer structure and the time rate of change of the multipath radio channel. Equalizers require periodic retraining in order to maintain effective ISI cancellation, and are commonly used in digital communication systems where user data is segmented into short time blocks. Time division multiple access (TDMA) wireless systems are particularly well suited for equalizers. As discussed in Chapter 8, TDMA systems send data in fixed-length time blocks, and the training sequence is usually sent at the beginning of a block. Each time a new data block is received, the equalizer is retrained using the same training sequence [EIA90].

An equalizer is usually implemented at baseband or at IF in a receiver. Since the baseband complex envelope expression can be used to represent bandpass waveforms [Cou93], the channel response, demodulated signal, and adaptive equalizer algorithms are usually simulated and implemented at baseband [Lo90], [Cro89].

Figure 6.1 shows a block diagram of a communication system with an adaptive equalizer in the receiver. If $x(t)$ is the original information signal, and $f(t)$ is the combined complex baseband impulse response of the transmitter, channel, and the RF/IF sections of the receiver, the signal received by the equalizer may be expressed as

$$y(t) = x(t) \otimes f^*(t) + n_b(t) \tag{6.1}$$

where $f^*(t)$ is the complex conjugate of $f(t)$, $n_b(t)$ is the baseband noise at the input of the equalizer, and $\otimes$ denotes the convolution operation. If the impulse response of the equalizer is $h_{eq}(t)$, then the output of the equalizer is

$$\hat{d}(t) = x(t) \otimes f^*(t) \otimes h_{eq}(t) + n_b(t) \otimes h_{eq}(t) \quad (6.2)$$
$$= x(t) \otimes g(t) + n_b(t) \otimes h_{eq}(t)$$

where $g(t)$ is the combined impulse response of the transmitter, channel, RF/IF sections of the receiver, and the equalizer. The complex baseband impulse response of a transversal filter equalizer is given by

$$h_{eq}(t) = \sum_n c_n \delta(t - nT) \quad (6.3)$$

where c_n are the complex filter coefficients of the equalizer. The desired output of the equalizer is *x(t)*, the original source data. Assume that $n_b(t) = 0$. Then, in order to force $\hat{d}(t) = x(t)$ in equation (6.2), $g(t)$ must be equal to

$$g(t) = f^*(t) \otimes h_{eq}(t) = \delta(t) \quad (6.4)$$

The goal of equalization is to satisfy equation (6.4). In the frequency domain, equation (6.4) can be expressed as

$$H_{eq}(f) F^*(-f) = 1 \quad (6.5)$$

where $H_{eq}(f)$ and $F(f)$ are Fourier transforms of $h_{eq}(t)$ and *f(t)*, respectively.

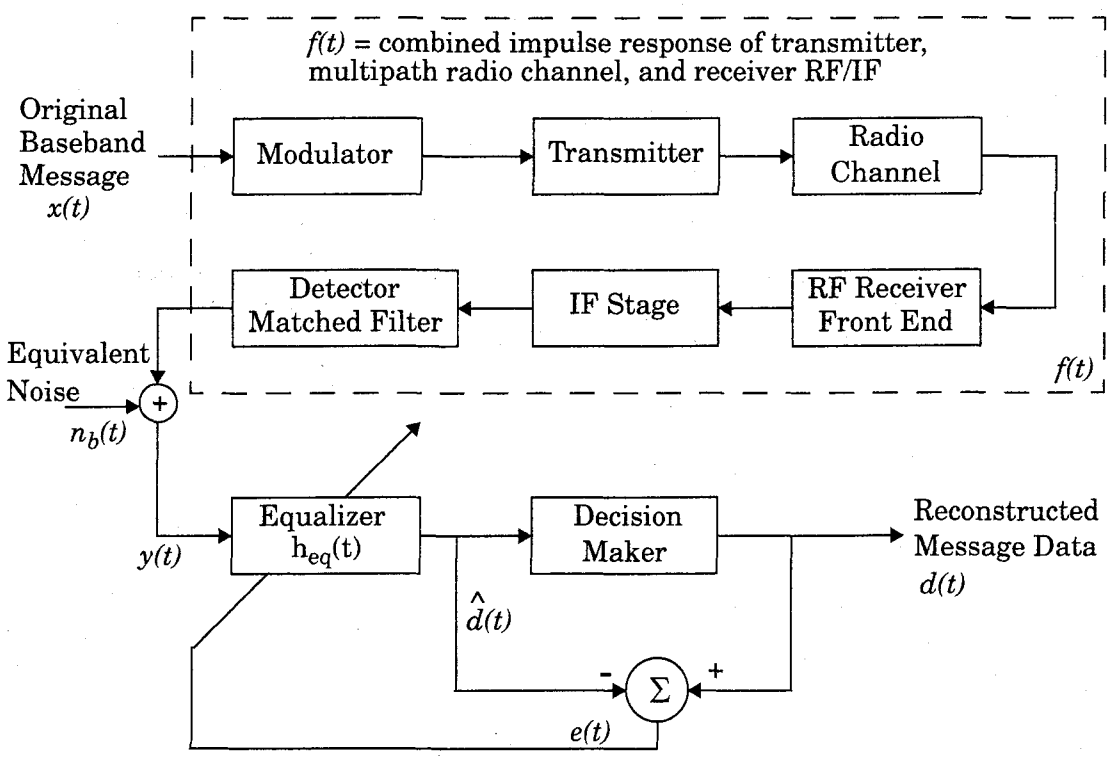

Figure 6.1
Block diagram of a simplified communications system using an adaptive equalizer at the receiver.

Equation (6.5) indicates that an equalizer is actually an inverse filter of the channel. If the channel is frequency selective, the equalizer enhances the fre-

quency components with small amplitudes and attenuates the strong frequencies in the received frequency spectrum in order to provide a flat, composite, received frequency response and linear phase response. For a time-varying channel, an adaptive equalizer is designed to track the channel variations so that equation (6.5) is approximately satisfied.

6.3 A Generic Adaptive Equalizer

An adaptive equalizer is a time-varying filter which must constantly be returned. The basic structure of an adaptive equalizer is shown in Figure 6.2, where the subscript k is used to denote a discrete time index (in section 6.4, another notation is introduced to represent discrete time events — both notations have exactly the same meaning).

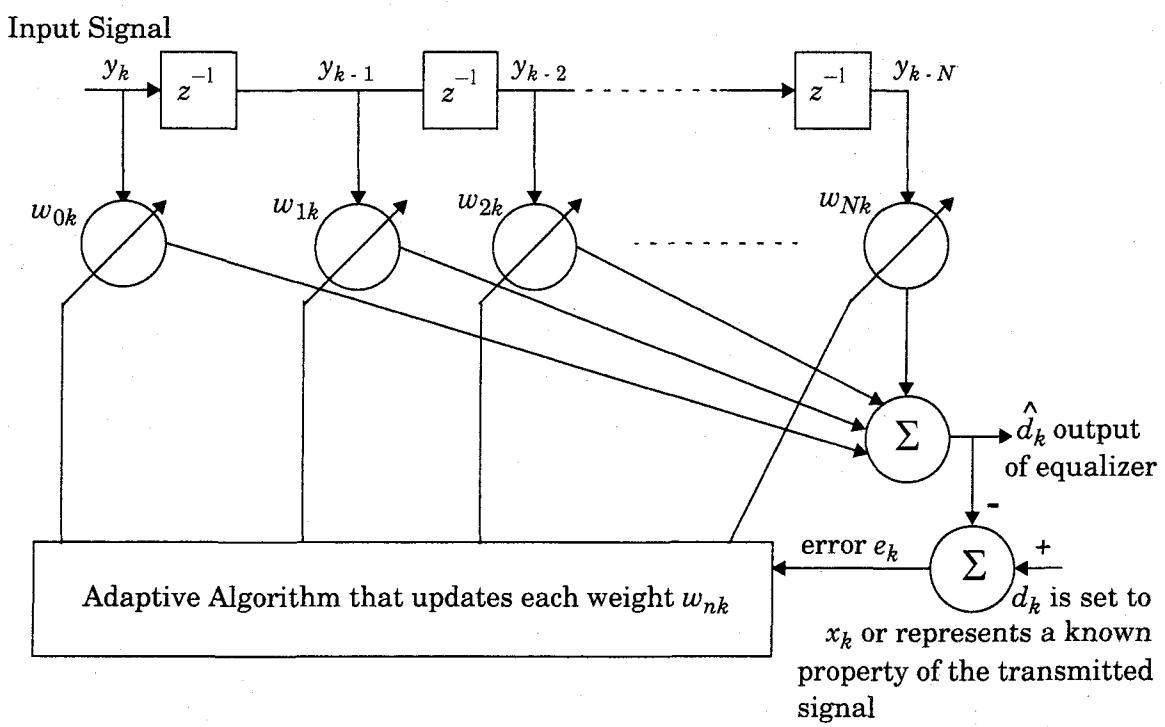

Figure 6.2
A basic linear equalizer during training.

Notice in Figure 6.2 that there is a single input y_k at any time instant. The value of y_k depends upon the instantaneous state of the radio channel and the specific value of the noise (see Figure 6.1). As such, y_k is a random process. The adaptive equalizer structure shown above is called a *transversal filter*, and in this case has N delay elements, $N+1$ taps, and $N+1$ tunable complex multipliers, called *weights*. The weights of the filter are described by their physical location in the delay line structure, and have a second subscript, k, to explicitly show they vary with time. These weights are updated continuously by the adaptive

algorithm, either on a sample by sample basis (i.e., whenever k is incremented by 1) or on a block by block basis (i.e., whenever a specified number of samples have been clocked into the equalizer).

The adaptive algorithm is controlled by the error signal e_k. This error signal is derived by comparing the output of the equalizer, $\hat{d}_k$, with some signal d_k which is either an exact scaled replica of the transmitted signal x_k or which represents a known property of the transmitted signal. The adaptive algorithm uses e_k to minimize a *cost function* and updates the equalizer weights in a manner that iteratively reduces the cost function. For example, the least mean squares (LMS) algorithm searches for the optimum or near-optimum filter weights by performing the following iterative operation:

$$\text{New weights} = \text{Previous weights} + (\text{constant}) \times (\text{Previous error}) \times (\text{Current error}) \quad (6.6.a)$$

where

$$\text{Previous error} = \text{Previous desired output} - \text{Previous actual output} \quad (6.6.b)$$

and the constant may be adjusted by the algorithm to control the variation between filter weights on successive iterations. This process is repeated rapidly in a programming loop while the equalizer attempts to *converge*, and many techniques (such as gradient or steepest decent algorithms) may be used to minimize the error. Upon reaching convergence, the adaptive algorithm freezes the filter weights until the error signal exceeds an acceptable level or until a new training sequence is sent.

Based on classical equalization theory [Wid85], [Qur85], the most common cost function is the mean square error (MSE) between the desired signal and the output of the equalizer. The MSE is denoted by $E[e(k)e^*(k)]$, and when a replica of the transmitted signal is required at the output of the equalizer (i.e., when d_k is set equal to x_k and is known *a priori*), a known *training sequence* must be periodically transmitted. By detecting the training sequence, the adaptive algorithm in the receiver is able to compute and minimize the cost function by driving the tap weights until the next training sequence is sent.

A more recent class of adaptive algorithms are able to exploit characteristics of the transmitted signal and do not require training sequences. These modern algorithms are able to acquire equalization through property restoral techniques of the transmitted signal, and are called *blind algorithms* because they provide equalizer convergence without burdening the transmitter with training overhead. These techniques include algorithms such as the *constant modulus algorithm* (CMA) and the *spectral coherence restoral algorithm* (SCORE). CMA is used for constant envelope modulation, and forces the equalizer weights to maintain a constant envelope on the received signal [Tre83], whereas SCORE exploits spectral redundancy or cyclostationarity in the transmitted signal [Gar91]. Blind algorithms are not described in this text, but are becoming important for wireless applications.

To study the adaptive equalizer of Figure 6.2, it is helpful to use vector and matrix algebra. Define the input signal to the equalizer as a vector $\boldsymbol{y}_k$ where

$$\boldsymbol{y}_k = \begin{bmatrix} y_k & y_{k-1} & y_{k-2} & \cdots & y_{k-N} \end{bmatrix}^T \tag{6.7}$$

It should be clear that the output of the adaptive equalizer is a scaler given by

$$\hat{d}_k = \sum_{n=0}^{N} w_{nk} y_{k-n} \tag{6.8}$$

and following equation (6.7) a weight vector can be written as

$$\boldsymbol{w}_k = \begin{bmatrix} w_{0k} & w_{1k} & w_{2k} & \cdots & w_{Nk} \end{bmatrix}^T \tag{6.9}$$

Using (6.7) and (6.9), (6.8) may be written in vector notation as

$$\hat{d}_k = \boldsymbol{y}_k^T \boldsymbol{w}_k = \boldsymbol{w}_k^T \boldsymbol{y}_k \tag{6.10}$$

It follows that when the desired equalizer output is known (i.e., $d_k = x_k$), the error signal e_k is given by

$$e_k = d_k - \hat{d}_k = x_k - \hat{d}_k \tag{6.11}$$

and from (6.10)

$$e_k = x_k - \boldsymbol{y}_k^T \boldsymbol{w}_k = x_k - \boldsymbol{w}_k^T \boldsymbol{y}_k \tag{6.12}$$

To compute the mean square error $|e_k|^2$ at time instant k, equation (6.12) is squared to obtain

$$|e_k|^2 = x_k^2 + \boldsymbol{w}_k^T \boldsymbol{y}_k \boldsymbol{y}_k^T \boldsymbol{w}_k - 2x_k \boldsymbol{y}_k^T \boldsymbol{w}_k \tag{6.13}$$

Taking the expected value of $|e_k|^2$ over k (which in practice amounts to computing a time average) yields

$$E\left[|e_k|^2\right] = E\left[x_k^2\right] + \boldsymbol{w}_k^T E\left[\boldsymbol{y}_k \boldsymbol{y}_k^T\right] \boldsymbol{w}_k - 2E\left[x_k \boldsymbol{y}_k^T\right] \boldsymbol{w}_k \tag{6.14}$$

Notice that the filter weights $\boldsymbol{w}_k$ are not included in the time average since, for convenience, it is assumed that they have converged to the optimum value and are not varying with time.

Equation (6.14) would be trivial to simplify if x_k and y_k were independent. However, this is not true in general since the input vector should be correlated with the desired output of the equalizer (otherwise, the equalizer would have a very difficult time extracting the desired signal). Instead, the cross correlation vector $\boldsymbol{p}$ between the desired response and the input signal is defined as

$$\boldsymbol{p} = E\left[x_k \boldsymbol{y}_k\right] = E\begin{bmatrix} x_k y_k & x_k y_{k-1} & x_k y_{k-2} & \cdots & x_k y_{k-N} \end{bmatrix}^T \tag{6.15}$$

and the *input correlation matrix* is defined as the $(N+1) \times (N+1)$ square matrix $\boldsymbol{R}$ where

$$\boldsymbol{R} = E[\boldsymbol{y}_k \boldsymbol{y}_k^*] = E\begin{bmatrix} y_k^2 & y_k y_{k-1} & y_k y_{k-2} & \cdots & y_k y_{k-N} \\ y_{k-1} y_k & y_{k-1}^2 & y_{k-1} y_{k-2} & \cdots & y_{k-1} y_{k-N} \\ \cdots & \cdots & \cdots & \cdots & \cdots \\ y_{k-N} y_k & y_{k-N} y_{k-1} & y_{k-N} y_{k-2} & \cdots & y_{k-N}^2 \end{bmatrix} \tag{6.16}$$

The matrix $\boldsymbol{R}$ is sometimes called the *input covariance matrix*. The major diagonal of $\boldsymbol{R}$ contains the mean square values of each input sample, and the cross terms specify the autocorrelation terms resulting from delayed samples of the input signal.

If x_k and $\boldsymbol{y}_k$ are stationary, then the elements in $\boldsymbol{R}$ and $\boldsymbol{p}$ are second order statistics which do not vary with time. Using equations (6.15) and (6.16), (6.14) may be rewritten as

$$\text{Mean Square Error} \equiv \xi = E\left[x_k^2\right] + \boldsymbol{w}^T \boldsymbol{R} \boldsymbol{w} - 2\boldsymbol{p}^T \boldsymbol{w} \tag{6.17}$$

By minimizing equation (6.17) in terms of the weight vector $\boldsymbol{w}_k$, it becomes possible to adaptively tune the equalizer to provide a flat spectral response (minimal ISI) in the received signal. This is due to the fact that when the input signal $\boldsymbol{y}_k$ and the desired response x_k are stationary, the mean square error (MSE) is quadratic on $\boldsymbol{w}_k$, and minimizing the MSE leads to optimal solutions for $\boldsymbol{w}_k$.

Example 6.1

The MSE of equation (6.17) is a multidimensional function. When two tap weights are used in an equalizer, then the MSE function is a bowl-shaped paraboloid where MSE is plotted on the vertical axis and weights w_0 and w_1 are plotted on the horizontal axes. If more than two tap-weights are used in the equalizer, then the error function is a hyperparaboloid. In all cases the error function is concave upward, which implies that a minimum may be found [Wid85].

To determine the minimum MSE (MMSE), the gradient of (6.17) can be used. As long as $\boldsymbol{R}$ is nonsingular (has an inverse), the MMSE occurs when $\boldsymbol{w}_k$ are such that the gradient is zero. The gradient of ξ is defined as

$$\nabla \equiv \frac{\partial \xi}{\partial \boldsymbol{w}} = \left[\frac{\partial \xi}{\partial w_0} \frac{\partial \xi}{\partial w_1} \cdots \frac{\partial \xi}{\partial w_N}\right]^T \tag{E6.1}$$

By expanding (6.17) and differentiating with respect to each signal in the weight vector, it can be shown that equation (E6.1) yields

$$\nabla = 2\boldsymbol{R}\boldsymbol{w} - 2\boldsymbol{p} \tag{E6.2}$$

Setting $\nabla = 0$ in (E6.2), the optimum weight vector $\hat{\boldsymbol{w}}$ for MMSE is given by

$$\hat{\boldsymbol{w}} = \boldsymbol{R}^{-1}\boldsymbol{p} \tag{E6.3}$$

Example 6.2

Four matrix algebra rules are useful in the study of adaptive equalizers [Wid85]:

1. Differentiation of $\boldsymbol{w}^T\boldsymbol{R}\boldsymbol{w}$ can be differentiated as the product $(\boldsymbol{w}^T)\,(\boldsymbol{R}\boldsymbol{w})$.

2. For any square matrix, $\boldsymbol{A}\boldsymbol{A}^{-1} = \boldsymbol{I}$.

3. For any matrix product, $(\boldsymbol{A}\boldsymbol{B})^T = \boldsymbol{B}^T\boldsymbol{A}^T$.

4. For any symmetric matrix, $\boldsymbol{A}^T = \boldsymbol{A}$ and $(\boldsymbol{A}^{-1})^T = \boldsymbol{A}^{-1}$.

Using (E6.3) to substitute $\hat{\boldsymbol{w}}$ for $\boldsymbol{w}$ in equation (6.17), and using the above rules, ξ_{min} is found to be

$$\xi_{min} = \text{MMSE} = E\left[x_k^2\right] - \boldsymbol{p}^T\boldsymbol{R}^{-1}\boldsymbol{p} = E\left[x_k^2\right] - \boldsymbol{p}^T\hat{\boldsymbol{w}} \tag{E6.4}$$

Equation (E6.4) solves the MMSE for optimum weights.

6.4 Equalizers in a Communications Receiver

The previous section demonstrated how a generic adaptive equalizer works and defined common notation for algorithm design and analysis. This section describes how the equalizer fits into the wireless communications link.

Figure 6.1 shows that the received signal includes channel noise. Because the noise $n_b(t)$ is present, an equalizer is unable to achieve perfect performance. Thus there is always some residual ISI and some small tracking error. Noise makes equation (6.4) hard to realize in practice. Therefore, the instantaneous combined frequency response will not always be flat, resulting in some finite *prediction error.* The prediction error of the equalizer is defined in equation (6.19).

Because adaptive equalizers are implemented using digital logic, it is most convenient to represent all time signals in discrete form. Let T represent some increment of time between successive observations of signal states. Letting $t = t_n$ where n is an integer that represents time $t_n = nT$, time waveforms may be equivalently expressed as a sequence on n in the discrete domain. Using this notation, equation (6.2) may be expressed as

$$\hat{d}(n) = x(n) \otimes g(n) + n_b(n) \otimes h_{eq}(n) \tag{6.18}$$

The prediction error is

$$e(n) = d(n) - \hat{d}(n) = d(n) - [x(n) \otimes g(n) + n_b(n) \otimes h_{eq}(n)] \tag{6.19}$$

The *mean squared error* $E\left[|e(n)|^2\right]$ is one of the most important measures of how well an equalizer works. $E\left[|e(n)|^2\right]$ is the expected value (ensemble average) of the squared prediction error $|e(n)|^2$, but time averaging can be used if $e(n)$ is ergodic. In practice, ergodicity is impossible to prove, and algorithms are developed and implemented using time averages instead of ensemble aver-

ages. This proves to be highly effective, and in general, better equalizers provide smaller values of $E[|e(n)|^2]$.

Minimizing the mean square error tends to reduce the bit error rate. This can be understood with a simple intuitive explanation. Suppose $e(n)$ is Gaussian distributed with zero mean. Then $E[|e(n)|^2]$ is the variance (or the power) of the error signal. If the variance is minimized then there is less chance of perturbing the output signal *d(n)*. Thus the decision device is likely to detect *d(n)* as the transmitted signal *x(n)* (see Figure 6.1). Consequently, there is a smaller probability of error when $E[|e(n)|^2]$ is minimized. For wireless communication links, it would be best to minimize the instantaneous probability of error (P_e) instead of the mean squared error, but minimizing P_e generally results in nonlinear equations, which are much more difficult to solve in real-time than the linear equations (6.1) - (6.19) [Pro89].

6.5 Survey of Equalization Techniques

Equalization techniques can be subdivided into two general categories — linear and nonlinear equalization. These categories are determined from how the output of an adaptive equalizer is used for subsequent control (feedback) of the equalizer. In general, the analog signal $\hat{d}(t)$ is processed by the decision making device in the receiver. The decision maker determines the value of the digital data bit being received and applies a slicing or thresholding operation (a nonlinear operation) in order to determine the value of *d(t)* (see Figure 6.1). If *d(t)* is not used in the feedback path to adapt the equalizer, the equalization is *linear*. On the other hand, if *d(t)* is fed back to change the subsequent outputs of the equalizer, the equalization is *nonlinear*. Many filter structures are used to implement linear and nonlinear equalizers. Further, for each structure, there are numerous algorithms used to adapt the equalizer. Figure 6.3 provides a general categorization of the equalization techniques according to the types, structures, and algorithms used.

The most common equalizer structure is a *linear transversal equalizer* (LTE). A linear transversal filter is made up of tapped delay lines, with the tappings spaced a symbol period (T_s) apart, as shown in Figure 6.4. Assuming that the delay elements have unity gain and delay T_s, the transfer function of a linear transversal equalizer can be written as a function of the delay operator $\exp(-j\omega T_s)$ or z^{-1}. The simplest LTE uses only feedforward taps, and the transfer function of the equalizer filter is a polynomial in z^{-1}. This filter has many zeroes but poles only at $z = 0$, and is called a *finite impulse response* (FIR) filter, or simply a transversal filter. If the equalizer has both feedforward and feedback taps, its transfer function is a rational function of z^{-1}, and is called an *infinite impulse response* (IIR) filter with poles and zeros. Figure 6.5 shows a tapped delay line filter with both feedforward and feedback taps. Since IIR filters tend to

be unstable when used in channels where the strongest pulse arrives after an echo pulse (i.e., leading echoes), they are rarely used.

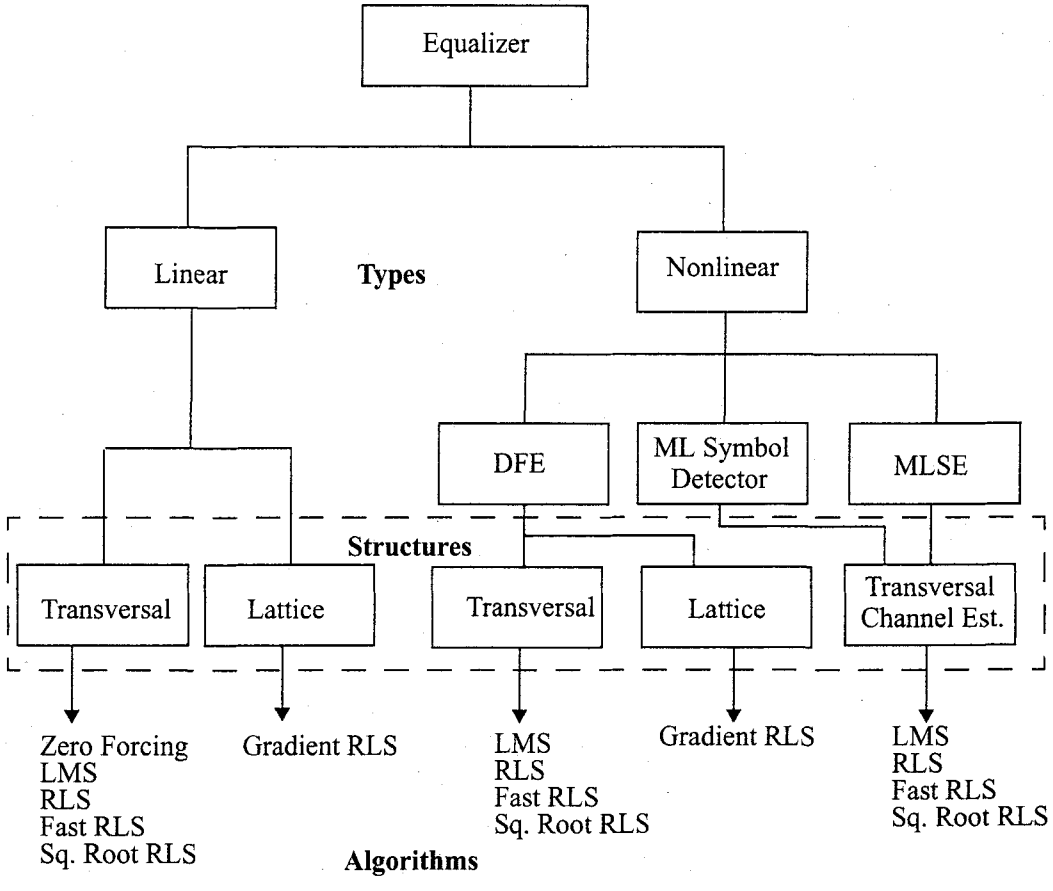

Figure 6.3
Classification of equalizers.

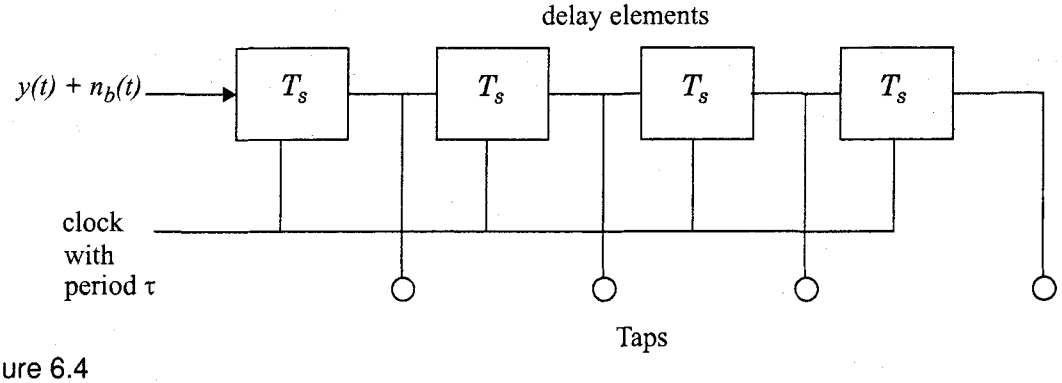

Figure 6.4
Basic linear transversal equalizer structure.

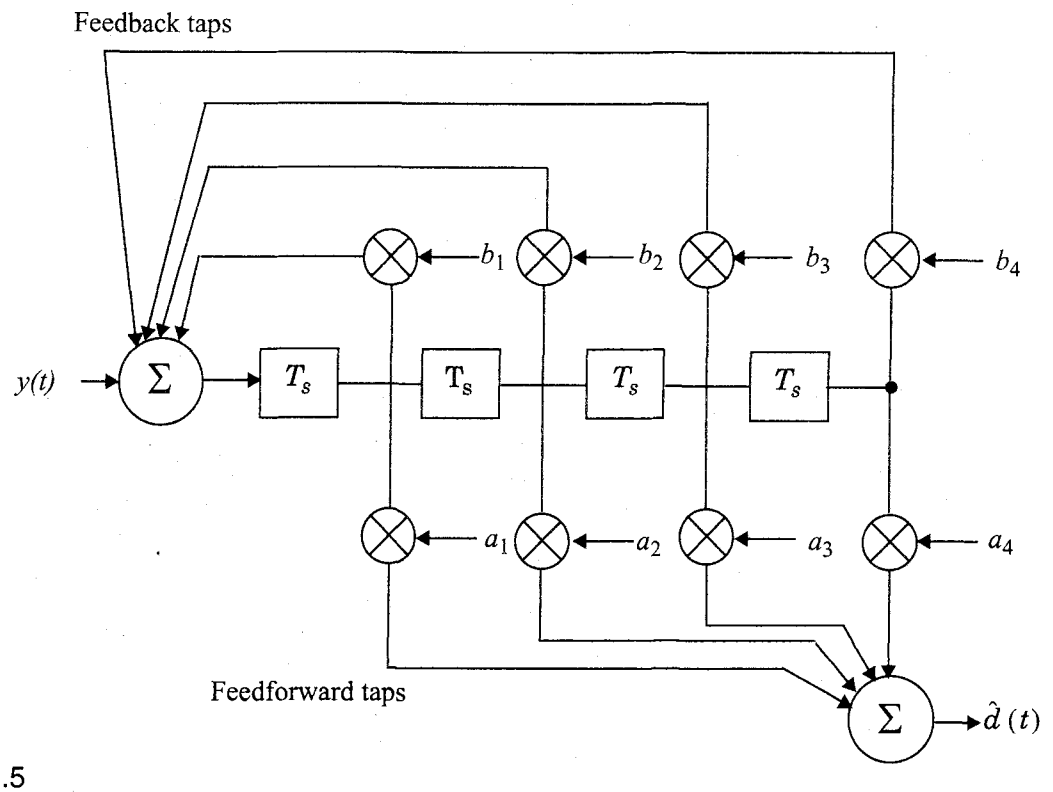

Figure 6.5
Tapped delay line filter with both feedforward and feedback taps.

6.6 Linear Equalizers

As mentioned in section 6.5, a linear equalizer can be implemented as an FIR filter, otherwise known as the transversal filter. This type of equalizer is the simplest type available. In such an equalizer, the current and past values of the received signal are linearly weighted by the filter coefficient and summed to produce the output, as shown in Figure 6.6. If the delays and the tap gains are analog, the continuous output of the equalizer is sampled at the symbol rate and the samples are applied to the decision device. The implementation is, however, usually carried out in the digital domain where the samples of the received signal are stored in a shift register. The output of this transversal filter before decision making (threshold detection) is [Kor85]

$$\hat{d}_k = \sum_{n=-N_1}^{N_2} (c_n^*) y_{k-n} \tag{6.20}$$

where c_n^* represents the complex filter coefficients or tap weights, $\hat{d}_k$ is the output at time index k, y_i is the input received signal at time $t_0 + iT$, t_0 is the equalizer starting time, and $N = N_1 + N_2 + 1$ is the number of taps. The values N_1 and N_2 denote the number of taps used in the forward and reverse portions

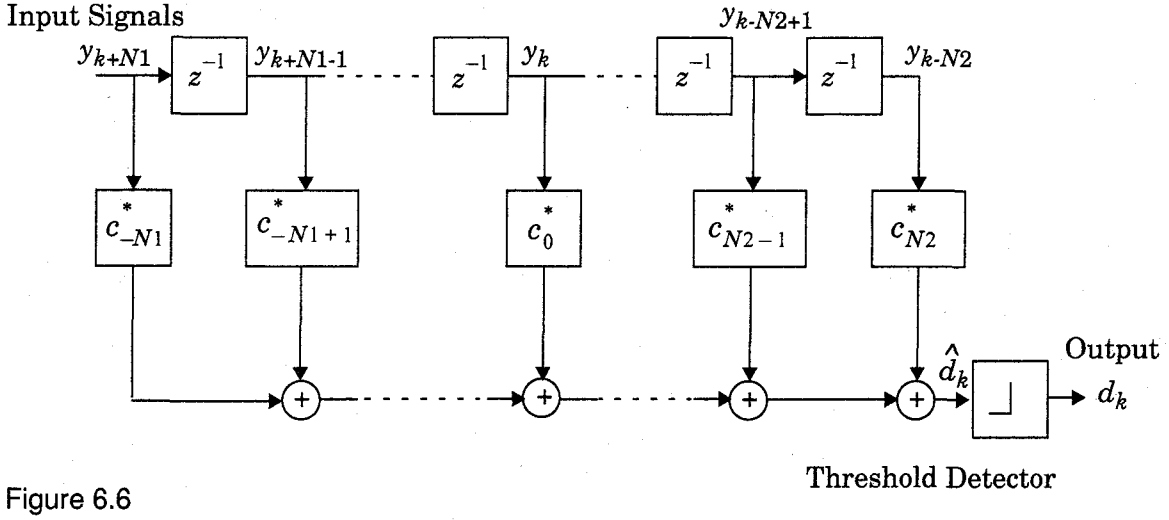

Figure 6.6
Structure of a linear transversal equalizer.

of the equalizer, respectively. The minimum mean squared error $E[|e(n)|^2]$ that a linear transversal equalizer can achieve is [Pro89]

$$E[|e(n)|^2] = \frac{T}{2\pi}\int_{-\pi/T}^{\pi/T}\frac{N_0}{|F(e^{j\omega T})|^2 + N_0}d\omega \tag{6.21}$$

where $F(e^{j\omega T})$ is the frequency response of the channel, and N_0 is the noise spectral density.

The linear equalizer can also be implemented as a *lattice filter*, whose structure is shown in Figure 6.7. The input signal y_k is transformed into a set of N intermediate forward and backward error signals, $f_n(k)$ and $b_n(k)$ respectively, which are used as inputs to the tap multipliers and are used to calculate the updated coefficients. Each stage of the lattice is then characterized by the following recursive equations [Bin88]:

$$f_1(k) = b_1(k) = y(k) \tag{6.22}$$

$$f_n(k) = y(k) - \sum_{i=1}^{n} K_i y(k-i) = f_{n-1}(k) + K_{n-1}(k)\, b_{n-1}(k-1) \tag{6.23}$$

$$b_n(k) = y(k-n) - \sum_{i=1}^{n} K_i y(k-n+i) \tag{6.24}$$

$$= b_{n-1}(k-1) + K_{n-1}(k) f_{n-1}(k)$$

where $K_n(k)$ is the reflection coefficient for the nth stage of the lattice. The backward error signals, b_n, are then used as inputs to the tap weights, and the output of the equalizer is given by

$$\hat{d}_k = \sum_{n=1}^{N} c_n(k)\, b_n(k) \tag{6.25}$$

Two main advantages of the lattice equalizer is its numerical stability and faster convergence. Also, the unique structure of the lattice filter allows the dynamic assignment of the most effective length of the lattice equalizer. Hence, if the channel is not very time dispersive, only a fraction of the stages are used. When the channel becomes more time dispersive, the length of the equalizer can be increased by the algorithm without stopping the operation of the equalizer. The structure of a lattice equalizer, however, is more complicated than a linear transversal equalizer.

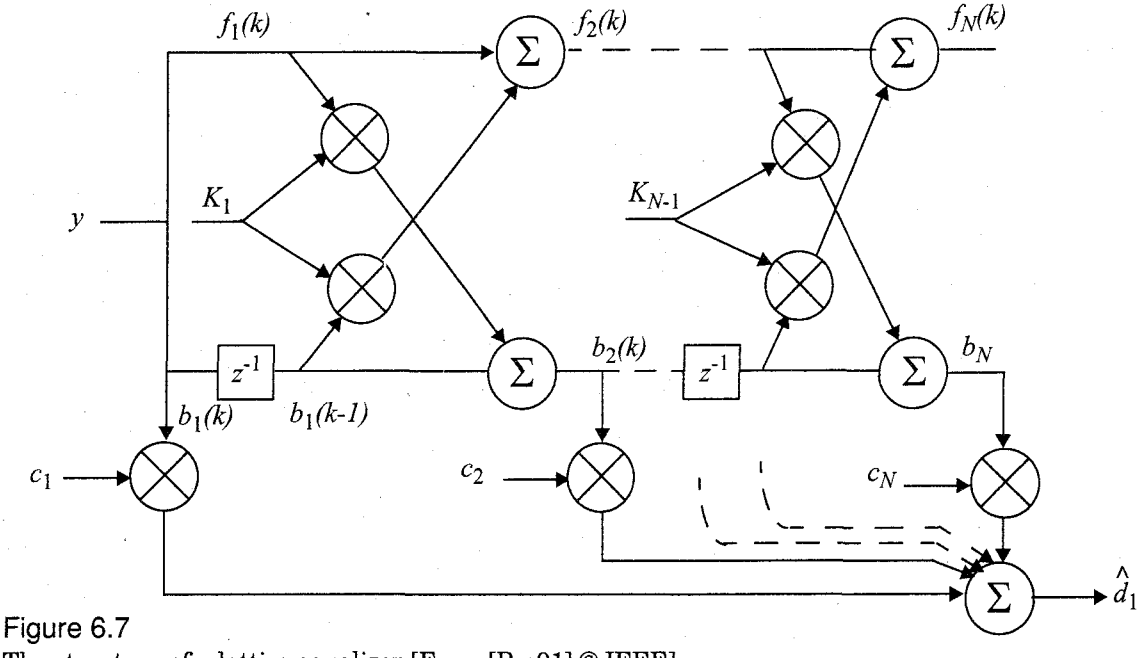

Figure 6.7
The structure of a lattice equalizer [From [Pro91] © IEEE].

6.7 Nonlinear Equalization

Nonlinear equalizers are used in applications where the channel distortion is too severe for a linear equalizer to handle. Linear equalizers do not perform well on channels which have deep spectral nulls in the passband. In an attempt to compensate for the distortion, the linear equalizer places too much gain in the vicinity of the spectral null, thereby enhancing the noise present in those frequencies.

Three very effective nonlinear methods have been developed which offer improvements over linear equalization techniques. These are [Pro91]:

1. Decision Feedback Equalization (DFE)
2. Maximum Likelihood Symbol Detection
3. Maximum Likelihood Sequence Estimation (MLSE)

6.7.1 Decision Feedback Equalization (DFE)

The basic idea behind decision feedback equalization is that once an information symbol has been detected and decided upon, the ISI that it induces on future symbols can be estimated and subtracted out before detection of subsequent symbols [Pro89]. The DFE can be realized in either the direct transversal form or as a lattice filter. The direct form is shown in Figure 6.8. It consists of a feedforward filter (FFF) and a feedback filter (FBF). The FBF is driven by decisions on the output of the detector, and its coefficients can be adjusted to cancel the ISI on the current symbol from past detected symbols. The equalizer has $N_1 + N_2 + 1$ taps in the feed forward filter and N_3 taps in the feedback filter, and its output can be expressed as:

$$\hat{d}_k = \sum_{n=-N_1}^{N_2} c_n^* y_{k-n} + \sum_{i=1}^{N_3} F_i d_{k-i} \tag{6.26}$$

where c_n^* and y_n are tap gains and the inputs, respectively, to the forward filter, F_i^* are tap gains for the feedback filter, and $d_i (i < k)$ is the previous decision made on the detected signal. That is, once $\hat{d}_k$ is obtained using equation (6.26), d_k is decided from it. Then, d_k along with previous decisions $d_{k-1}, d_{k-2}, \ldots$ are fed back into the equalizer, and $\hat{d}_{k+1}$ is obtained using equation (6.26).

The minimum mean squared error a DFE can achieve is [Pro89]

$$E\left[|e(n)|^2\right]_{min} = \exp\left\{\frac{T}{2\pi}\int_{-\pi/T}^{\pi/T} \ln\left[\frac{N_0}{\left|F(e^{j\omega T})\right|^2 + N_0}\right] d\omega\right\} \tag{6.27}$$

It can be shown that the minimum MSE for a DFE in equation (6.27) is always smaller than that of an LTE in equation (6.21) unless $\left|F(e^{j\omega T})\right|$ is a constant (i.e, when adaptive equalization is not needed) [Pro89]. If there are nulls in $\left|F(e^{j\omega T})\right|$, a DFE has significantly smaller minimum MSE than an LTE. Therefore, an LTE is well behaved when the channel spectrum is comparatively flat, but if the channel is severely distorted or exhibits nulls in the spectrum, the performance of an LTE deteriorates and the mean squared error of a DFE is much better than a LTE. Also, an LTE has difficulty equalizing a nonminimum phase channel, where the strongest energy arrives after the first arriving signal component. Thus, a DFE is more appropriate for severely distorted wireless channels.

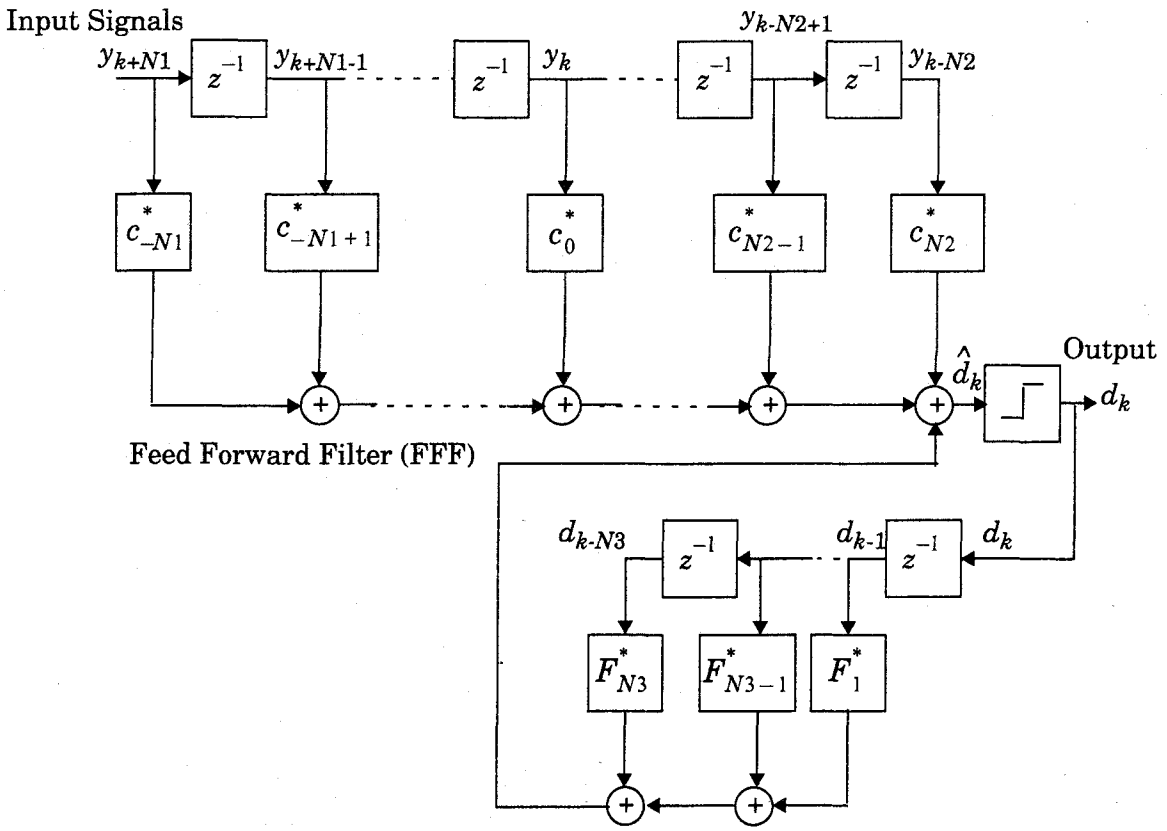

Figure 6.8
Decision feedback equalizer (DFE).

The lattice implementation of the DFE is equivalent to a transversal DFE having a feed forward filter of length N_1 and a feedback filter of length N_2, where $N_1 > N_2$.

Another form of DFE proposed by Belfiore and Park [Bel79] is called a *predictive DFE*, and is shown in Figure 6.9. It also consists of a feed forward filter (FFF) as in the conventional DFE. However, the feedback filter (FBF) is driven by an input sequence formed by the difference of the output of the detector and the output of the feed forward filter. Hence, the FBF here is called a *noise predictor* because it predicts the noise and the residual ISI contained in the signal at the FFF output and subtracts from it the detector output after some feedback delay. The predictive DFE performs as well as the conventional DFE as the limit in the number of taps in the FFF and the FBF approach infinity. The FBF in the predictive DFE can also be realized as a lattice structure [Zho90]. The RLS lattice algorithm (discussed in Section 6.8) can be used in this case to yield fast convergence.

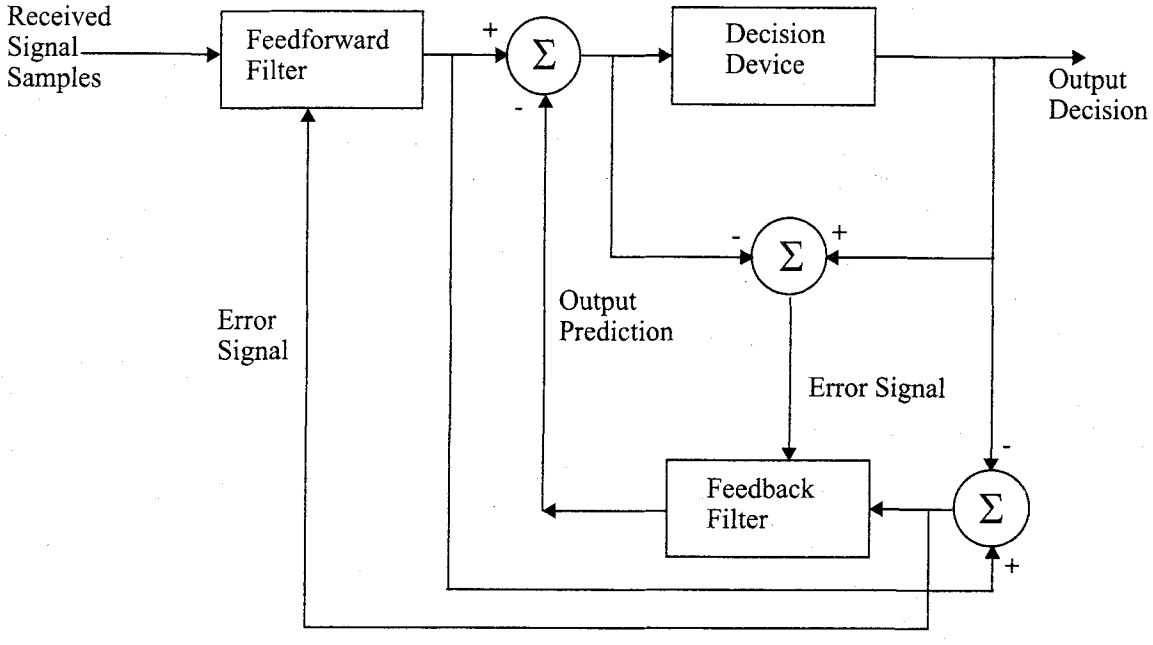

Figure 6.9
Predictive decision feedback equalizer.

6.7.2 Maximum Likelihood Sequence Estimation (MLSE) Equalizer

The MSE-based linear equalizers described previously are optimum with respect to the criterion of minimum probability of symbol error when the channel does not introduce any amplitude distortion. Yet this is precisely the condition in which an equalizer is needed for a mobile communications link. This limitation on MSE-based equalizers led researchers to investigate optimum or nearly optimum nonlinear structures. These equalizers use various forms of the classical maximum likelihood receiver structure. Using a channel impulse response simulator within the algorithm, the MLSE tests all possible data sequences (rather than decoding each received symbol by itself), and chooses the data sequence with the maximum probability as the output. An MLSE usually has a large computational requirement, especially when the delay spread of the channel is large. Using the MLSE as an equalizer was first proposed by Forney [For78] in which he set up a basic MLSE estimator structure and implemented it with the Viterbi algorithm. This algorithm, described in Section 6.15, was recognized to be a maximum likelihood sequence estimator (MLSE) of the state sequences of a finite state Markov process observed in memoryless noise. It has recently been implemented successfully for equalizers in mobile radio channels.

The MLSE can be viewed as a problem in estimating the state of a discrete-time finite state machine, which in this case happens to be the radio channel with coefficients f_k, and with a channel state which at any instant of time is estimated by the receiver based on the L most recent input samples. Thus the chan-

nel has M^L states, where M is the size of the symbol alphabet of the modulation. That is, an M^L trellis is used by the receiver to model the channel over time. The Viterbi algorithm then tracks the state of the channel by the paths through the trellis and gives at stage k a rank ordering of the M^L most probable sequences terminating in the most recent L symbols.

The block diagram of a MLSE receiver based on the DFE is shown in Figure 6.10. The MLSE is optimal in the sense that it minimizes the probability of a sequence error. The MLSE requires knowledge of the channel characteristics in order to compute the metrics for making decisions. The MLSE also requires knowledge of the statistical distribution of the noise corrupting the signal. Thus, the probability distribution of the noise determines the form of the metric for optimum demodulation of the received signal. Notice that the matched filter operates on the continuous time signal, whereas the MLSE and channel estimator rely on discretized (nonlinear) samples.

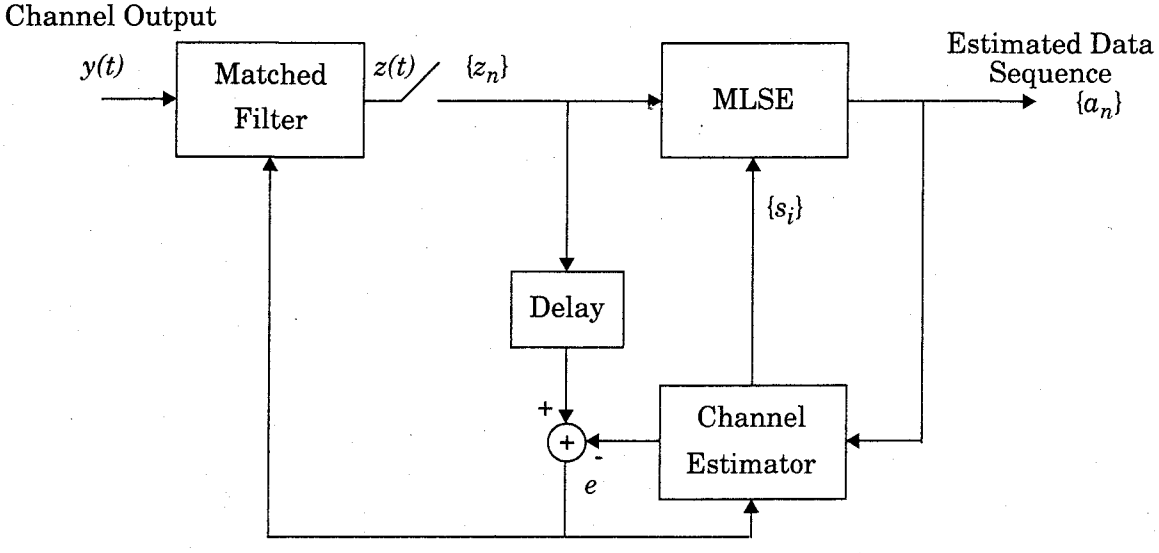

Figure 6.10
The structure of a maximum likelihood sequence estimator (MLSE) with an adaptive matched filter.

6.8 Algorithms for Adaptive Equalization

Since an adaptive equalizer compensates for an unknown and time-varying channel, it requires a specific algorithm to update the equalizer coefficients and track the channel variations. A wide range of algorithms exist to adapt the filter coefficients. The development of adaptive algorithms is a complex undertaking, and it is beyond the scope of this text to delve into great detail on how this is done. Excellent references exist which treat algorithm development [Wid85], [Hay86], [Pro91]. This section describes some practical issues regarding equalizer algorithm design, and outlines three of the basic algorithms for adaptive equalization. Though the algorithms detailed in this section are derived for the

linear, transversal equalizer, they can be extended to other equalizer structures, including nonlinear equalizers.

The performance of an algorithm is determined by various factors which include:

- **Rate of convergence** — This is defined as the number of iterations required for the algorithm, in response to stationary inputs, to converge close enough to the optimum solution. A fast rate of convergence allows the algorithm to adapt rapidly to a stationary environment of unknown statistics. Furthermore, it enables the algorithm to track statistical variations when operating in a nonstationary environment.
- **Misadjustment** — For an algorithm of interest, this parameter provides a quantitative measure of the amount by which the final value of the mean square error, averaged over an ensemble of adaptive filters, deviates from the optimal minimum mean square error.
- **Computational complexity** — This is the number of operations required to make one complete iteration of the algorithm.
- **Numerical properties** — When an algorithm is implemented numerically, inaccuracies are produced due to round-off noise and representation errors in the computer. These kinds of errors influence the stability of the algorithm.

In practice, the cost of the computing platform, the power budget, and the radio propagation characteristics dominate the choice of an equalizer structure and its algorithm. In portable radio applications, battery drain at the subscriber unit is a paramount consideration, as customer talk time needs to be maximized. Equalizers are implemented only if they can provide sufficient link improvement to justify the cost and power burden.

The radio channel characteristics and intended use of the subscriber equipment is also key. The speed of the mobile unit determines the channel fading rate and the Doppler spread, which is directly related to the coherence time of the channel (see Chapter 4). The choice of algorithm, and its corresponding rate of convergence, depends on the channel data rate and coherence time.

The maximum expected time delay spread of the channel dictates the number of taps used in the equalizer design. An equalizer can only equalize over delay intervals less than or equal to the maximum delay within the filter structure. For example, if each delay element in an equalizer (such as the ones shown in Figure 6.2 — Figure 6.8) offers a 10 microsecond delay, and 4 delay elements are used to provide a 5 tap equalizer, then the maximum delay spread that could be successfully equalized is $4 \times 10\mu s = 40\mu s$. Transmissions with multipath delay spread in excess of $40\mu s$ could not be equalized. Since the circuit complexity and processing time increases with the number of taps and delay elements, it is important to know the maximum number of delay elements before selecting an equalizer structure and its algorithm. The effects of channel fading are discussed by Proakis [Pro91], with regard to the design of the U.S. digital cellular equal-

izer. A study which considered a number of equalizers for a wide range of channel conditions was conducted by Rappaport, et. al. [Rap93a].

Example 6.3

Consider the design of the U.S. digital cellular equalizer [Pro91]. If f = 900 MHz and the mobile velocity v = 80 km/hr, determine the following:
(a) the maximum Doppler shift
(b) the coherence time of the channel
(c) the maximum number of symbols that could be transmitted without updating the equalizer, assuming that the symbol rate is 24.3 ksymbols/sec

Solution to Example 6.3

(a) From equation (4.2), the maximum Doppler shift is given by

$$f_d = \frac{v}{\lambda} = \frac{(80,000/3600)\text{ m/s}}{(1/3)\text{ m}} = 66.67\text{ Hz}$$

(b) From equation (4.40.c), the coherence time is approximately

$$T_c = \sqrt{\frac{9}{16\pi f_d^2}} = \frac{0.423}{66.67} = 6.34\text{ msec}$$

Note that if (4.40.a) or (4.40.b) were used, T_C would increase or decrease by a factor of 2 – 3.

(c) To ensure coherence over a TDMA time slot, data must be sent during a 6.34 ms interval. For R_s=24.3 ksymbols/sec, the number of bits that can be sent is

$$N_b = R_s T_C = 24,300 \times 0.00634 = 154\text{ symbols}$$

As shown in Chapter 10, each time slot in the U.S. digital cellular standard has a 6.67 ms duration and 162 symbols per time slot, which are very close to values in this example.

Three classic equalizer algorithms are discussed below. These include the zero forcing (ZF) algorithm, the least mean squares (LMS) algorithm, and the recursive least squares (RLS) algorithm.

6.8.1 Zero Forcing Algorithm

In a zero forcing equalizer, the equalizer coefficients c_n are chosen to force the samples of the combined channel and equalizer impulse response to zero at all but one of the NT spaced sample points in the tapped delay line filter. By letting the number of coefficients increase without bound, an infinite length equalizer with zero ISI at the output can be obtained. When each of the delay elements provide a time delay equal to the symbol duration T, the frequency response $H_{eq}(f)$ of the equalizer is periodic with a period equal to the symbol rate $1/T$. The combined response of the channel with the equalizer must satisfy Nyquist's first criterion (see Chapter 5)

$$H_{ch}(f)H_{eq}(f) = 1,\ |f| < 1/2T \tag{6.28}$$

where $H_{ch}(f)$ is the folded frequency response of the channel. Thus, an infinite length, zero, ISI equalizer is simply an inverse filter which inverts the folded frequency response of the channel. This infinite length equalizer is usually implemented by a truncated length version.

The zero forcing algorithm was developed by Lucky [Luc65] for wireline communication. The zero forcing equalizer has the disadvantage that the inverse filter may excessively amplify noise at frequencies where the folded channel spectrum has high attenuation. The ZF equalizer thus neglects the effect of noise altogether, and is not often used for wireless links.

6.8.2 Least Mean Square Algorithm

A more robust equalizer is the LMS equalizer where the criterion used is the minimization of the mean square error (MSE) between the desired equalizer output and the actual equalizer output. Using the notation developed in section 6.3, the LMS algorithm can be readily understood.

Referring to Figure 6.2 the prediction error is given by

$$e_k = d_k - \hat{d}_k = x_k - \hat{d}_k \tag{6.29}$$

and from (6.10)

$$e_k = x_k - \boldsymbol{y}_k^T \boldsymbol{w}_k = x_k - \boldsymbol{w}_k^T \boldsymbol{y}_k \tag{6.30}$$

To compute the mean square error $|e_k|^2$ at time instant k, equation (6.12) is squared to obtain

$$\xi = E[e_k^* e_k] \tag{6.31}$$

The LMS algorithm seeks to minimize the mean square error given in equation (6.31).

For a specific channel condition, the prediction error e_k is dependent on the tap gain vector $\boldsymbol{w}_N$, so the MSE of an equalizer is a function of $\boldsymbol{w}_N$. Let the cost function $J(\boldsymbol{w}_N)$ denote the mean squared error as a function of tap gain vector $\boldsymbol{w}_N$. Following the derivation in section 6.3, in order to minimize the MSE, it is required to set the derivative of equation (6.32) to zero.

$$\frac{\partial}{\partial \boldsymbol{w}_N} J(\boldsymbol{w}_N) = -2\boldsymbol{p}_N + 2\boldsymbol{R}_{NN}\boldsymbol{w}_N = 0 \tag{6.32}$$

Simplifying equation (6.32) (see Example 6.1 and Example 6.2)

$$\boldsymbol{R}_{NN}\hat{\boldsymbol{w}}_N = \boldsymbol{p}_N \tag{6.33}$$

Equation (6.33) is a classic result, and is called the *normal equation*, since the error is minimized and is made orthogonal (normal) to the projection related to the desired signal x_k. When equation (6.33) is satisfied, the MMSE of the equalizer is

$$J_{opt} = J(\hat{\boldsymbol{w}}_N) = E\left[x_k x_k^*\right] - \boldsymbol{p}_N^T \hat{\boldsymbol{w}}_N \tag{6.34}$$

To obtain the optimal tap gain vector $\hat{\boldsymbol{w}}_N$, the normal equation in (6.33) must be solved iteratively as the equalizer converges to an acceptably small value of J_{opt}. There are several ways to do this, and many variants of the LMS algorithm have been built upon the solution of equation (6.34). One obvious technique is to calculate

$$\hat{\boldsymbol{w}} = \boldsymbol{R}_{NN}^{-1} \boldsymbol{p}_N \tag{6.35}$$

However, inverting a matrix requires $O(N^3)$ arithmetic operations [Joh82]. Other methods such as Gaussian elimination [Joh82] and Cholesky factorization [Bie77] require $O(N^2)$ operations per iteration. The advantage of these methods which directly solve equation (6.35) is that only N symbol inputs are required to solve the normal equation. Consequently, a long training sequence is not necessary.

In practice, the minimization of the MSE is carried out recursively by use of the *stochastic gradient algorithm* introduced by Widrow [Wid66]. This is more commonly called the *Least Mean Square* (LMS) *algorithm*. The LMS algorithm is the simplest equalization algorithm and requires only $2N+1$ operations per iteration. The filter weights are updated by the update equations given below [Ale86]. Letting the variable n denote the sequence of iterations, LMS is computed iteratively by

$$\hat{d}_k(n) = \boldsymbol{w}_N^T(n)\boldsymbol{y}_N(n) \tag{6.36.a}$$

$$e_k(n) = x_k(n) - \hat{d}_k(n) \tag{6.36.b}$$

$$\boldsymbol{w}_N(n+1) = \boldsymbol{w}_N(n) - \alpha e_k^*(n)\boldsymbol{y}_N(n) \tag{6.36.c}$$

where the subscript N denotes the number of delay stages in the equalizer, and α is the step size which controls the convergence rate and stability of the algorithm.

The LMS equalizer maximizes the signal to distortion ratio at its output within the constraints of the equalizer filter length. If an input signal has a time dispersion characteristic that is greater than the propagation delay through the equalizer, then the equalizer will be unable to reduce distortion. The convergence rate of the LMS algorithm is slow due to the fact that there is only one parameter, the step size α, that controls the adaptation rate. To prevent the adaptation from becoming unstable, the value of α is chosen from

$$0 < \alpha < 2/\sum_{i=1}^{N} \lambda_i \tag{6.37}$$

where λ_i is the ith eigenvalue of the covariance matrix $\boldsymbol{R}_{NN}$. Since $\sum_{i=1}^{N} \lambda_i = \boldsymbol{y}_N^T(n)\boldsymbol{y}_N(n)$, the step size α can be controlled by the total input power in order to avoid instability in the equalizer [Hay86].

6.8.3 Recursive Least Squares Algorithm

The convergence rate of the gradient-based LMS algorithm is very slow, especially when the eigenvalues of the input covariance matrix $\boldsymbol{R}_{NN}$ have a very large spread, i.e, $\lambda_{max}/\lambda_{min} \gg 1$. In order to achieve faster convergence, complex algorithms which involve additional parameters are used. Faster converging algorithms are based on a least squares approach, as opposed to the statistical approach used in the LMS algorithm. That is, rapid convergence relies on error measures expressed in terms of a time average of the actual received signal instead of a statistical average. This leads to the family of powerful, albeit complex, adaptive signal processing techniques known as *recursive least squares* (RLS), which significantly improves the convergence of adaptive equalizers.

The least square error based on the time average is defined as [Hay86], [Pro91]

$$J(n) = \sum_{i=1}^{n} \lambda^{n-i} e^*(i,n)\, e(i,n) \tag{6.38}$$

where λ is the weighting factor close to 1, but smaller than 1, $e^*(i,n)$ is the complex conjugate of $e(i,n)$, and the error $e(i,n)$ is

$$e(i,n) = x(i) - \boldsymbol{y}_N^T(i)\,\boldsymbol{w}_N(n) \qquad 0 \le i \le n \tag{6.39}$$

and

$$\boldsymbol{y}_N(i) = [y(i), y(i-1), ..., y(i-N+1)]^T \tag{6.40}$$

where $\boldsymbol{y}_N(i)$ is the data input vector at time i, and $\boldsymbol{w}_N(n)$ is the new tap gain vector at time n. Therefore, $e(i,n)$ is the error using the new tap gain at time n to test the old data at time i, and $J(n)$ is the cumulative squared error of the new tap gains on all the old data.

The RLS solution requires finding the tap gain vector of the equalizer $\boldsymbol{w}_N(n)$ such that the cumulative squared error $J(n)$ is minimized. It uses all the previous data to test the new tap gains. The parameter λ is a data weighting factor that weights recent data more heavily in the computations, so that $J(n)$ tends to forget the old data in a nonstationary environment. If the channel is stationary, λ may be set to 1 [Pro89].

To obtain the minimum of least square error $J(n)$, the gradient of $J(n)$ in equation (6.38) is set to zero,

$$\frac{\partial}{\partial \boldsymbol{w}_N} J(n) = 0 \tag{6.41}$$

Using equations (6.39) – (6.41), it can be shown that [Pro89]

$$\boldsymbol{R}_{NN}(n)\,\hat{\boldsymbol{w}}_N(n) = \boldsymbol{p}_N(n) \tag{6.42}$$

where $\hat{\boldsymbol{w}}_N$ is the optimal tap gain vector of the RLS equalizer,

$$\boldsymbol{R}_{NN}(n) = \sum_{i=1}^{n} \lambda^{n-i} \boldsymbol{y}_N^*(i)\,\boldsymbol{y}_N^T(i) \tag{6.43}$$

$$\boldsymbol{p}_N(n) = \sum_{i=1}^{n} \lambda^{n-i} x^*(i)\,\boldsymbol{y}_N(i) \tag{6.44}$$

The matrix $\boldsymbol{R}_{NN}(n)$ in equation (6.43) is the deterministic correlation matrix of input data of the equalizer $\boldsymbol{y}_N(i)$, and $\boldsymbol{p}_N(i)$ in equation (6.44) is the deterministic crosscorrelation vector between inputs of the equalizer $\boldsymbol{y}_N(i)$ and the desired output $d(i)$, where $d(i) = x(i)$. To compute the equalizer weight vector $\hat{\boldsymbol{w}}_N$ using equation (6.42), it is required to compute $\boldsymbol{R}_{NN}^{-1}(n)$.

From the definition of $\boldsymbol{R}_{NN}(n)$ in equation (6.43), it is possible to obtain a recursive equation expressing $\boldsymbol{R}_{NN}(n)$ in terms of $\boldsymbol{R}_{NN}(n-1)$.

$$\boldsymbol{R}_{NN}(n) = \lambda \boldsymbol{R}_{NN}(n-1) + \boldsymbol{y}_N(n)\,\boldsymbol{y}_N^T(n) \tag{6.45}$$

Since the three terms in equation (6.45) are all N by N matrices, a matrix inverse lemma [Bie77] can be used to derive a recursive update for $\boldsymbol{R}_{NN}^{-1}$ in terms of the previous inverse, $\boldsymbol{R}_{NN}^{-1}(n-1)$.

$$\boldsymbol{R}_{NN}^{-1}(n) = \frac{1}{\lambda}\left[\boldsymbol{R}_{NN}^{-1}(n-1) - \frac{\boldsymbol{R}_{NN}^{-1}(n-1)\,\boldsymbol{y}_N(n)\,\boldsymbol{y}_N^T(n)\,\boldsymbol{R}_{NN}^{-1}(n-1)}{\lambda + \mu(n)}\right] \tag{6.46}$$

where

$$\mu(n) = \boldsymbol{y}_N^T(n)\,\boldsymbol{R}_{NN}^{-1}(n-1)\,\boldsymbol{y}_N(n) \tag{6.47}$$

Based on these recursive equations, the RLS minimization leads to the following weight update equations:

$$\boldsymbol{w}_N(n) = \boldsymbol{w}_N(n-1) + \boldsymbol{k}_N(n)\,e^*(n, n-1) \tag{6.48}$$

where

$$\boldsymbol{k}_N(n) = \frac{\boldsymbol{R}_{NN}^{-1}(n-1)\,\boldsymbol{y}_N(n)}{\lambda + \mu(n)} \tag{6.49}$$

The RLS algorithm may be summarized as follows:

1. Initialize $w(0) = k(0) = x(0) = 0$, $\boldsymbol{R}^{-1}(0) = \delta \boldsymbol{I}_{NN}$, where $\boldsymbol{I}_{NN}$ is an

$N \times N$ identity matrix, and δ is a large positive constant.

2. Recursively compute the following:

$$\hat{d}(n) = \boldsymbol{w}^T(n-1)\boldsymbol{y}(n) \tag{6.50}$$

$$e(n) = x(n) - \hat{d}(n) \tag{6.51}$$

$$\boldsymbol{k}(n) = \frac{\boldsymbol{R}^{-1}(n-1)\boldsymbol{y}(n)}{\lambda + \boldsymbol{y}^T(n)\boldsymbol{R}^{-1}(n-1)\boldsymbol{y}(n)} \tag{6.52}$$

$$\boldsymbol{R}^{-1}(n) = \frac{1}{\lambda}[\boldsymbol{R}^{-1}(n-1) - \boldsymbol{k}(n)\boldsymbol{y}^T(n)\boldsymbol{R}^{-1}(n-1)] \tag{6.53}$$

$$\boldsymbol{w}(n) = \boldsymbol{w}(n-1) + \boldsymbol{k}(n)e^*(n) \tag{6.54}$$

In equation (6.53), λ is the weighting coefficient that can change the performance of the equalizer. If a channel is time-invariant, λ can be set to 1. Usually $0.8 < \lambda < 1$ is used. The value of λ has no influence on the rate of convergence, but does determines the tracking ability of the RLS equalizers. The smaller the λ, the better the tracking ability of the equalizer. However, if λ is too small, the equalizer will be unstable [Lin84]. The RLS algorithm described above, called the *Kalman RLS* algorithm, use $2.5N^2 + 4.5N$ arithmetic operations per iteration.

6.8.4 Summary of Algorithms

There are number of variations of the LMS and RLS algorithms that exist for adapting an equalizer. Table 6.1 shows the computational requirements of different algorithms, and lists some advantages and disadvantages of each algorithm. Note that the RLS algorithms have similar convergence and tracking performances, which are much better than the LMS algorithm. However, these RLS algorithms usually have high computational requirement and complex program structures. Also, some RLS algorithms tend to be unstable. The fast transversal filter (FTF) algorithm requires the least computation among the RLS algorithms, and it can use a rescue variable to avoid instability. However, rescue techniques tend to be a bit tricky for widely varying mobile radio channels, and the FTF is not widely used.

6.9 Fractionally Spaced Equalizers

The equalizers discussed so far have tap spacings at the symbol rate. It is well known that the optimum receiver for a communication signal corrupted by Gaussian noise consists of a matched filter sampled periodically at the symbol rate of the message. In the presence of channel distortion, the matched filter prior to the equalizer must be matched to the channel and the corrupted signal.

Table 6.1 Comparison of Various Algorithms for Adaptive Equalization [Pro91]

Algorithm	Number of Multiply Operations	Advantages	Disadvantages
LMS Gradient DFE	$2N + 1$	Low computational complexity, simple program	Slow convergence, poor tracking
Kalman RLS	$2.5N^2 + 4.5N$	Fast convergence, good tracking ability	High computational complexity
FTF	$7N + 14$	Fast convergence, good tracking, low computational complexity	Complex programming, unstable (but can use rescue method)
Gradient Lattice	$13N - 8$	Stable, low computational complexity, flexible structure	Performance not as good as other RLS, complex programming
Gradient Lattice DFE	$13N_1 + 33N_2 - 36$	Low computational complexity	Complex programming
Fast Kalman DFE	$20N + 5$	Can be used for DFE, fast convergence and good tracking	Complex programming, computation not low, unstable
Square Root RLS DFE	$1.5N^2 + 6.5N$	Better numerical properties	High computational complexity

In practice, the channel response is unknown, and hence the optimum matched filter must be adaptively estimated. A suboptimal solution in which the matched filter is matched to the transmitted signal pulse may result in a significant degradation in performance. In addition, such a suboptimal filter is extremely sensitive to any timing error in the sampling of its output [Qur77]. A *fractionally spaced equalizer* (FSE) is based on sampling the incoming signal at least as fast as the Nyquist rate [Pro91]. The FSE compensates for the channel distortion before aliasing effects occur due to the symbol rate sampling. In addition, the equalizer can compensate for any timing delay for any arbitrary timing phase. In effect, the FSE incorporates the functions of a matched filter and equalizer into a single filter structure. Simulation results demonstrating the effectiveness of the FSE over a symbol rate equalizer have been given in the papers by Qureshi and Forney [Qur77], and Gitlin and Weinstein [Git81].

Nonlinear equalizers based on MLSE techniques appear to be gaining popularity in modern wireless systems (these were described in Section 6.7.2). The interested reader may find Chapter 6 of [Ste94] useful for further work in this area.

6.10 Diversity Techniques

Diversity is a powerful communication receiver technique that provides wireless link improvement at relatively low cost. Unlike equalization, diversity requires no training overhead since a training sequence is not required by the transmitter. Furthermore, there are a wide range of diversity implementations, many which are very practical and provide significant link improvement with little added cost.

Diversity exploits the random nature of radio propagation by finding independent (or at least highly uncorrelated) signal paths for communication. In virtually all applications, diversity decisions are made by the receiver, and are unknown to the transmitter.

The diversity concept can be explained simply. If one radio path undergoes a deep fade, another independent path may have a strong signal. By having more than one path to select from, both the instantaneous and average SNRs at the receiver may be improved, often by as much as 20 dB to 30 dB.

As shown in Chapters 3 and 4, there are two types of fading – small-scale and large-scale fading. Small-scale fades are characterized by deep and rapid amplitude fluctuations which occur as the mobile moves over distances of just a few wavelengths. These fades are caused by multiple reflections from the surroundings in the vicinity of the mobile. Small-scale fading typically results in a Rayleigh fading distribution of signal strength over small distances. In order to prevent deep fades from occurring, *microscopic diversity techniques* can exploit the rapidly changing signal. For example, the small-scale fading shown in Figure 3.1 reveals that if two antennas are separated by a fraction of a meter, one may receive a null while the other receives a strong signal. By selecting the best signal at all times, a receiver can mitigate small-scale fading effects (this is called *antenna diversity* or *space diversity*).

Large-scale fading is caused by shadowing due to variations in both the terrain profile and the nature of the surroundings. In deeply shadowed conditions, the received signal strength at a mobile can drop well below that of free space. In Chapter 3, large-scale fading was shown to be log-normally distributed with a standard deviation of about 10 dB in urban environments. By selecting a base station which is not shadowed when others are, the mobile can improve substantially the average signal-to-noise ratio on the forward link. This is called *macroscopic diversity*, since the mobile is taking advantage of large separations between the serving base stations.

Macroscopic diversity is also useful at the base station receiver. By using base station antennas that are sufficiently separated in space, the base station is able to improve the reverse link by selecting the antenna with the strongest signal from the mobile.

6.10.1 Derivation of Selection Diversity Improvement

Before discussing the many diversity techniques that are used, it is worthwhile to quantitatively determine the advantage that can be achieved using diversity. Consider M independent Rayleigh fading channels available at a receiver. Each channel is called a diversity *branch*. Further assume that each branch has the same average *SNR* given by

$$SNR = \Gamma = \frac{E_b}{N_0}\overline{\alpha^2} \tag{6.55}$$

If each branch has an instantaneous $SNR = \gamma_i$, then from equation (5.154), the pdf of γ_i is

$$p(\gamma_i) = \frac{1}{\Gamma} e^{\frac{-\gamma_i}{\Gamma}} \quad \gamma_i \geq 0 \tag{6.56}$$

where Γ is the mean *SNR* of each branch. The probability that a single branch has *SNR* less than some threshold γ is

$$Pr[\gamma_i \leq \gamma] = \int_0^{\infty} p(\gamma_i)\, d\gamma_i = \int_0^{\infty} \frac{1}{\Gamma} e^{\frac{-\gamma_i}{\Gamma}} d\gamma_i \tag{6.57}$$

$$= 1 - e^{\frac{-\gamma}{\Gamma}}$$

Now, the probability that all M independent diversity branches receive signals which are simultaneously less than some specific *SNR* threshold γ is

$$Pr[\gamma_1, ..., \gamma_M \leq \gamma] = (1 - e^{-\gamma/\Gamma})^M = P_M(\gamma) \tag{6.58}$$

$P_M(\gamma)$ in equation (6.58) is the probability of all branches failing to achieve $SNR = \gamma$. If a single branch achieves $SNR > \gamma$ then the probability that $SNR > \gamma$ for any one branch is given by

$$Pr[\gamma_i > \gamma] = 1 - P_M(\gamma) = 1 - (1 - e^{-\gamma/\Gamma})^M \tag{6.59}$$

Equation (6.59) is an expression for the probability of exceeding a threshold when *selection diversity* is used [Jak71], and is plotted in Figure 6.11.

To determine the average signal-to-noise ratio of the received signal when diversity is used, it is first necessary to find the pdf of the fading signal. For selection diversity, the average SNR is found by first computing the derivative of $P_M(\gamma)$. Proceeding along these lines,

$$p_M(\gamma) = \frac{d}{d\gamma} P_M(\gamma) = \frac{M}{\Gamma}(1 - e^{-\gamma/\Gamma})^{M-1} e^{-\gamma/\Gamma} \tag{6.60}$$

Then, the mean *SNR*, $\bar{\gamma}$, may be expressed as

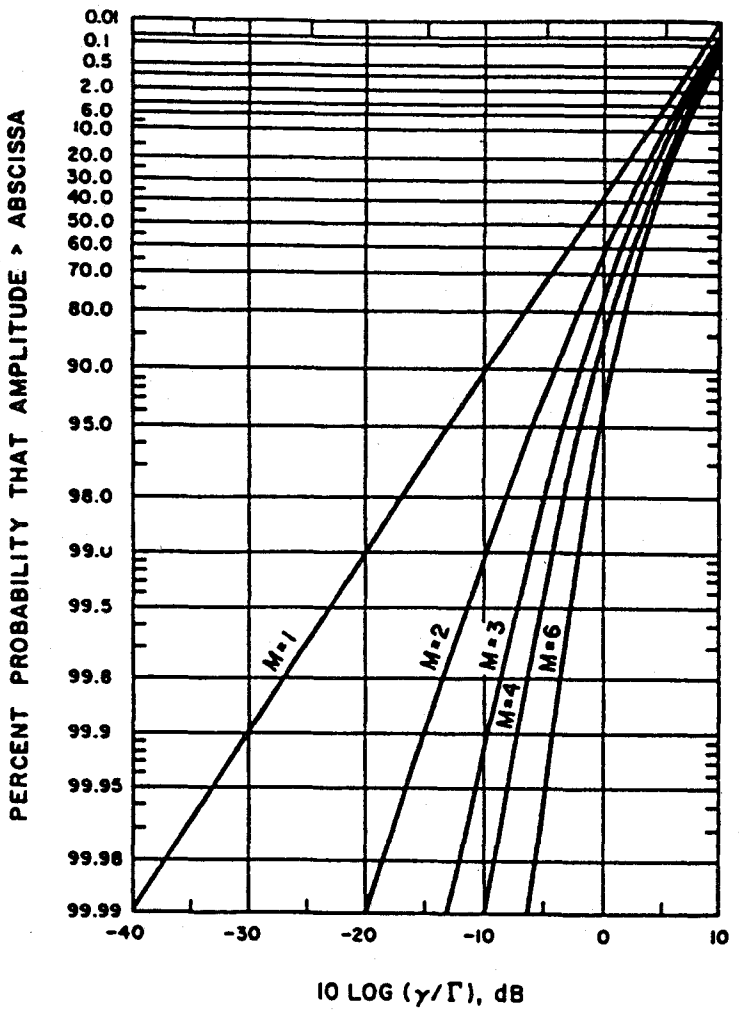

Figure 6.11
Graph of probability distributions of $SNR = \gamma$ threshold for M branch selection diversity. The term γ represents the mean SNR on each branch [From [Jak71] © IEEE].

$$\bar{\gamma} = \int_0^\infty \gamma p_M(\gamma)\, d\gamma = \Gamma \int_0^\infty Mx\,(1-e^{-x})^{M-1} e^{-x} dx \tag{6.61}$$

where $x = \gamma/\Gamma$. Equation (6.61) is evaluated to yield the average SNR improvement offered by selection diversity.

$$\frac{\bar{\gamma}}{\Gamma} = \sum_{k=1}^{M} \frac{1}{k} \tag{6.62}$$

The following example illustrates the advantage that diversity provides.

Example 6.4

Assume four branch diversity is used, where each branch receives an independent Rayleigh fading signal. If the average *SNR* is 20 dB, determine the probability that the *SNR* will drop below 10 dB. Compare this with the case of a single receiver without diversity.

Solution to Example 6.4

For this example the specified threshold $\gamma = 10$ dB, $\Gamma = 20$ dB, and there are four branches. Thus $\gamma/\Gamma = 0.1$ and using equation (6.58),

$$P_4(10 \text{ dB}) = (1-e^{-0.1})^4 = 0.000082$$

When diversity is not used, equation (6.58) may be evaluated using $M = 1$.

$$P_1(10 \text{ dB}) = (1-e^{-0.1})^1 = 0.095$$

Notice that without diversity the *SNR* drops below the specified threshold with a probability that is three orders of magnitude greater than if four branch diversity is used!

From equation (6.62) it can be seen that the average SNR in the branch which is selected using selection diversity naturally increases, since it is always guaranteed to be above the specified threshold. Thus, selection diversity offers an average improvement in the link margin without requiring additional transmitter power or sophisticated receiver circuitry. The diversity improvement can be directly related to the average bit error rate for various modulations by using the principles discussed in section 5.11.1.

Selection diversity is easy to implement because all that is needed is a side monitoring station and an antenna switch at the receiver. However, it is not an optimal diversity technique because it does not use all of the possible branches simultaneously. *Maximal ratio combining* uses each of the M branches in a co-phased and weighted manner such that the highest achievable SNR is available at the receiver at all times.

6.10.2 Derivation of Maximal Ratio Combining Improvement

In maximal ratio combining, the voltage signals r_i from each of the M diversity branches are co-phased to provide coherent voltage addition and are individually weighted to provide optimal SNR. If each branch has gain G_i, then the resulting signal envelope applied to the detector is

$$r_M = \sum_{i=1}^{M} G_i r_i \tag{6.63}$$

Assuming that each branch has the same average noise power N, the total noise power N_T applied to the detector is simply the weighted sum of the noise in each branch. Thus

$$N_T = N\sum_{i=1}^{M} G_i^2 \tag{6.64}$$

which results in an SNR applied to the detector, γ_M, given by

$$\gamma_M = \frac{r_m^2}{2N_T} \tag{6.65}$$

Using Chebychev's inequality [Cou93], γ_M is maximized when $G_i = r_i/N$ which leads to

$$\gamma_M = \frac{1}{2}\frac{\sum\left(r_i^2/N\right)^2}{N\sum\left(r_i^2/N^2\right)} = \frac{1}{2}\sum_{i=1}^{M}\frac{r_i^2}{N} = \sum_{i=1}^{M}\gamma_i \tag{6.66}$$

Thus the SNR out of the diversity combiner (see in Figure 6.14) is simply the sum of the SNRs in each branch.

The value for γ_i is $r_i^2/2N$, where r_i is equal to $r(t)$ as defined in equation (4.67). As shown in Chapter 4, the received signal envelope for a fading mobile radio signal can be modeled from two independent Gaussian random variables T_c and T_s, each having zero mean and equal variance σ^2. That is,

$$\gamma_i = \frac{1}{2N}r_i^2 = \frac{1}{2N}\left(T_c^2 + T_s^2\right) \tag{6.67}$$

Hence γ_M is a Chi-square distribution of $2M$ Gaussian random variables with variance $\sigma^2/(2N) = \Gamma/2$, where Γ is defined in equation (6.55). The resulting pdf for γ_M can be shown to be

$$p(\gamma_M) = \frac{\gamma_M^{M-1}e^{-\gamma_M/\Gamma}}{\Gamma^M(M-1)!} \quad \text{for } \gamma_M \geq 0 \tag{6.68}$$

The probability that γ_M is less than some SNR threshold γ is

$$Pr\{\gamma_M \leq \gamma\} = \int_0^{\gamma} p(\gamma_M)\,d\gamma_M = 1 - e^{-\gamma/\Gamma}\sum_{k=1}^{M}\frac{(\gamma/\Gamma)^{k-1}}{(k-1)!} \tag{6.69}$$

Equation (6.69) is the probability distribution for maximal ratio combining [Jak71]. It follows directly from equation (6.66) that the average SNR, $\overline{\gamma_M}$, is simply the sum of the individual $\overline{\gamma_i}$ from each branch. In other words,

$$\overline{\gamma_M} = \sum_{i=1}^{M}\overline{\gamma_i} = \sum_{i=1}^{M}\Gamma = M\Gamma \tag{6.70}$$

The control algorithms for setting the gains and phases for maximal ratio combining receivers are similar to those required in equalizers and RAKE receivers. Figure 6.14 and Figure 6.16 illustrate maximal ratio combining structures. Maximal ratio combining is discussed in Section 6.10.3.3, and can be applied to

virtually any diversity application, although often at much greater cost and complexity than other diversity techniques.

6.10.3 Practical Space Diversity Considerations

Space diversity, also known as antenna diversity, is one of the most popular forms of diversity used in wireless systems. Conventional cellular radio systems consist of an elevated base station antenna and a mobile antenna close to the ground. The existence of a direct path between the transmitter and the receiver is not guaranteed and the possibility of a number of scatterers in the vicinity of the mobile suggests a Rayleigh fading signal. From this model [Jak70], Jakes deduced that the signals received from spatially separated antennas on the mobile would have essentially uncorrelated envelopes for antenna separations of one half wavelength or more.

The concept of antenna space diversity is also used in base station design. At each cell site, multiple base station receiving antennas are used to provide diversity reception. However, since the important scatterers are generally on the ground in the vicinity of the mobile, the base station antennas must be spaced considerably far apart to achieve decorrelation. Separations on the order of several tens of wavelengths are required at the base station. Space diversity can thus be used at either the mobile or base station, or both. Figure 6.12 shows a general block diagram of a space diversity scheme [Cox83a].

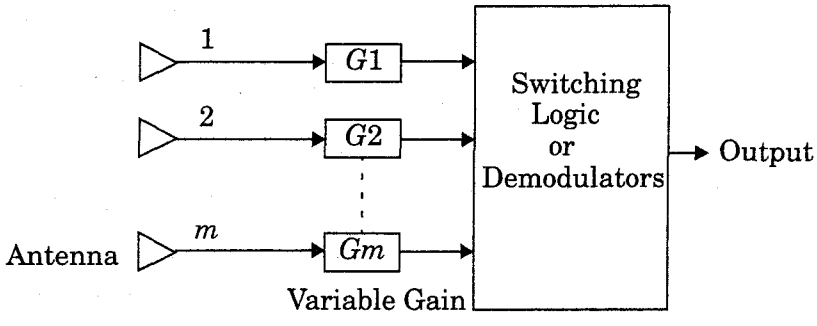

Figure 6.12
Generalized block diagram for space diversity.

Space diversity reception methods can be classified into four categories [Jak71]:

1. Selection diversity
2. Feedback diversity
3. Maximal ratio combining
4. Equal gain diversity

6.10.3.1 Selection Diversity

Selection diversity is the simplest diversity technique analyzed in section 6.10.1. A block diagram of this method is similar to that shown in Figure 6.12, where m demodulators are used to provide m diversity branches whose gains are adjusted to provide the same average SNR for each branch. As derived in section 6.10.1, the receiver branch having the highest instantaneous SNR is connected to the demodulator. The antenna signals themselves could be sampled and the best one sent to a single demodulator. In practice, the branch with the largest $(S+N)/N$ is used, since it is difficult to measure SNR. A practical selection diversity system cannot function on a truly instantaneous basis, but must be designed so that the internal time constants of the selection circuitry are shorter than the reciprocal of the signal fading rate.

6.10.3.2 Feedback or Scanning Diversity

Scanning diversity is very similar to selection diversity except that instead of always using the best of M signals, the M signals are scanned in a fixed sequence until one is found to be above a predetermined threshold. This signal is then received until it falls below threshold and the scanning process is again initiated. The resulting fading statistics are somewhat inferior to those obtained by the other methods but the advantage with this method is that it is very simple to implement — only one receiver is required. A block diagram of this method is shown in Figure 6.13.

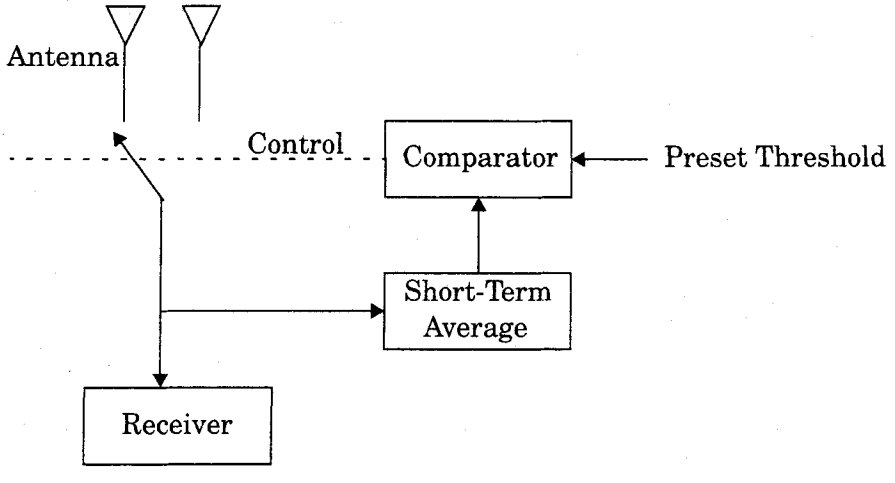

Figure 6.13
Basic form of scanning diversity.

6.10.3.3 Maximal Ratio Combining

In this method first proposed by Kahn [Kah54], the signals from all of the M branches are weighted according to their individual signal voltage to noise power ratios and then summed. Figure 6.14 shows a block diagram of the technique. Here, the individual signals must be co-phased before being summed

(unlike selection diversity) which generally requires an individual receiver and phasing circuit for each antenna element. Maximal ratio combining produces an output SNR equal to the sum of the individual SNRs, as explained in section 6.10.2. Thus, it has the advantage of producing an output with an acceptable SNR even when none of the individual signals are themselves acceptable. This technique gives the best statistical reduction of fading of any known linear diversity combiner. Modern DSP techniques and digital receivers are now making this optimal form of diversity practical.

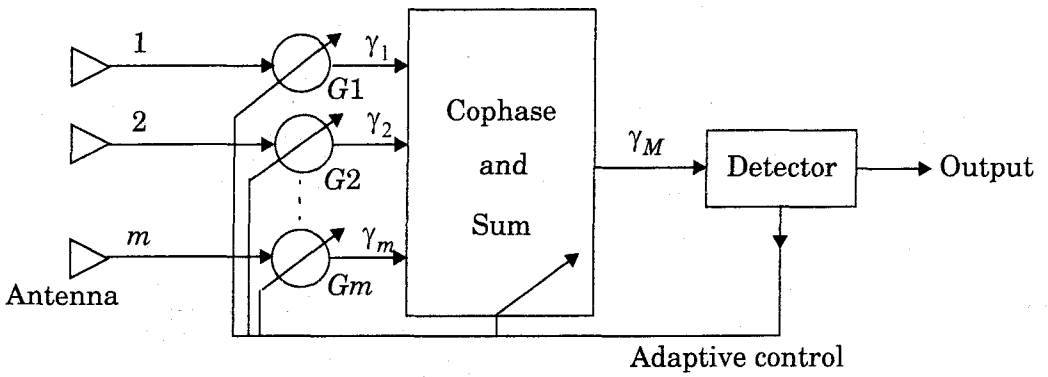

Figure 6.14
Maximal ratio combiner.

6.10.3.4 Equal Gain Combining

In certain cases, it is not convenient to provide for the variable weighting capability required for true maximal ratio combining. In such cases, the branch weights are all set to unity but the signals from each branch are co-phased to provide *equal gain combining* diversity. This allows the receiver to exploit signals that are simultaneously received on each branch. The possibility of producing an acceptable signal from a number of unacceptable inputs is still retained, and performance is only marginally inferior to maximal ratio combining and superior to selection diversity.

6.10.4 Polarization Diversity

At the base station, space diversity is considerably less practical than at the mobile because the narrow angle of incident fields requires large antenna spacings [Vau90]. The comparatively high cost of using space diversity at the base station prompts the consideration of using orthogonal polarization to exploit polarization diversity. While this only provides two diversity branches it does allow the antenna elements to be co-located.

In the early days of cellular radio, all subscriber units were mounted in vehicles and used vertical whip antennas. Today, however, over half of the subscriber units are portable. This means that most subscribers are no longer using vertical polarization due to hand-tilting when the portable cellular phone is

used. This recent phenomenon has sparked interest in polarization diversity at the base station.

Measured horizontal and vertical polarization paths between a mobile and a base station are reported to be uncorrelated by Lee and Yeh [Lee72]. The decorrelation for the signals in each polarization is caused by multiple reflections in the channel between the mobile and base station antennas. Chapter 3 showed that the reflection coefficient for each polarization is different, which results in different amplitudes and phases for each, or at least some, of the reflections. After sufficient random reflections, the polarization state of the signal will be independent of the transmitted polarization. In practice, however, there is some dependence of the received polarization on the transmitted polarization.

Circular and linear polarized antennas have been used to characterize multipath inside buildings [Haw91], [Rap92a], [Ho94]. When the path was obstructed, polarization diversity was found to dramatically reduce the multipath delay spread without significantly decreasing the received power.

While polarization diversity has been studied in the past, it has primarily been used for fixed radio links which vary slowly in time. Line-of-sight microwave links, for example, typically use polarization diversity to support two simultaneous users on the same radio channel. Since the channel does not change much in such a link, there is little likelihood of cross polarization interference. As portable users proliferate, polarization diversity is likely to become more important for improving link margin and capacity. An outline of a theoretical model for the base station *polarization diversity reception* as suggested by Kozono [Koz85] is given below.

Theoretical Model for Polarization Diversity

It is assumed that the signal is transmitted from a mobile with vertical (or horizontal) polarization. It is received at the base station by a polarization diversity antenna with 2 branches. Figure 6.15 shows the theoretical model and the system coordinates. As seen in the figure, a polarization diversity antenna is composed of two antenna elements V_1 and V_2, which make a $\pm\alpha$ angle (polarization angle) with the Y axis. A mobile station is located in the direction of offset angle β from the main beam direction of the diversity antenna as seen in Figure 6.15(b).

Some of the vertically polarized signals transmitted are converted to the horizontal polarized signal because of multipath propagation. The signal arriving at the base station can be expressed as

$$x = r_1 \cos(\omega t + \phi_1) \tag{6.71.a}$$

$$y = r_2 \cos(\omega t + \phi_2) \tag{6.71.b}$$

where x and y are signal levels which are received when $\beta = 0$. It is assumed that r_1 and r_2 have independent Rayleigh distributions, and ϕ_1 and ϕ_2 have independent uniform distributions.

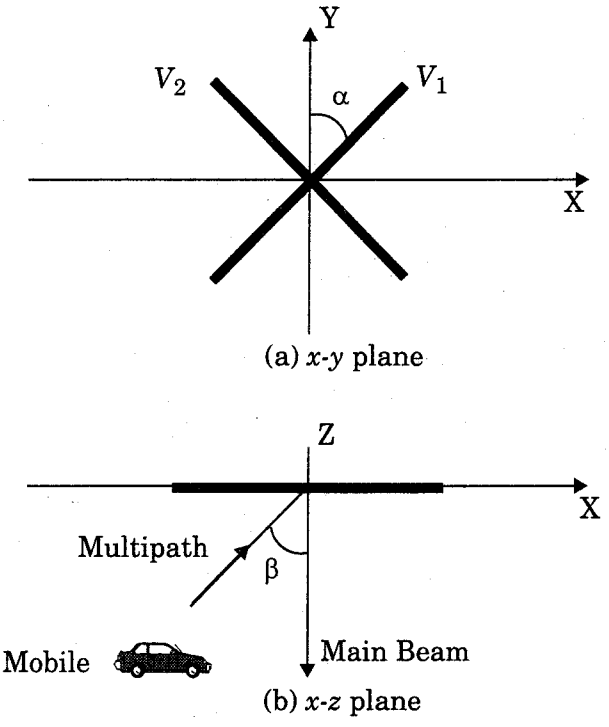

Figure 6.15
Theoretical Model for base station polarization diversity based on [Koz85].

The received signal values at elements V_1 and V_2 can be written as:

$$v_1 = (ar_1\cos\phi_1 + r_2 b\cos\phi_2)\cos\omega t - (ar_1\sin\phi_1 + r_2 b\sin\phi_2)\sin\omega t \quad (6.72)$$

$$v_2 = (-ar_1\cos\phi_1 + r_2 b\cos\phi_2)\cos\omega t - (-ar_1\sin\phi_1 + r_2 b\sin\phi_2)\sin\omega t \quad (6.73)$$

where $a = \sin\alpha\cos\beta$ and $b = \cos\alpha$.

The correlation coefficient ρ can be written as

$$\rho = \left(\frac{\tan^2(\alpha)\cos^2(\beta) - \Gamma}{\tan^2(\alpha)\cos^2(\beta) + \Gamma}\right)^2 \quad (6.74)$$

where

$$\Gamma = \frac{\langle R_2^2\rangle}{\langle R_1^2\rangle} \quad (6.75)$$

where

$$R_1 = \sqrt{r_1^2 a^2 + r_2^2 b^2 + 2r_1 r_2 ab\cos(\phi_1 + \phi_2)} \quad (6.76)$$

$$R_2 = \sqrt{r_1^2 a^2 + r_2^2 b^2 - 2r_1 r_2 ab\cos(\phi_1 + \phi_2)} \quad (6.77)$$

Here, Γ is the cross polarization discrimination of the propagation path between a mobile and a base station.

The correlation coefficient is determined by three factors: polarization angle; offset angle from the main beam direction of the diversity antenna and the cross polarization discrimination. The correlation coefficient generally becomes higher as offset angle β becomes larger. Also, ρ generally becomes lower as polarization angle α increases. This is because the horizontal polarization component becomes larger as α increases.

Because antenna elements V_1 and V_2 are polarized at $\pm\alpha$ to the vertical, the received signal level is lower than that received by a vertically polarized antenna. The average value of signal loss L, relative to that received using vertical polarization is given by

$$L = a^2/\Gamma + b^2 \tag{6.78}$$

The results of practical experiments carried out using polarization diversity [Koz85] show that polarization diversity is a viable diversity reception technique.

6.10.5 Frequency Diversity

Frequency diversity transmits information on more than one carrier frequency. The rationale behind this technique is that frequencies separated by more than the coherence bandwidth of the channel will not experience the same fades [Lem91]. Theoretically, if the channels are uncorrelated, the probability of simultaneous fading will be the product of the individual fading probabilities (see equation (6.58)).

Frequency diversity is often employed in microwave line-of-sight links which carry several channels in a frequency division multiplex mode (FDM). Due to tropospheric propagation and resulting refraction, deep fading sometimes occurs. In practice, *1:N protection switching* is provided by a radio licensee, wherein one frequency is nominally idle but is available on a stand-by basis to provide frequency diversity switching for any one of the N other carriers (frequencies) being used on the same link, each carrying independent traffic. When diversity is needed, the appropriate traffic is simply switched to the backup frequency. This technique has the disadvantage that it not only requires spare bandwidth but also requires that there be as many receivers as there are channels used for the frequency diversity. However, for critical traffic, the expense may be justified.

6.10.6 Time Diversity

Time diversity repeatedly transmits information at time spacings that exceed the coherence time of the channel, so that multiple repetitions of the signal will be received with independent fading conditions, thereby providing for diversity. One modern implementation of time diversity involves the use of the

RAKE receiver for spread spectrum CDMA, where the multipath channel provides redundancy in the transmitted message.

6.11 RAKE Receiver

In CDMA spread spectrum systems (see Chapter 5), the chip rate is typically much greater than the flat fading bandwidth of the channel. Whereas conventional modulation techniques require an equalizer to undo the intersymbol interference between adjacent symbols, CDMA spreading codes are designed to provide very low correlation between successive chips. Thus, propagation delay spread in the radio channel merely provides multiple versions of the transmitted signal at the receiver. If these multipath components are delayed in time by more than a chip duration, they appear like uncorrelated noise at a CDMA receiver, and equalization is not required.

However, since there is useful information in the multipath components, CDMA receivers may combine the time delayed versions of the original signal transmission in order to improve the signal to noise ratio at the receiver. A RAKE receiver does just this – it attempts to collect the time-shifted versions of the original signal by providing a separate correlation receiver for each of the multipath signals. The RAKE receiver, shown in Figure 6.16, is essentially a diversity receiver designed specifically for CDMA, where the diversity is provided by the fact that the multipath components are practically uncorrelated from one another when their relative propagation delays exceed a chip period.

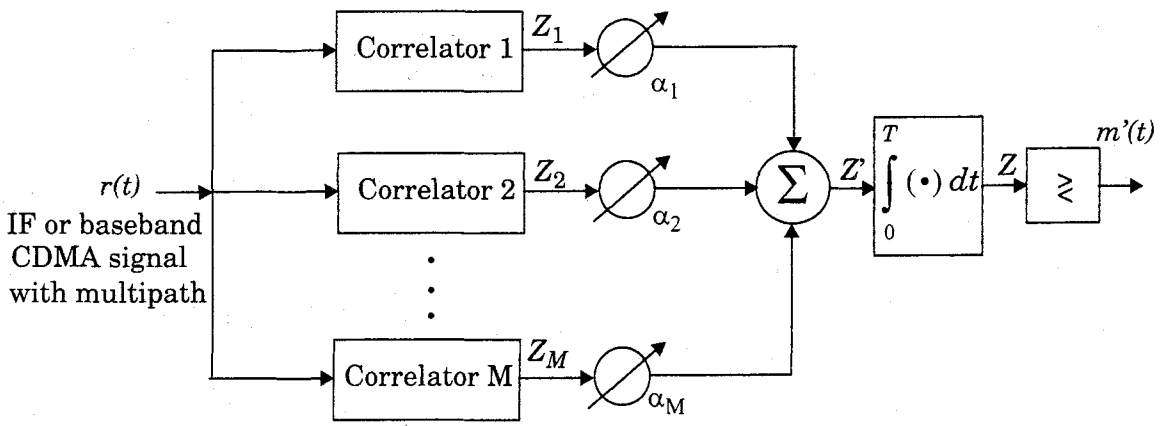

Figure 6.16
An M-branch (M-finger) RAKE receiver implementation. Each correlator detects a time shifted version of the original CDMA transmission, and each finger of the RAKE correlates to a portion of the signal which is delayed by at least one chip in time from the other fingers.

A RAKE receiver utilizes multiple correlators to separately detect the M strongest multipath components. The outputs of each correlator are weighted to provide a better estimate of the transmitted signal than is provided by a single

component. Demodulation and bit decisions are then based on the weighted outputs of the M correlators.

The basic idea of a RAKE receiver was first proposed by Price and Green [Pri58]. In outdoor environments, the delay between multipath components is usually large and, if the chip rate is properly selected, the low autocorrelation properties of a CDMA spreading sequence can assure that multipath components will appear nearly uncorrelated with each other.

Assume M correlators are used in a CDMA receiver to capture the M strongest multipath components. A weighting network is used to provide a linear combination of the correlator output for bit detection. Correlator 1 is synchronized to the strongest multipath m_1. Multipath component m_2 arrives τ_1 later than component m_1. The second correlator is synchronized to m_2. It correlates strongly with m_2 but has low correlation with m_1. Note that if only a single correlator is used in the receiver (see Figure 5.52), once the output of the single correlator is corrupted by fading, the receiver cannot correct the value. Bit decisions based on only a single correlation may produce a large bit error rate. In a RAKE receiver, if the output from one correlator is corrupted by fading, the others may not be, and the corrupted signal may be discounted through the weighting process. Decisions based on the combination of the M separate decision statistics offered by the RAKE provide a form of diversity which can overcome fading and thereby improve CDMA reception.

The M decision statistics are weighted to form an overall decision statistic as shown in Figure 6.16. The outputs of the M correlators are denoted as $Z_1, Z_2, \ldots$ and Z_M. They are weighted by $\alpha_1, \alpha_2, \ldots$ and α_M, respectively. The weighting coefficients are based on the power or the SNR from each correlator output. If the power or SNR is small out of a particular correlator, it will be assigned a small weighting factor. Just as in the case of a maximal ratio combining diversity scheme, the overall signal Z' is given by

$$Z' = \sum_{m=1}^{M} \alpha_m Z_m \tag{6.79}$$

The weighting coefficients, α_m, are normalized to the output signal power of the correlator in such a way that the coefficients sum to unity, as shown in equation (6.80).

$$\alpha_m = \frac{Z_m^2}{\sum_{m=1}^{M} Z_m^2} \tag{6.80}$$

As in the case of adaptive equalizers and diversity combining, there are many ways to generate the weighting coefficients. However, due to multiple access interference, RAKE fingers with strong multipath amplitudes will not

necessarily provide strong output after correlation. Choosing weighting coefficients based on the actual outputs of the correlators yields better RAKE performance.

6.12 Interleaving

Interleaving is used to obtain time diversity in a digital communications system without adding any overhead. Interleaving has become an extremely useful technique in all second generation digital cellular systems, due to the rapid proliferation of digital speech coders which transform analog voices into efficient digital messages that are transmitted over wireless links (speech coders are presented in Chapter 7).

Because speech coders attempt to represent a wide range of voices in a uniform and efficient digital format, the encoded data bits (called *source bits*) carry a great deal of information, and as explained in Chapters 7 and 10, some source bits are more important than others and must be protected from errors. It is typical for many speech coders to produce several "important" bits in succession, and it is the function of the interleaver to spread these bits out in time so that if there is a deep fade or noise burst, the important bits from a block of source data are not corrupted at the same time. By spreading the source bits over time, it becomes possible to make use of error control coding (called *channel coding*) which protects the source data from corruption by the channel. Since error control codes are designed to protect against channel errors that may occur randomly or in a bursty manner, interleavers scramble the time order of source bits before they are channel coded.

An interleaver can be one of two forms – a block structure or a convolutional structure. A block interleaver formats the encoded data into a rectangular array of m rows and n columns, and interleaves nm bits at a time. Usually, each row contains a word of source data having n bits. An interleaver of degree m (or depth m) consists of m rows. The structure of a block interleaver is shown in Figure 6.17. As seen, source bits are placed into the interleaver by sequentially increasing the row number for each successive bit, and filling the columns. The interleaved source data is then read out row-wise and transmitted over the channel. This has the effect of separating the original source bits by m bit periods.

At the receiver, the de-interleaver stores the received data by sequentially increasing the row number of each successive bit, and then clocks out the data row-wise, one word (row) at a time.

Convolutional interleavers can be used in place of block interleavers in much the same fashion. Convolutional interleavers are ideally suited for use with convolutional codes.

There is an inherent delay associated with an interleaver since the received message block cannot be fully decoded until all of the nm bits arrive at the receiver and are de-interleaved. In practice, human speech is tolerable to listen

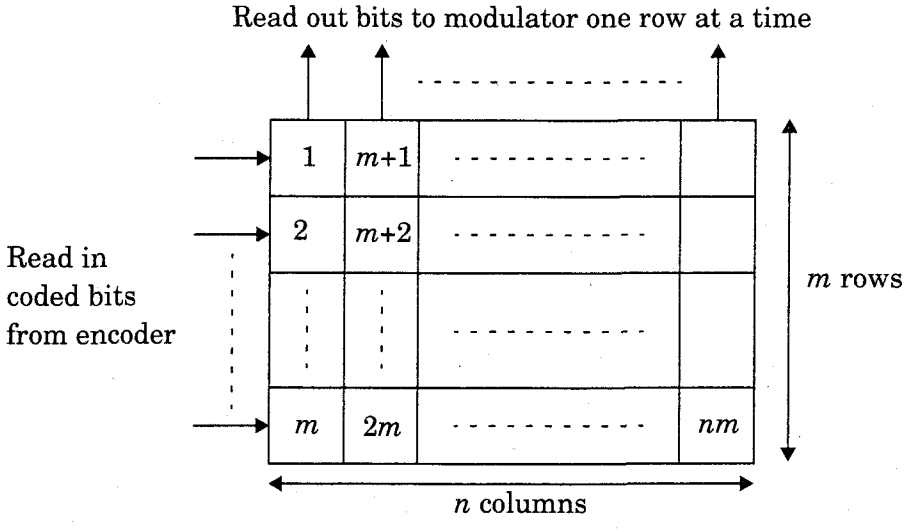

Figure 6.17
Block interleaver where source bits are read into columns and read out as n-bit rows.

to until delays of greater than 40 ms occur. It is for this reason that all of the wireless data interleavers have delays which do not exceed 40ms. The interleaver word size and depth are closely related to the type of speech coder used, the source coding rate and the maximum tolerable delay.

6.13 Fundamentals of Channel Coding

Channel coding protects digital data from errors by selectively introducing redundancies in the transmitted data. Channel codes that are used to detect errors are called *error detection codes,* while codes that can detect and correct errors are called *error correction codes.*

In 1948, Shannon demonstrated that by proper encoding of the information, errors induced by a noisy channel can be reduced to any desired level without sacrificing the rate of information transfer [Sha48]. Shannon's channel capacity formula is applicable to the AWGN channel and is given by

$$C = B\log_2\left(1 + \frac{P}{N_0 B}\right) = B\log_2\left(1 + \frac{S}{N}\right) \tag{6.81}$$

where C is the channel capacity (bits per second), B is the transmission bandwidth (Hz), P is the received signal power (watts), and N_0 is the single-sided noise power density (watts/Hz). The received power at a receiver is given as

$$P = E_b R_b \tag{6.82}$$

where E_b is the average bit energy, and R_b is the transmission bit rate. Equation (6.81) can be normalized by the transmission bandwidth and is given by

$$\frac{C}{B} = \log_2\left(1 + \frac{E_b}{N_0}\frac{R_b}{B}\right) \tag{6.83}$$

where C/B denotes *bandwidth efficiency.*

The basic purpose of error detection and error correction techniques is to introduce redundancies in the data to improve wireless link performance. The introduction of redundant bits increases the raw data rate used in the link, hence increases the bandwidth requirement for a fixed source data rate. This reduces the bandwidth efficiency of the link in high SNR conditions, but provides excellent BER performance at low SNR values.

It is well known that the use of orthogonal signaling allows the probability of error to become arbitrarily small by expanding the signal set, i.e., by making the number of waveforms $M \to \infty$, provided that the SNR per bit exceeds the Shannon limit of $SNR_b \geq -1.6$ dB [Vit79]. In the limit, Shannon's result indicates that extremely wideband signals could be used to achieve error free communications, as long as sufficient SNR exists. Error control coding waveforms, on the other hand, have bandwidth expansion factors that grow only linearly with the code block length. Error correction coding thus offers advantages in bandwidth limited applications, and also provides link protection in power limited applications.

A channel coder operates on digital message (or source) data by encoding the source information into a code sequence for transmission through the channel. There are two basic types of error correction and detection codes: *block codes* and *convolutional codes.*

6.14 Block Codes

Block codes are *forward error correction* (FEC) codes that enable a limited number of errors to be detected and corrected without retransmission. Block codes can be used to improve the performance of a communications system when other means of improvement (such as increasing transmitter power or using a more sophisticated demodulator) are impractical.

In block codes, parity bits are added to blocks of message bits to make *codewords* or *code blocks.* In a block encoder, k information bits are encoded into n code bits. A total of $n-k$ redundant bits are added to the k information bits for the purpose of detecting and correcting errors [Lin83]. The block code is referred to as an (n, k) code, and the rate of the code is defined as $R_c = k/n$ and is equal to the rate of information divided by the raw channel rate.

The ability of a block code to correct errors is a function of the *code distance.* Many families of codes exist that provide varying degrees of error protection [Cou93], [Hay94], [Lin83], [Skl93], and [Vit79].

Example 6.5

Interleavers and block codes are typically combined for wireless speech transmission. Consider an interleaver with m rows and n-bit words. Assume each word of the interleaver is actually made up of k source bits and $(n\text{-}k)$ bits from a block code. The resulting interleaver/coder combination will break up a burst of channel errors of length $l = mb$ into m bursts of length b.

Thus an (n, k) code that can handle burst errors of length $b < (n-k)/2$ can be combined with an interleaver of degree m to create an interleaved (mn,mk) block code that can handle bursts of length mb. As long as mb or fewer bits are corrupted during the transmission of the coded speech signal from the interleaver, the received data will be error free.

Besides the code rate, other important parameters are the distance and the weight of a code. These are defined below.

Distance of a Code — The distance of a codeword is the number of elements in which two codewords C_i and C_j differ

$$d(C_i, C_j) = \sum_{l=1}^{N} C_{i,l} \oplus C_{j,l} \, (modulo-q) \tag{6.84}$$

where d is the distance of the codeword and q is the number of possible values of C_i and C_j. If the code used is binary, the distance is known as the *Hamming distance*. The minimum distance d_{min} is the smallest distance for the given set and is given as

$$d_{min} = Min\{d(C_i, C_j)\} \tag{6.85}$$

Weight of a Code — The weight of a codeword is given by the number of nonzero elements in the codeword. For a binary code, the weight is basically the number of 1's in the codeword and is given as

$$w(C_i) = \sum_{l=1}^{N} C_{i,l} \tag{6.86}$$

Properties of Block Codes

Linearity — Suppose C_i and C_j are two code words in an (n, k) block code. Let α_1 and α_2 be any two elements selected from the alphabet. Then the code is said to be linear if and only if $\alpha_1 C_1 + \alpha_2 C_2$ is also a code word. A linear code must contain the all-zero code word. Consequently, a constant-weight code is nonlinear.

Systematic — A systematic code is one in which the parity bits are appended to the end of the information bits. For an (n, k) code, the first k bits are identical to the information bits, and the remaining $n-k$ bits of each code word are linear combinations of the k information bits.

Cyclic — Cyclic codes are a subset of the class of linear codes which satisfy the following cyclic shift property: If $C = [c_{n-1}, c_{n-2}, ..., c_0]$ is a code word of a cyclic code, then $[c_{n-2}, c_{n-3}, ..., c_0, c_{n-1}]$, obtained by a cyclic shift of the elements of C, is also a code word. That is, all cyclic shifts of C are code words. As a consequence of the cyclic property, the codes possess a considerable amount of structure which can be exploited in the encoding and decoding operations.

Encoding and decoding techniques make use of the mathematical constructs know as *finite fields*. Finite fields are algebraic systems which contain a finite set of elements. Addition, subtraction, multiplication, and division of finite field elements is accomplished without leaving the set (i.e., the sum/product of two field elements is a field element). Addition and multiplication must satisfy the commutative, associative, and distributive laws. A formal definition of a finite field is given below:

Let F be a finite set of elements on which two binary operations — addition and multiplication are defined. The set F together with the two binary operations is a field if the following conditions are satisfied:

- F is a commutative group under addition. The identity element with respect to addition is called the *zero* element and is denoted by 0.
- The set of nonzero elements in F is a commutative group under multiplication. The identity element with respect to multiplication is called the *unit* element and is denoted by 1.
- Multiplication is distributive over addition; that is, for any three elements a, b, and c in F.

$$a \cdot (b + c) = a \cdot b + a \cdot c$$

The *additive inverse* of a field element a, denoted by $-a$, is the field element which produces the sum 0 when added to a $[a + (-a) = 0]$. The multiplicative inverse of a, denoted by a^{-1}, is the field element which produces the product 1 when multiplied by a $[a \cdot a^{-1} = 1]$.

Four basic properties of fields can be derived from the definition of a field. They are as follows:

Property I: $a \cdot 0 = 0 = 0 \cdot a$

Property II: For nonzero field elements a and b, $a \cdot b \neq 0$

Property III: $a \cdot b = 0$ and $a \neq 0$ imply $b = 0$

Property IV: $-(a \cdot b) = (-a) \cdot b = a \cdot (-b)$

For any prime number p, there exists a finite field which contains p elements. This prime field is denoted as $GF(p)$ because finite fields are also called *Galois fields*, in honor of their discoverer [Lin83]. It is also possible to extend the prime field $GF(p)$ to a field of p^m elements which is called an *extension field* of $GF(p)$ and is denoted by $GF(p^m)$, where m is a positive integer. Codes with symbols from the binary field $GF(2)$ or its extension field $GF(2^m)$ are most commonly used in digital data transmission and storage systems, since information in these systems is always encoded in binary form in practice.

In binary arithmetic, modulo-2 addition and multiplication are used. This arithmetic is actually equivalent to ordinary arithmetic except that 2 is considered equal to 0 $(1 + 1 = 2 = 0)$. Note that since 1+1 = 0, 1= -1, and hence for the arithmetic used to generate error control codes, addition is equivalent to subtraction.

Reed-Solomon codes make use of nonbinary field $GF(2^m)$. These fields have more than 2 elements and are extensions of the binary field $GF(2) = \{0, 1\}$. The additional elements in the extension field $GF(2^m)$ cannot be 0 or 1 since all of the elements are unique, so a new symbol α is used to represent the other elements in the field. Each nonzero element can be represented by a power of α.

The multiplication operation " $\cdot$ " for the extension field must be defined so that the remaining elements of the field can be represented as sequence of powers of α. The multiplication operation can be used to produce the *infinite* set of elements F shown below

$$F = \{0, 1, \alpha, \alpha^2, ..., \alpha^j, ...\} = \{0, \alpha^0, \alpha^1, \alpha^2, ..., \alpha^j, ...\} \tag{6.87}$$

To obtain the *finite* set of elements of $GF(2^m)$ from F, a condition must be imposed on F so that it may contain only 2^m elements and is a closed set under multiplication (i.e., multiplication of two field elements is performed without leaving the set). The condition which closes the set of field elements under multiplication is known as the irreducible polynomial, and it typically takes the following form [Rhe89]:

$$\alpha^{(2^m-1)} + 1 = 0 \text{ or equivalently } \alpha^{(2^m-1)} = 1 = \alpha^0 \tag{6.88}$$

Using the irreducible polynomial, any element which has a power greater than $2^m - 2$ can be reduced to an element with a power less than $2^m - 2$ as follows:

$$\alpha^{(2^m+n)} = \alpha^{(2^m-1)} \cdot \alpha^{n+1} = \alpha^{n+1} \tag{6.89}$$

The sequence of elements F thus becomes the following sequence F^*, whose nonzero terms are closed under multiplication:

$$F^* = \{0, 1, \alpha, \alpha^2, ..., \alpha^{2^m-2}, \alpha^{2^m-1}, \alpha^{2^m}, ...\} \tag{6.90}$$

$$= \{0, \alpha^0, \alpha^1, \alpha^2, ..., \alpha^{2^m-2}, \alpha^0, \alpha, \alpha^2, ...\}$$

Take the first 2^m terms of F^* and you have the elements of the finite field $GF(2^m)$ in their *power representation*

$$GF(2^m) = \{0, 1, \alpha, \alpha^2, ..., \alpha^{2^m-2}\} = \{0, \alpha^0, \alpha, \alpha^2, ..., \alpha^{2^m-2}\} \tag{6.91}$$

It can be shown that each of the 2^m elements of the finite field can be represented as a distinct polynomial of degree $m-1$ or less (the element 0 is represented by the *zero polynomial*, a polynomial with no nonzero terms) [Rhe89]. Each of the nonzero elements of $GF(2^m)$, can be denoted as a polynomial $a_i(x)$, where at least one of the m coefficients is nonzero.

$$\alpha^i = a_i(x) = a_{i,0} + a_{i,1}x + a_{i,2}x^2 + ... + a_{i,m-1}x^{m-1} \tag{6.92}$$

Addition of two elements of the finite field is then defined as the modulo-2 addition of each of the polynomial coefficients of like powers, as shown below.

$$\alpha^i + \alpha^j = (a_{i,0} + a_{j,0}) + (a_{i,1} + a_{j,1})x + ... + (a_{i,m-1} + a_{j,m-1})x^{m-1} \tag{6.93}$$

Thus $GF(2^m)$ may be constructed, and using equations (6.92) and (6.93) the polynomial representation for the 2^m elements of the field may be obtained.

6.14.1 Examples of Block Codes

Hamming Codes

Hamming codes were among the first of the nontrivial error correction codes [Ham50]. These codes and their variations have been used for error control in digital communication systems. There are both binary and nonbinary Hamming codes. A binary Hamming code has the property that

$$(n, k) = (2^m - 1, 2^m - 1 - m) \tag{6.94}$$

where k is the number of information bits used to form a n bit codeword, and m is any positive integer. The number of parity symbols are $n-k = m$.

Hadamard Codes

Hadamard codes are obtained by selecting as codewords the rows of a Hadamard matrix. A Hadamard matrix A is a $N \times N$ matrix of 1s and 0s such that each row differs from any other row in exactly $N/2$ locations. One row contains all zeros with the remainder containing $N/2$ zeros and $N/2$ ones. The minimum distance for these codes is $N/2$.

For $N = 2$, the Hadamard matrix A is

$$A = \begin{bmatrix} 0 & 0 \\ 0 & 1 \end{bmatrix} \tag{6.95}$$

In addition to the special case considered above when $N = 2^m$ (m being a positive integer), Hadamard codes of other block lengths are possible, but the codes are not linear.

Golay Codes

Golay codes are linear binary (23,12) codes with a minimum distance of 7 and a error correction capability of 3 bits [Gol49]. This is a special, one of a kind code in that this is the only nontrivial example of a perfect code. Every codeword

lies within distance 3 of any codeword, thus making maximum likelihood decoding possible.

Cyclic Codes

Cyclic codes are a subset of the class of linear codes which satisfy the cyclic property as discussed before. As a result of this property, these codes possess a considerable amount of structure which can be exploited.

A cyclic code can be generated by using a generator polynomial $g(p)$ of degree $(n - k)$. The generator polynomial of an (n, k) cyclic code is a factor of $p^n + 1$ and has the general form

$$g(p) = p^{n-k} + g_{n-k-1}p^{n-k-1} + \ldots\ldots + g_1 p + 1 \tag{6.96}$$

A message polynomial $x(p)$ can also be defined as

$$x(p) = x_{k-1}p^{k-1} + \ldots\ldots + x_1 p + x_0 \tag{6.97}$$

where $(x_{k-1}, \ldots., x_0)$ represents the k information bits. The resultant codeword $c(p)$ can be written as

$$c(p) = x(p)g(p) \tag{6.98}$$

where $c(p)$ is a polynomial of degree less than n.

Encoding for a cyclic code is usually performed by a linear feedback shift register based on either the generator or parity polynomial.

BCH Codes

BCH cyclic codes are among the most important block codes since they exist for a wide range of rates, achieve significant coding gains, and can be implemented even at high speeds [Bos60]. The block length of the codes is $n = 2^m - 1$ for $m \geq 3$, and the number of errors that they can correct is bounded by $t < (2^m - 1)/2$. The binary BCH codes can be generalized to create classes of nonbinary codes which use m bits per code symbol. The most important and common class of nonbinary BCH codes is the family of codes known as Reed-Solomon codes. The (63,47) Reed-Solomon code in U.S. *Cellular Digital Packet Data* (CDPD) uses $m = 6$ bits per code symbol.

Reed-Solomon Codes

Reed-Solomon (RS) are nonbinary codes which are capable of correcting errors which appear in bursts and are commonly used in concatenated coding systems [Ree60]. The block length of these codes is $n = 2^m - 1$. These can be extended to 2^m or $2^m + 1$. The number of parity symbols that must be used to correct e errors is $n - k = 2e$. The minimum distance $d_{min} = 2e + 1$. RS codes achieve the largest possible d_{min} of any linear code.

6.14.2 Case Study of Reed-Solomon Codes

For the purpose of explanation, the field choice will be $GF(64)$, since this is the same field used in CDPD systems. In this case, $m = 6$, so each of the 64 field elements is represented by a 6 bit symbol.

A finite field entity $p(X)$ is introduced in order to map the 64 distinct 6-bit symbols to the elements of the field. An irreducible polynomial $p(X)$ of degree m is said to be *primitive* if the smallest integer n for which $p(X)$ divides $X^n + 1$ is $n = 2^m - 1$. This primitive polynomial $p(X)$ is typical of the form

$$p(X) = 1 + X + X^m \tag{6.99}$$

In the case of the Reed-Solomon code used for CDPD, this is indeed the form of $p(X)$. Regardless, these polynomials have been tabulated for a wide range of field sizes, so $p(X)$ should be considered a known quantity. CDPD's primitive polynomial is

$$p_{CDPD}(X) = 1 + X + X^6 \tag{6.100}$$

In order to map symbols to field elements, set the primitive polynomial $p(\alpha) = 0$. This yields the following result, which closes the set of field elements:

$$\alpha^6 + \alpha + 1 = 0 \tag{6.101}$$

Table 6.2 shows the proper mapping of 6 bit symbols to field elements. These elements were generated by starting with the element $1(\alpha^0)$ and multiplying by α to obtain the next field element. Any element which contains an α^5 term will yield an α^6 term in the next element, but α^6 is not in $GF(64)$. The primitive polynomial rule is used to convert α^6 to $\alpha + 1$. Also note that $\alpha^{62} \cdot \alpha = \alpha^{63} = \alpha^0 = 1$. This simple result is critical when implementing finite field multiplication in software. Multiplication can be accomplished quickly and efficiently by using modulo $2^m - 1$ addition of the powers of the elemental operands. For the 63, 47 Reed-Solomon code used in CDPD systems, multiplication of two field elements corresponds to adding the powers of the two operands modulo-63 to arrive at the power of the product.

Addition in $GF(2^m)$ corresponds to modulo-2 adding the coefficients of the polynomial representation of the elements. Since the coefficients are either 1's or 0's (because the field is an extension of the binary field $GF(2)$), this can simply be implemented with the bit-wise exclusive-OR of the 6 bit symbol representation of the elemental operands. Some examples of finite field addition in $GF(64)$ are shown below.

$$\alpha^{27} + \alpha^5 = (001110)_2 XOR (100000)_2 = (101110)_2 = \alpha^{55} \tag{6.102.a}$$

$$\alpha^{19} + \alpha^{62} = (011110)_2 XOR (100001)_2 = (111111)_2 = \alpha^{58} \tag{6.102.b}$$

6.14.2.1 Reed-Solomon Encoding

In the discussion of a Reed Solomon encoder, the following polynomials are used frequently:

$d(x)$: raw information polynomial
$p(x)$: parity polynomial
$c(x)$: codeword polynomial
$g(x)$: generator polynomial
$q(x)$: quotient polynomial
$r(x)$: remainder polynomial

Let

$$d(x) = c_{n-1}x^{n-1} + c_{n-2}x^{n-2} + ... + c_{2t+1}x^{2t+1} + c_{2t}x^{2t} \tag{6.103}$$

be the information polynomial and

$$p(x) = c_0 + c_1x + ... + c_{2t-1}x^{2t-1} \tag{6.104}$$

be the parity polynomial (c_i are all elements of *GF(64)*). The encoded RS polynomial can thus be expressed as

$$c(x) = d(x) + p(x) = \sum_{i=0}^{n-1} c_i x^i \tag{6.105}$$

A vector of n field elements $(c_0, c_1, ..., c_{n-1})$ is a code word if and only if it is a multiple of the generator polynomial *g(x)*. The generator polynomial for a t-error, correcting, Reed-Solomon code has the form

$$g(x) = (x+\alpha)(x+\alpha^2).....(x+\alpha^{2t}) = \sum_{i=0}^{2t} g_i x^i \tag{6.106}$$

A common method for encoding a cyclic code is to derive $p(x)$ by dividing $d(x)$ by *g(x)*. This yields an irrelevant quotient polynomial $q(x)$ and an important polynomial $r(x)$ as follows:

$$d(x) = g(x)q(x) + r(x) \tag{6.107}$$

Thus the codeword polynomial can be expressed as

$$c(x) = p(x) + g(x)q(x) + r(x) \tag{6.108}$$

If the parity polynomial is defined as being equal to the negatives of the coefficients of *r(x)*, then it follows that

$$c(x) = g(x)q(x) \tag{6.109}$$

Thus ensuring that the codeword polynomial is a multiple of the generator polynomial, a Reed-Solomon encoder can be constructed by performing the above division process to obtain *p(X)*. The straightforward method of obtaining the remainder from the division process by the monic polynomial $g(x)$ is to connect a shift register according to $g(x)$ as shown in Figure 6.18. Each "+" represents

Table 6.2 Three Representations of the Elements of GF(64)

Power Representation	Polynomial Representation	6-Bit Symbol Representation
$0 = \alpha^{63}$	0	0 0 0 0 0 0
$1 = \alpha^{0}$	1	0 0 0 0 0 1
α	x^1	0 0 0 0 1 0
α^2	x^2	0 0 0 1 0 0
α^3	x^3	0 0 1 0 0 0
α^4	x^4	0 1 0 0 0 0
α^5	x^5	1 0 0 0 0 0
α^6	$x^1 + 1$	0 0 0 0 1 1
α^7	$x^2 + x^1$	0 0 0 1 1 0
α^8	$x^3 + x^2$	0 0 1 1 0 0
α^9	$x^4 + x^3$	0 1 1 0 0 0
α^{10}	$x^5 + x^4$	1 1 0 0 0 0
α^{11}	$x^5 + x^1 + 1$	1 0 0 0 1 1
α^{12}	$x^2 + 1$	0 0 0 1 0 1
α^{13}	$x^3 + x^1$	0 0 1 0 1 0
α^{14}	$x^4 + x^2$	0 1 0 1 0 0
α^{15}	$x^5 + x^3$	1 0 1 0 0 0
α^{16}	$x^4 + x^1 + 1$	0 1 0 0 1 1
α^{17}	$x^5 + x^2 + x^1$	1 0 0 1 1 0
α^{18}	$x^3 + x^2 + x^1 + 1$	0 0 1 1 1 1
α^{19}	$x^4 + x^3 + x^2 + x^1$	0 1 1 1 1 0
α^{20}	$x^5 + x^4 + x^3 + x^2$	1 1 1 1 0 0
α^{21}	$x^5 + x^4 + x^3 + x^1 + 1$	1 1 1 0 1 1
α^{22}	$x^5 + x^4 + x^2 + 1$	1 1 0 1 0 1
α^{23}	$x^5 + x^3 + 1$	1 0 1 0 0 1
α^{24}	$x^4 + 1$	0 1 0 0 0 1
α^{25}	$x^5 + x^1$	1 0 0 0 1 0
α^{26}	$x^2 + x^1 + 1$	0 0 0 1 1 1
α^{27}	$x^3 + x^2 + x^1$	0 0 1 1 1 0
α^{28}	$x^4 + x^3 + x^2$	0 1 1 1 0 0
α^{29}	$x^5 + x^4 + x^3$	1 1 1 0 0 0
α^{30}	$x^5 + x^4 + x^1 + 1$	1 1 0 0 1 1
α^{31}	$x^5 + x^2 + 1$	1 0 0 1 0 1
α^{32}	$x^3 + 1$	0 0 1 0 0 1
α^{33}	$x^4 + x^1$	0 1 0 0 1 0
α^{34}	$x^5 + x^2$	1 0 0 1 0 0
α^{35}	$x^3 + x^1 + 1$	0 0 1 0 1 1
α^{36}	$x^4 + x^2 + x^1$	0 1 0 1 1 0
α^{37}	$x^5 + x^3 + x^2$	1 0 1 1 0 0
α^{38}	$x^4 + x^3 + x^1 + 1$	0 1 1 0 1 1
α^{39}	$x^5 + x^4 + x^2 + x^1$	1 1 0 1 1 0
α^{40}	$x^5 + x^3 + x^2 + x^1 + 1$	1 0 1 1 1 1
α^{41}	$x^4 + x^3 + x^2 + 1$	0 1 1 1 0 1
α^{42}	$x^5 + x^4 + x^3 + x^1$	1 1 1 0 1 0
α^{43}	$x^5 + x^4 + x^2 + x^1 + 1$	1 1 0 1 1 1
α^{44}	$x^5 + x^3 + x^2 + 1$	1 0 1 1 0 1
α^{45}	$x^4 + x^3 + 1$	0 1 1 0 0 1
α^{46}	$x^5 + x^4 + x^1$	1 1 0 0 1 0
α^{47}	$x^5 + x^2 + x^1 + 1$	1 0 0 1 1 1
α^{48}	$x^3 + x^2 + 1$	0 0 1 1 0 1
α^{49}	$x^4 + x^3 + x^1$	0 1 1 0 1 0
α^{50}	$x^5 + x^4 + x^2$	1 1 0 1 0 0
α^{51}	$x^5 + x^3 + x^1 + 1$	1 0 1 0 1 1
α^{52}	$x^4 + x^2 + 1$	0 1 0 1 0 1
α^{53}	$x^5 + x^3 + x^1$	1 0 1 0 1 0
α^{54}	$x^4 + x^2 + x^1 + 1$	0 1 0 1 1 1
α^{55}	$x^5 + x^3 + x^2 + x^1$	1 0 1 1 1 0
α^{56}	$x^4 + x^3 + x^2 + x^1 + 1$	0 1 1 1 1 1
α^{57}	$x^5 + x^4 + x^3 + x^2 + x^1$	1 1 1 1 1 0
α^{58}	$x^5 + x^4 + x^3 + x^2 + x^1 + 1$	1 1 1 1 1 1
α^{59}	$x^5 + x^4 + x^3 + x^2 + 1$	1 1 1 1 0 1
α^{60}	$x^5 + x^4 + x^3 + 1$	1 1 1 0 0 1
α^{61}	$x^5 + x^4 + 1$	1 1 0 0 0 1
α^{62}	$x^5 + 1$	1 0 0 0 0 1

an exclusive-OR of two m-bit numbers, each X represents a multiplication of two m-bit numbers under $GF(2^m)$, and each m-bit register contains an m-bit number denoted by b_i.

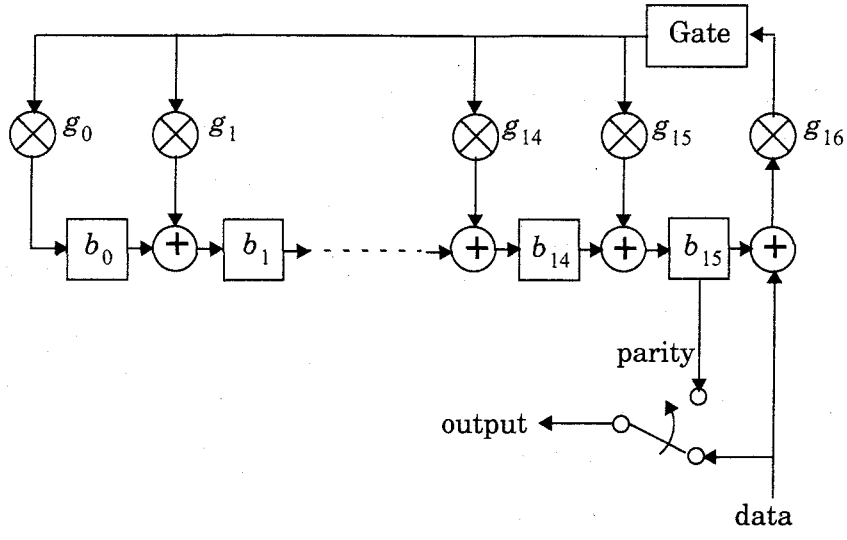

Figure 6.18
Reed-Solomon encoding circuit.

Initially, all registers are set to 0, and the switch is set to the data position. Code symbols c_{n-1} through c_{n-k} are sequentially shifted into the circuit and simultaneously transmitted to the output line. As soon as code symbol c_{n-k} enters the circuit, the switch is flipped to the parity position, and the gate to the feedback network is opened so that no further feedback is provided. At that same instant, the registers b_0 through b_{2t-1} contain the parity symbols p_0 through p_{2t-1} which correspond directly to the coefficients of the parity polynomial. They can be sequentially shifted to the output to complete the Reed-Solomon encoding process.

6.14.2.2 Reed Solomon Decoding

Suppose that a codeword

$$c(x) = v_0 + v_1 x + ... + v_{n-1} x^{n-1} \tag{6.110}$$

is transmitted and that channel errors result in the received codeword

$$r(x) = r_0 + r_1 x + ... + r_{n-1} x^{n-1} \tag{6.111}$$

The error pattern $e(x)$ is the difference between $c(x)$ and $r(x)$. Using equations (6.110) and (6.111),

$$e(x) = r(x) - c(x) = e_0 + e_1 x + ... + e_{n-1} x^{n-1} \tag{6.112}$$

Let the $2t$ *partial syndromes* S_i, $1 < i \leq 2t$, be defined as $S_i = r(\alpha^i)$. Since $\alpha^1, \alpha^2, ..., \alpha^{2t}$ are roots of each transmitted codeword $c(x)$ (because each codeword is a multiple of the generator polynomial $g(x)$), it follows that $c(\alpha^i) = 0$

and $S_i = c(\alpha^i) + e(\alpha^i) = e(\alpha^i)$. Thus, it is clear that the $2t$ partial syndromes S_i depend only on the error pattern $e(x)$ and not on the specific received codeword *r(x)*.

Suppose the error pattern contains k errors $(k \le t)$ at locations $x^{j_1}, x^{j_2}, \ldots\ldots, x^{j_k}$, where $0 \le j_1 < j_2 < \ldots\ldots < j_k < n-1$. Let the error magnitude at each location x^{j_i} be denoted as e_{j_i}. Then $e(x)$ has the form:

$$e(x) = e_{j_1} x^{j_1} + e_{j_2} x^{j_2} + \ldots\ldots + e_{j_k} x^{j_k} \tag{6.113}$$

Define the set of error locator numbers $\beta_i = \alpha^{j_i}$, i = 1,2,.....,k. Then the set of $2t$ partial syndromes yields the following system of equations:

$$S_1 = e_{j_1}\beta_1 + e_{j_2}\beta_2 + \ldots\ldots + e_{j_k}\beta_k \tag{6.114.a}$$

$$S_2 = e_{j_1}\beta_1^2 + e_{j_2}\beta_2^2 + \ldots\ldots + e_{j_k}\beta_k^2 \tag{6.114.b}$$

$$\ldots\ldots\ldots\ldots$$

$$S_{2t} = e_{j_1}\beta_1^{2t} + e_{j_2}\beta_2^{2t} + \ldots\ldots + e_{j_k}\beta_k^{2t} \tag{6.114.c}$$

Any algorithm which solves this system of equations is a Reed-Solomon decoding algorithm. The error magnitudes e_{j_i} are found directly, and the error locations x^{j_i} can be determined from β_i.

Reed-Solomon decoders can be implemented in hardware, software, or a mix of hardware and software. Hardware implementations are typically very fast, but they cannot be used for a wide variety of Reed-Solomon code sizes. For example, there are several single-chip, Reed-Solomon decoders available which decode codes commonly used in satellite communications, digital video applications, and compact disk technology. These hardware decoders can operate at rates up to 10 Mbits per second. However, since this specific family of codes operates on 8-bit symbols from $GF(255)$, the $(63, 47)$ Reed-Solomon code used in CDPD systems cannot be decoded with these chips. Since CDPD operates at the much slower rate of 19.2 kbps, a real-time software implementation of a $(63, 47)$ Reed-Solomon decoder can be achieved. A software approach may be more attractive to a CDPD system developer, because it will have a shorter development time, lower development cost, and greater flexibility.

A typical Reed-Solomon decoder uses five distinct algorithms. The first algorithm calculates the $2t$ partial syndromes S_i. The second step in the RS decoding process is the Berlekamp-Massey algorithm which calculates the error locator polynomial $\sigma(x)$. This polynomial is a function of the error locations in the received codeword *r(x)*, but it does not directly indicate which symbols of the received codeword are in error. A Chien search algorithm is then used to calculate these specific error locations from the error locator polynomial. The fourth

step in the decoding process is the calculation of the magnitude of the error at each location. Finally, knowing both the error locations in the received codeword and the magnitude of the error at each location, an error correction algorithm may be implemented to correct up to t errors successfully [Rhe89].

Syndrome Calculation

The syndrome of a cyclic code is typically defined as the remainder obtained by dividing the received codeword $r(x)$ by the generator polynomial *g(x)*. However, for Reed-Solomon codes, $2t$ *partial syndromes* are computed. Each partial syndrome S_i is defined as the remainder obtained when dividing the received codeword $r(x)$ by $x + \alpha^i$.

$$S_i = rem\left[\frac{r(x)}{x+\alpha^i}\right], \; i = 1, 2, ..., 2t \tag{6.115}$$

The division of two polynomials results in a quotient polynomial $q(x)$ and a remainder polynomial *rem(x)*. The degree of the remainder $rem(x)$ must be less than the degree of the dividing polynomial *p(x)*. Thus, if $p(x)$ has degree 1 (i.e., $p(x) = x + \alpha^i$), $rem(x)$ must have degree 0. In other words, $rem(x)$ is simply a field element and can be denoted as *rem*. Thus the determination of the $2t$ partial syndromes begins with the calculation

$$\frac{r(x)}{x+\alpha^i} = q(x) + \frac{rem}{x+\alpha^i} \tag{6.116}$$

Rearranging the above equation yields

$$r(x) = q(x) \cdot (x+\alpha^i) + rem \tag{6.117}$$

Letting $x = \alpha^i$,

$$\begin{aligned} r(\alpha^i) &= q(\alpha^i) \cdot (\alpha^i + \alpha^i) + rem \\ &= rem = S_i \end{aligned} \tag{6.118}$$

Thus, the calculation of the $2t$ partial syndromes S_i can be simplified from a full-blown polynomial division (which is computationally intense) to merely evaluating the received polynomial $r(x)$ at $x = \alpha^i$ [Rhe89]:

$$S_i = r(\alpha^i), \; i = 1, 2, ..., 2t \tag{6.119}$$

Also

$$r(x) = r_0 + r_1 x + ... + r_{n-1} x^{n-1} \tag{6.120}$$

Thus $r(\alpha^i)$ has the form

$$r(\alpha^i) = r_0 + r_1 \alpha^i + r_2 \alpha^{2i} + ... + r_{n-1} \alpha^{(n-1)i} \tag{6.121}$$

The evaluation of $r(\alpha^i)$ can be implemented very efficiently in software by arranging the function so that it has the following form

$$r(\alpha^i) = \Big(\ldots\ldots \Big(\Big(r_{n-1}\alpha^i + r_{n-2} \Big)\alpha^i + r_{n-3} \Big)\alpha^i + \ldots\ldots \Big)\alpha^i + r_0 \qquad (6.122)$$

Error Locator Polynomial Calculation

The Reed-Solomon decoding process is simply any implementation which solves equations (6.114.a) through (6.114.c). These $2t$ equations are symmetric function in $\beta_1, \beta_2, \ldots\ldots, \beta_k$, known as *power-sum symmetric functions*. We now define the polynomial

$$\sigma(x) = (1 + \beta_1 x)(1 + \beta_2 x) \ldots\ldots (1 + \beta_k x) = \sigma_0 + \sigma_1 x + \ldots\ldots + \sigma_k x^k \qquad (6.123)$$

The roots of $\sigma(x)$ are $\beta_1^{-1}, \beta_2^{-1}, \ldots\ldots, \beta_k^{-1}$, which are the inverses of the error location numbers β_i. Thus, $\sigma(x)$ is called the *error locator polynomial* because it indirectly contains the exact locations of each of the errors in $r(x)$. Note that $\sigma(x)$ is an unknown polynomial whose coefficients must also be determined during the Reed-Solomon decoding process.

The coefficients of $\sigma(x)$ and the error-location numbers β_i are related by the following equations

$$\sigma_0 = 1 \qquad (6.124.a)$$

$$\sigma_1 = \beta_1 + \beta_2 + \ldots\ldots + \beta_k \qquad (6.124.b)$$

$$\sigma_2 = \beta_1\beta_2 + \beta_2\beta_3 + \ldots\ldots + \beta_{k-1}\beta_k \qquad (6.124.c)$$

$$\ldots\ldots\ldots\ldots$$

$$\sigma_k = \beta_1\beta_2\beta_3 \ldots\ldots \beta_k \qquad (6.124.d)$$

The unknown quantities σ_i and β_i can be related to the known partial syndromes S_j by the following set of equations known as *Newton's Identities.*

$$S_1 + \sigma_1 = 0 \qquad (6.125.a)$$

$$S_2 + \sigma_1 S_1 + 2\sigma_2 = 0 \qquad (6.125.b)$$

$$S_3 + \sigma_2 S_2 + \sigma_1 S_1 + 3\sigma_3 = 0 \qquad (6.125.c)$$

$$S_k + \sigma_1 S_{k-1} + \ldots\ldots + \sigma_{k-1} S_1 + k\sigma_k = 0 \qquad (6.125.d)$$

The most common method for determining $\sigma(x)$ is the Berlekamp-Massey algorithm [Lin83].

6.15 Convolutional Codes

Convolutional codes are fundamentally different from block codes in that information sequences are not grouped into distinct blocks and encoded [Vit79]. Instead a continuous sequence of information bits is mapped into a continuous sequence of encoder output bits. This mapping is highly structured enabling a decoding method considerably different from that of block codes to be employed.

It can be argued that convolutional coding can achieve a larger coding gain than can be achieved using a block coding with the same complexity.

A convolutional code is generated by passing the information sequence through a finite state shift register. In general, the shift register contains $N(k\ bit)$ stages and m linear algebraic function generators based on the generator polynomials as shown in Figure 6.19. The input data is shifted into and along the shift register k bits at a time. The number of output bits for each k bit input data sequence is n bits. The code rate $R_C = k/n$. The parameter N is called the constraint length and indicates the number of input data bits that the current output is dependent upon. It determines how powerful and complex the code is. Following, is an outline of the various ways of representing convolutional codes,

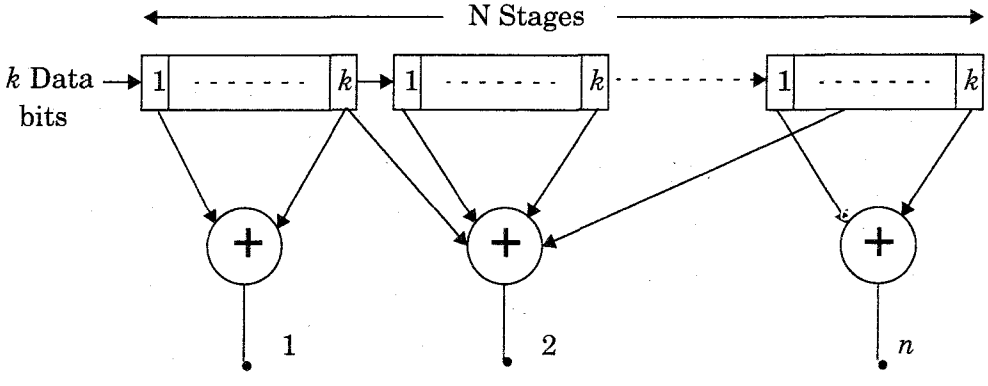

Figure 6.19
General block diagram of convolutional encoder.

Generator Matrix — The generator matrix for a convolutional code is semi-infinite since the input is semi-infinite in length. Hence, this may not be a convenient way of representing a convolutional code.

Generator Polynomials — Here, we specify a set of n vectors, one for each of the n modulo-2 adders used. Each vector of dimension $2k$ indicates the connection of the encoder to that modulo-2 adder. A 1 in the i th position of the vector indicates that the corresponding shift register stage is connected and a 0 indicates no connection.

Logic Table — A logic table can be built showing the outputs of the convolutional encoder and the state of the encoder for the input sequence present in the shift register.

State Diagram — Since the output of the encoder is determined by the input and the current state of the encoder, a state diagram can be used to represent the encoding process. The state diagram is simply a graph of the possible states of the encoder and the possible transitions from one state to another.

Tree Diagram — The tree diagram shows the structure of the encoder in the form of a tree with the branches representing the various states and the outputs of the coder.

Trellis Diagram — Close observation of the tree reveals that the structure repeats itself once the number of stages is greater than the constraint length. It is observed that all branches emanating from two nodes having the same state are identical in the sense that they generate identical output sequences. This means that the two nodes having the same label can be merged. By doing this throughout the tree diagram, we can obtain another diagram called a Trellis diagram which is a more compact representation.

6.15.1 Decoding of Convolutional Codes

The function of the decoder is to estimate the encoded input information using a rule or method that results in the minimum possible number of errors. There is a one-to-one correspondence between the information sequence and the code sequence. Further, any information and code sequence pair is uniquely associated with a path through the trellis. Thus, the job of the convolutional decoder is to estimate the path through the trellis that was followed by the encoder.

There are a number of techniques for decoding convolutional codes. The most important of these methods is the Viterbi algorithm which performs maximum likelihood decoding of convolutional codes. The algorithm was first described by A.J. Viterbi [Vit67], [For78]. Both hard and soft decision decoding can be implemented for convolutional codes. Soft decision decoding is superior by about 2-3 dB.

6.15.1.1 The Viterbi Algorithm

The Viterbi algorithm can be described as follows:

Let the trellis node corresponding to state S_j at time i be denoted $S_{j,i}$. Each node in the trellis is to be assigned a value $V(S_{j,i})$ based on a metric. The node values are computed in the following manner.

1 Set $V(S_{0,0}) = 0$ and $i = 1$.

2 At time i, compute the partial path metrics for all paths entering each node.

3 Set $V(S_{j,i})$ equal to the smallest partial path metric entering the node corresponding to state S_j at time i. Ties can be broken by previous node choosing a path randomly. The nonsurviving branches are deleted from the trellis. In this manner, a group of minimum paths is created from $S_{0,0}$.

4 If $i < L + m$, where L is the number of input code segments (k bits for each segment) and m is the length of the longest shift register in the encoder, let $i = i + 1$ and go back to step 2.

Once all node values have been computed, start at state S_0, time $i = L + m$, and follow the surviving branches backward through the trellis. The path thus defined is unique and corresponds to the decoded output. When hard decision decoding is performed, the metric used is the Hamming distance, while the Euclidean distance is used for soft decision decoding.

6.15.1.2 Other Decoding Algorithms for Convolutional Codes

Fano's Sequential Decoding

Fano's algorithm searches for the most probable path through the trellis by examining one path at a time [Fan63]. The increment added to the metric along each branch is proportional to the probability of the received signal for that branch, as in Viterbi decoding, with the exception that an additional negative constant is added to each branch metric. The value of this constant is selected such that the metric for the correct path will increase on the average while the metric for any incorrect path will decrease on the average. By comparing the metric of a candidate path with an increasing threshold, the algorithm detects and discards incorrect paths. The error rate performance of the Fano algorithm is comparable to that of Viterbi decoding. However, in comparison to Viterbi decoding, sequential decoding has a significantly larger delay. It's advantages over Viterbi decoding is that it requires less storage, and thus codes with larger constraint lengths can be employed.

The Stack Algorithm

In contrast to the Viterbi algorithm which keeps track of $2^{(N-1)k}$ paths and their corresponding metrics, the stack algorithm deals with fewer paths and their corresponding metrics. In a stack algorithm, the more probable paths are ordered according to their metrics, with the path at the top of the stack having the largest metric. At each step of the algorithm, only the path at the top of the stack is extended by one branch. This yields 2^k successors and their metrics. These 2^k successors along with the other paths are then reordered according to the values of the metrics, and all paths with metrics that fall below some preselected amount from the metric of the top path may be discarded. Then the process of extending the path with the largest metric is repeated. In comparison with Viterbi decoding, the stack algorithm requires fewer metric calculations, but this computational savings is offset to a large extent by the computations involved in reordering the stack after every iteration. In comparison with the Fano algorithm, the stack algorithm is computationally simpler since there is no retracing over the same path, but on the other hand, the stack algorithm requires more storage than the Fano algorithm.

Feedback Decoding

Here, the decoder makes a hard decision on the information bit at stage j based on the metrics computed from stage j to stage $j + m$, where m is a preselected positive integer. Thus the decision on whether the information bit was a 1 or a 0 depends on whether the minimum Hamming distance path which begins

at stage j and ends at stage $j+m$ contains a 0 or 1 in the branch emanating from stage j. Once a decision is made, only that part of the tree which stems from the bit selected at stage j, is kept and the remainder is discarded. This is the feedback feature of the decoder. The next step is to extend the part of the tree that has survived to stage $j+1+m$ and to consider the paths from stage $j+1$ to $j+1+m$ in deciding on the bit at stage $j+1$. This procedure is repeated at every stage. The parameter m is simply the number of stages in the tree that the decoder looks ahead before making a hard decision. Instead of computing the metrics, the feedback decoder can be implemented by computing the syndrome from the received sequence and using a table look up method to correct errors. For some convolutional codes, the feedback decoder can be simplified to a majority logic decoder or a threshold decoder.

6.16 Coding Gain

The advantage of error control codes, whether they be block codes or convolutional codes, is that they provide a *coding gain* for the communications link. The coding gain describes how much better the decoded message performs as compared to the raw bit error performance of the coded transmission. Coding gain is what allows a channel error rate of 10^{-2} to support decoded data rates which are 10^{-5} or better.

Each error control code has a particular coding gain. Depending on the particular code, the decoder implementation, and the channel BER probability, P_c. It can be shown that a good approximation for the decoded message error probability, P_B is given by

$$P_B \cong \frac{1}{n} \sum_{i=t+1}^{n} i \binom{n}{i} P_c^i (1-P_c)^{n-i} \tag{6.126}$$

where t denotes the number of errors that can be corrected in an *(n,k)* block code. Thus, given a known channel BER, it is possible to determine the decoded message error rate easily. The coding gain measures the amount of additional SNR that would be required to provide the same BER performance for an uncoded message signal.

6.17 Trellis Coded Modulation

Trellis coded modulation (TCM) is a technique which combines both coding and modulation to achieve significant coding gains without compromising bandwidth efficiency [Ung87]. TCM schemes employ redundant nonbinary modulation in combination with a finite state encoder which decides the selection of modulation signals to generate coded signal sequences. TCM uses signal set expansion to provide redundancy for coding and to design coding and signal mapping functions jointly so as to maximize directly the free distance (minimum

Euclidean distance) between the coded signals. In the receiver, the signals are decoded by a soft decision maximum likelihood sequence decoder. Coding gains as large as 6 dB can be obtained without any bandwidth expansion or reduction in the effective information rate.

Example 6.6

Equalization

The IS-54 standard specifies the use of decision feedback equalizers (DFE).

Diversity

1. The U.S AMPS system makes use of spatial selection diversity.
2. The USDC standard specifies the use of polarization diversity.

Channel Coding

1. The IS-95 standard as proposed makes use of a rate 1/3, constraint length L=9 convolutional code with block interleaving. The interleaver used is a 32*18 block interleaver.
2. The AMPS system makes use of a (40,28) BCH code for the forward channel and a (48,30) BCH code for the reverse channel.

Equalization, diversity, and channel coding, as discussed, have the same goal of improving the reliability and quality of the communication service. Each technique has it's own advantages and disadvantages. The trade-offs to be considered are those of complexity/power/cost versus system performance. Each technique is capable of improving system performance significantly.

6.18 Problems

6.1 Use identical notation described in Section 6.3, except now let $d_k = \sum_{n=0}^{N} w_{nk} y_{nk}$, and verify that the MSE is identical for the multiple input linear filter shown in Figure P6.1 (this structure is used for maximal ratio combining diversity, RAKE receivers, and adaptive antennas).

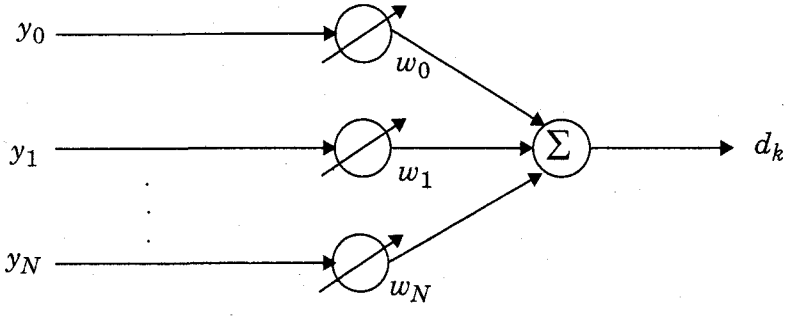

Figure P6.1: Multiple input adaptive linear combiner.

6.2 Consider the two-tap adaptive equalizer shown in Figure P6.2.
(a) Find an expression for MSE in terms of w_0, w_1, and N.
(b) If N>2, find the minimum MSE.

(c) If w_0=0, w_1=-2 and N=4 samples/cycle, what is the MSE?
(d) For parameters in (c), what is the MSE if d_k=2sin(2$\pi k/N$)?

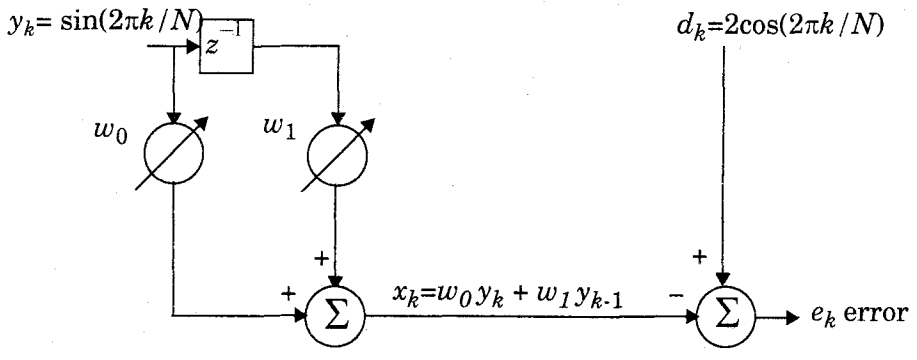

Figure P6.2: A two-tap adaptive linear equalizer.

6.3 For the equalizer in Figure P6.2, what weight values will produce a rms value of ε_k=2? Assume N=5, and express your answer in terms of w_0, and w_1.

6.4 If a digital signal processing chip can perform 1 million multiplications per second, determine the time required between each iteration for the following adaptive equalizer algorithms.
(a) LMS
(b) Kalman RLS
(c) Square root RLS DFE
(d) Gradient lattice DFE

6.5 Suppose a quick rule of thumb is that an RLS algorithm requires 50 iterations to converge, whereas the LMS algorithm requires 1000 iterations. For the DSP chip in Problem 6.4 determine the maximum symbol rate and maximum time interval before retraining if the equalizer requires 10% transmission overhead, and the following Doppler spreads are found in a 1900 MHz channel.
(a) 100 Hz
(b) 1000 Hz
(c) 10,000 Hz
(Hint: Consider the coherence time and its impact on equalizer training).

6.6 Use computer simulation to implement a 2 stage (3 tap) LMS equalizer based on the circuit shown in Figure 6.2. Assume each delay element offers 10 microseconds of delay, and the transmitted baseband signal *x(t)* is a rectangular binary pulse train of alternating 1's and 0's, where each pulse has a duration of 10 microseconds. Assume that *x(t)* passes through a time dispersive channel before being applied to the equalizer. If the channel is a stationary 2-ray channel, with equal amplitude impulses at t=0 and t=15 microseconds, use equations (6.35) — (6.37) to verify that the original *x(t)* can be recreated by the equalizer.
(a) Provide graphical data illustrating the equalizer converges.
(b) Plot the MMSE as a function of the number of iterations.
(c) How many iterations are required to obtain convergence?
(d) What happens if the second ray is placed at t=25 microseconds?
(e) What happens if the second ray is set equal to zero? (This effect is known as equalizer noise, and is the result of using an equalizer when one is not required by the channel).

6.7 Consider a single branch Rayleigh fading signal has a 20% chance of being 6 dB below some mean SNR threshold.
(a) Determine the mean of the Rayleigh fading signal as referenced to the threshold.
(b) Find the likelihood that a two branch selection diversity receiver will be 6 dB below the mean SNR threshold.
(c) Find the likelihood that a three branch selection diversity receiver will be 6 dB below the mean SNR threshold.
(d) Find the likelihood that a four branch selection diversity receiver will be 6 dB below the mean SNR threshold.
(e) Based on your answers above, is there a law of diminishing returns when diversity is used?

6.8 Using computer simulation, reconstruct Figure 6.11 which illustrates the improvements offered by selection diversity.

6.9 Prove that the maximal ratio combining results in equations (6.66) – (6.69) are accurate, and plot the probability distributions of $SNR = \gamma_M$ as a function of γ/Γ for 1, 2, 3, and 4-branch diversity.

6.10 Compare $\bar{\gamma}/\Gamma$ (selection diversity) with $\overline{\gamma_M}/\Gamma$ (maximal ratio combining) for 1 to 6 branches. Specifically, compare how the average SNR increases for each diversity scheme as a new branch is added. Does this make sense? What is the average SNR improvement offered by 6-branch maximal ratio combining as compared to 6-branch selection diversity? If $\gamma/\Gamma = 0.01$, determine the probability that the received signal will be below this threshold for maximal ratio combining and selection diversity (assume 6 branches are used). How does this compare with a single Rayleigh fading channel with the same threshold?

6.11 Extending the diversity concepts in this chapter and using the flat fading BER analysis of Chapter 5, it is possible to determine the BER for a wide range of modulation techniques when selection diversity is applied.
Define γ_0 as the required E_b/N_0 to achieve a specific BER = y in a flat Rayleigh fading channel, and let γ denote the random SNR due to fading. Furthermore let $P(\gamma)$ denote a function that describes the BER for a particular modulation when the $SNR = \gamma$. It follows:

$$y = Pr[P(\gamma) > x] = Pr\left[\gamma < P^{-1}(x)\right] = 1 - e^{(-P^{-1}(x))/\gamma_0}$$

(a) Find an expression that solves γ_0 in terms of $P^{-1}(x)$ and y.
(b) When M uncorrelated fading branches are used for diversity selection, write a new expression for y.
(c) Determine the required average E_b/N_0 for BPSK in order to sustain a 10^{-3} BER in a Rayleigh fading channel.
(d) When 4 branch diversity is used, determine the required average E_b/N_0 for BPSK in order to sustain a 10^{-3} BER in a Rayleigh fading channel.

* * *

APPENDIX F

Abbreviations and Acronyms

A

AC	Access Channel
ACA	Adaptive Channel Allocation
ACF	Autocorrelation function
ACI	Adjacent Channel interference
ACK	Acknowledge
ADM	Adaptive Delta Modulation
ADPCM	Adaptive Digital Pulse Code Modulation
AGCH	Access Grant Channel
AIN	Advanced Intelligent Network
AM	Amplitude Modulation
AMPS	Advanced Mobile Phone System
ANSI	American National Standards Institute
APC	Adaptive Predictive Coding
ARDIS	Advance Radio Data Information Systems
ARFCN	Absolute Radio Frequency Channel Numbers
ARQ	Automatic Repeat Request
ATC	Adaptive Transform Coding
ATM	Asynchronous Transfer Mode
AUC	Authentication Center
AWGN	Additive White Gaussian Noise

B

BER	Bit Error Rate
BERSIM	Bit Error Rate Simulator

BCH Bose-Chaudhuri-Hocquenghem, also Broadcast Channel
BCCH Broadcast Control Channel
BFSK Binary Frequency Shift Keying
BISDN Broadband Integrated Services Digital Network
BIU Base Station Interface Unit
BOC Bell Operating Company
BPSK Binary Phase Shift Keying
BRI Basic Rate Interface
BSC Base Station Controller
BSIC Base Station Identity Code
BSS Base Station Subsystem
BT 3 dB bandwidth-bit-duration product for GMSK
BTA Basic Trading Area
BTS Base Transceiver Station

C

CAI Common Air Interface
CB Citizens Band
CCCH Common Control Channel
CCH Control Channel
CCI Co-channel Interference
CCIR Consultative Committee for International Radiocommunications
CCITT International Telgraph and Telephone Consultative Committee
CCS Common Channel Signaling
CD Collision Detection
CDF Cumulative Distribution Function
CDMA Code Division Multiple Access
CDPD Cellular Digital Packet Data
CDVCC Coded Digital Verification Color Code
CELP Code Excited Linear Predictor
CFP Cordless Fixed Part
C/I Carrier-to-interference Ratio
CIC Circuit Identification Code
CIU Cellular Controller Interface Unit
CLNP Connectionless Protocol (Open System Interconnect)
CMA Constant modulus algorithm
CNS Comfort Noise Subsystem
CO Central Office
codec Coder/decoder
CPE Customer Premises Equipment
CPFSK Continuous Phase Frequency Shift Keying
CPP Cordless Portable Part
CRC Cyclic Redundancy Code
CSMA Carrier Sense Multiple Access

CT2 Cordless Telephone -2
CVSDM Continuously Variable Slope Delta Modulation
CW Continuous Wave

D

DAM Diagnostic Acceptability Measure
DBAS Database Service Mangement System
DCA Dynamic Channel Allocation
DCCH Dedicated Control Channel
DCE Data Circuit Terminating Equipment
DCS Digital Communication System
DCS1800 Digital Communication System — 1800
DCT Discrete Cosine Transform
DECT Digital European Cordless Telephone
DEM Digital Elevation Models
DFE Decision Feedback Equalization
DFT Discrete Fourier Transform
DLC Data Link Control
DM Delta Modulation
DPCM Differential Pulse Code Modulation
DQPSK Differential Quadrature Phase Shift Keying
DRT Diagnostic Rhyme Test
DS Direct Sequence
DSAT Digital Supervisory Audio Tone
DSE Data Switching Exchange
DS/FHMA Hybrid Direct Sequence/Frequency Hopped Multiple Access
DSP Digital Signal Processing
DS-SS Direct Sequence Spread Spectrum
DST Digital Signaling Tone
DTC Digital Traffic Channel
DTE Data Terminal Equipment
DTMF Dual Tone Multiple Frequency
DTX Discontinuous Transmission Mode
DUP Data User Part

E

EIA Electronic Industry Association
EIR Equipment Identity Register
EIRP Effective Isotropic Radiated Power
E_b/N_0 Bit Energy-to-noise Density
EOC Embedded Operations Channel
erf Error Function
erfc Complementary Error Function
ERMES European Radio Message System

E-SMR Extended — Specialized Mobile Radio
ESN Electronic Serial Number
E-TACS Extended Total Access Communication System
ETSI European Telecommunications Standard Institute

F

FACCH Fast Associated Control Channel
FAF Floor Attenuation Factor
FBF Feedback Filter
FC Fast Channel
FCC Federal Communications Commission, Inc., also Forward Control Channel
FCCH Frequency Correction Channel
FCDMA Hybrid FDMA/CDMA
FDD Frequency Division Duplex
FDMA Frequency Division Multiple Access
FDTC Forward Data Traffic Channel
FEC Forward Error Correction
FFF Feedforward Filter
FFSR Feedforward Signal Regeneration
FH Frequency Hopping
FHMA Frequency Hopped Multiple Access
FH-SS Frequency Hopped Spread Spectrum
FLEX 4-level FSK-based paging standard developed by Motorola
FM Frequency Modulation
FN Frame Number
FPLMTS Future Public Land Mobile Telephone System
FSE Fractionally Spaced Equalizer
FSK Frequency Shift Keying
FTF Fast Transversal Filter
FVC Forward Voice Channel

G

GIS Graphical Information System
GIU Gateway Interface Unit
GMSK Gaussian Minimum Shift Keying
GOS Grade of Service
GSC Golay Sequential Coding (a 600 bps paging standard)
GSM Global System for Mobile Communication

H

HDB Home Database
HLR Home Location Register

I

IDCT Inverse Discrete Cosine Transform
IDFT Inverse Discrete Fourier Transform
IEEE Institute of Electrical and Electronics Engineers
IF Intermediate Frequency
IFFT Inverse Fast Fourier Transform
IGA Improved Gaussian Approximation
IIR Infinite Impulse Response
IM Intermodulation
IMSI International Mobile Subscriber Identity
IMT-2000 International Mobile Telecommuncation 2000
IMTS Improved Mobile Telephone Service
IP Internet Protocol
IS-54 EIA Interim Standard for U.S. Digital Cellular (USDC)
IS-95 EIA Interim Standard for U.S. Code Division Multiple Access
IS-136 EIA Interim Standard 136 — USDC with Digital Control Channels
ISDN Integrated Services Digital Network
ISI Intersymbol Interference
ISM Industrial, Scientific, and Medical
ISUP ISDN User Part
ITFS Intructional Television Fixed Service
ITU International Telecommunications Union
IXC Interexchange Carrier

J

JDC Japanese Digital Cellular (later called Pacific Digital Cellular)
JRC Joint Radio Committee
JTACS Japanese Total Access Communication System
JTC Joint Technical Committee

L

LAN Local Area Network
LAR Log-area Ratio
LATA Local Access and Transport Area
LBT Listen-before-talk
LCC Lost Call Cleared
LCD Lost Call Delayed
LCR Level Crossing Rate
LEC Local Exchange Carrier
LEO Low Earth Orbit
LMS Least Mean Square
LOS Line-of-sight
LPC Linear Predictive Coding

LSSB Lower Single Side Band
LTE Linear Transversal Equalizer
LTP Long Term Prediction

M

MAC Medium Access Control
MAHO Mobile Assisted Handoff
MAN Metropolitan Area Network
M-ary Multiple Level Modulation
MDBS Mobile Database Stations
MDLP Mobile Data Link Protocol
MDS Multipoint Distribution Service
MFJ Modified Final Judgement
MFSK Minimum Frequency Shift Keying
MIN Mobile Identification Number
MIRS Motorola Integrated Radio System (for SMR use)
ML Maximal Length
MLSE Maximum Likelihood Sequence Estimation
MMDS Multichannel Multipoint Distribution Service
MMSE Minimum Mean Square Error
MOS Mean Opinion Score
MoU Memorandum of Understanding
MPE Multi-pulse Excited
MPSK Minimum Phase Shift Keying
MSB Most Significant Bit
MSC Mobile Switching Center
MSCID MSC Identification
MSE Mean Square Error
MSK Minimum Shift Keying
MSU Message Signal Unit
MTA Major Trading Area
MTP Message Transfer Part
MTSO Mobile Telephone Switching Office
MUX Multiplexer

N

NACK Negative Acknowledge
NAMPS Narrowband Advanced Mobile Phone System
NBFM Narrowband Frequency Modulation
NEC National
N-ISDN Narrowband Integrated Service Digital Network
NMT-450 Nordic Mobile Telephone — 450
NRZ Non-return to Zero
NSP Network Service Part

NSS Network and Switching subsystem
NTACS Narrowband Total Access Communication System
NTT Nippon Telephone

O

OBS Obstructed
OFDM Orthogonal Frequency Division Multiplexing
OMAP Operations Maintenance and Administration Part
OMC Operation Maintenance Center
OQPSK Offset Quadrature Phase Shift Keying
OSI Open System Interconnect
OSS Operation Support Subsystem

P

PABX Private Automatic Branch Exchange
PACS Personal Access Communication System
PAD Packet Assembler Disassembler
PBX Private Branch Exchange
PCH Paging Channel
PCM Pulse Code Modulation
PCN Personal Communication Network
PCS Personal Communication System
PDC Pacific Digital Cellular
pdf probability density function
PG Processing Gain
PH Portable Handset
PHP Personal Handy Phone
PHS Personal Handy Phone System
PL Path Loss
PLL Phase Locked Loop
PLMR Public Land Mobile Radio
PN Pseudo-noise
POCSAG Post Office Code Standard Advisory Group
PR Packet Radio
PRI Primary Rate Interface
PRMA Packet Reservation Multiple Access
PSD Power Spectral Density
PSK Phase Shift Keying
PSTN Public Switched Telephone Network
PTI Permanent Terminal Identifier

Q

QAM Quadrature Amplitude Modulation

QCELP Qualcomm Code Excited Linear Predictive Coder
QMF Quadrature Mirror Filter
QPSK Quadrature Phase Shift Keying

R

RACE Research on Advanced Communications in Europe
RACH Random Access Channel
RCC Reverse Control Channel
RCS Radar Cross Section
RD-LAP Radio Data Link Access Procedure
RDTC Reverse Data Traffic Channel
RELP Residual Excited Linear Predictor
RF Radio Frequency
RFP Radio Fixed Part
RLC Resistor Inductor Capacitor
RLS Recursive Least Square
RMD RAM Mobile Data
RPCU Radio Port Control Unit
RRMS Radio Resource Management Protocol
RS Reed Solomon
RSSI Received Signal Strength Indicator
RVC Reverse Voice Channel
Rx Receiver
RZ Return to Zero

S

SACCH Slow Associated Control Channel
SAT Supervisory Audio Tone
SBC System Broadcasting Channel
also Sub-band Coding
SC Slow Channel
SCCP Signaling Connection Control Part
SCH Synchronization Channel
SCM Station Class Mark
SCORE Spectral Coherence Restoral Algorithm
SCP Service Control Point
SDCCH Stand-alone Dedicated Control Channel
SDMA Space Division Multiple Access
SEIGA Simplified Expression for the Improved Gaussian Approximation
SELP Stochastically Excited Linaer Predictive coder
SEP Switching End Points
SFM Spectral Flatness Measure
S/I see SIR
SID Station Identity

SIM Subscriber Identity Module
SIR Signal-to-interference Ratio
SIRCIM Simulation of Indoor Radio Channel Imulse response Models
SISP Site Specific Propagation
SMR Specialized Mobile Radio
SMRCIM Simulation of Mobile Radio Channel Impulse Response Models
SMS Short Messaging Service
also Service Management System
S/N see SNR
SNR Signal-to-noise Ratio
SP Signaling Point
SQNR Signal-to-quantization Noise Ratio
SS Spread Spectrum
SSB Single Side Band
SSMA Spread Spectrum Multiple Access
SS7 Signaling System No. 7
ST Signaling Tone
STP Short Term Prediction,
also Signaling Transfer Point
SYN Synchronization channel

T

TACS Total Access Communications System
TCAP Transaction Capabilities Application Part
TCDMA Time Division CDMA
TCH Traffic Channel
TCM Trellis Coded Modulation
TDD Time Division Duplex
TDFH Time Division Frequency Hopping
TDMA Time Division Multiple
TDN Temporary Directory Number
TIA Telecommunications Industry Association
TIU Trunk Interface Unit
TTIB Transparent Tone-In-Band
TUP Telephone User Part
Tx Transmitter

U

UF Urban Factor
UMTS Universal Mobile Telecommunication System
U.S. United States of America
USGS United States Geological Survey
USSB Upper Single Side Band

V

VAD Voice Activity Detector
VCI Virtual Circuit Identifier
VCO Voltage Controlled Oscillator
VDB Visitor Database
VIU Visitor Interface Unit
VLSI Very Large-scale Integration
VMAC Voice Mobile Attenuation Code
VQ Vector Quantization
VSELP Vector Sum Excited Linear Predictor

W

WACS Wireless Access Communication System (later called PACS)
WAN Wide Area Network
WARC World Administrative Radio Conference
WIN Wireless Information Network
WIU Wireless Interface Unit
WLAN Wireless Local Area Network
WUPE Wireless User Premises Equipement

Z

ZF Zero forcing

APPENDIX G

References

[Abe70] Abend, K. and Fritchman, B. D., "Statistical Detection for Communication Channels with Intersymbol Interference," *Proceedings of IEEE*, pp. 779-785, May 1970.

[You79] Akaiwa, Y., and Nagata, Y., "Highly Efficient Digital Mobile Communications with a Linear Modulation Method," *IEEE Journal on Selected Areas in Communications*, Vol. SAC-5, No.5, pp. 890-895, June 1987.

[Ake88] Akerberg, D., "Properties of a TDMA Picocellular Office Communication System," *IEEE Globecom*, pp. 1343-1349, December 1988.

[Ale82] Alexander, S. E., "Radio Propagation Within Buildings at 900 MHZ," *Electronics Letters*, Vol. 18, No. 21, pp. 913-914, 1982.

[Ale86] Alexander, S. T., *Adaptive Signal Processing*, Springer-Verlag, 1986.

[Ame53]Ament, W. S., "Toward a Theory of Reflection by a Rough Surface," *Proceedings of the IRE*, Vol. 41, No. 1, pp. 142-146, January 1953.

[Amo80] Amoroso, F., "The Bandwidth of Digital Data Signals," *IEEE Communications Magazine*, pp. 13-24, November 1980.

[ANS95] ANSI J-STD-008 - Personal Station-Base Compatibility Requirements for 1.8-2.0 GHz Code Division Multiple Access (CDMA) Personal Communication Systems, March 1995.

[And94] Anderson, J.B., Rappaport, T.S., and Yoshida, S., "Propagation Measurements and Models for Wireless Communications Channels," *IEEE Communications Magazine*, November 1994.

[Anv91]Anvari, K., and Woo, D., "Susceptibility of $\pi/4$ DQPSK TDMA Channel To Receiver Impairments," *RF Design*, pp. 49-55, February 1991.

[Ash93] Ashitey, D., Sheikh, A., and Murthy, K. M. S., "Intelligent Personal Communication System," *43rd IEEE Vehicular Technology Conference*, pp. 696-699, 1993.

[Ata86] Atal, B. S., "High Quality Speech at Low Bit Rates: Multi-pulse and Stochastically Excited Linear Predictive Coders," *Proceedings of ICASSP*, pp. 1681 - 1684, 1986.

[Bay73] Bayless, J.W., et. al, "Voice Signals: Bit-by-bit," *IEEE Spectrum*, pp. 28 - 34, October 1973.

[Bel62] Bello, P.A., and Nelin, B. D., "The Influence of Fading Spectrum on the Binary Error Probabilities of Incoherent and Differentially Coherent Matched Filter Receivers," *IRE Transactions on Communication Systems*, Vol. CS-10, pp.160-168, June 1962.

[Bel79] Belfiori, C. A., and Park, J. H., "Decision Feedback Equalization," *Proceedings of IEEE*, Vol. 67, pp. 1143-1156, August 1979.

[Ber87] Bernhardt, R.C., "Macroscopic Diversity in Frequency Reuse Systems," *IEEE Journal on Selected Areas in Communications*, Vol-SAC 5, pp. 862-878, June 1987.

[Ber89] Bernhardt, R.C., "The Effect of Path Loss Models on the Simulated Performance of Portable Radio Systems," *IEEE Globecom*, pp. 1356-1360, 1989.

[Ber92] Bertsekas, D., and Gallager R., *Data Networks*, 2nd edition,Prentice-Hall, Englewood Cliffs, NJ, 1992.

[Bie77] Bierman, G. J., *Factorization Method for Discrete Sequential Estimation*, Academic Press, New York, 1977.

[Bin88] Bingham, J.A.C., *The Theory and Practice of Modem Design*, John Wiley & Sons, New York, 1988.

[Boi87] Boithias, L., *Radio Wave Propagation*, McGraw-Hill Inc., New York, 1987.

[Bos60] Bose, R. C., and Ray-Chaudhuri, D. K., "On a Class of Error Correcting Binary Group Codes," *Information and Control*, Vol. 3, pp. 68-70, March 1960.

[Bou88] Boucher, J. R., *Voice Teletraffic Systems Engineering*, Artech House, c. 1988.

[Bou91] Boucher, N., *Cellular Radio Handbook*, Quantum Publishing, c. 1991.

[Boy90] Boyles, S. M., Corn, R. L., and Moseley, L. R., "Common Channel Signaling: The Nexus of an Advanced Communications Network," *IEEE Communications Magazine*, pp. 57-63, July 1990.

[Bra68] Brady, P. T., "A Statistical Analysis of On-Off Patterns in 16 Conversations", *Bell System Technical Journal,* Vol. 47, pp73-91, 1968.

[Bra70] Brady, D. M., "An Adaptive Coherent Diversity Receiver for Data Transmission through Dispersive Media," *Proceedings of IEEE International Conference on Communications*, pp. 21-35, June 1970.

[Bue94] Buehrer, R. M., and Woerner, B. D., "Teaching Spread Spectrum for Commercial Wireless Communications", *IEEE Transaction on Education*, submitted November 1994, to appear.

[Bul47] Bullington, K., "Radio Propagation at Frequencies above 30 megacycles," *Proceedings of the IEEE*, 35, pp. 1122-1136, 1947.

[Bul89] Bultitude, R.J.C., and Bedal, G.K., "Propagation Characteristics on Microcellular Urban Mobile Radio Channels at 910 MHz," *IEEE Journal on Selected Areas in Communications*, Vol. 7, pp. 31-39, January 1989.

[Cal88] Calhuon, G., *Digital Cellular Radio,* Artech House Inc., 1988.

[Cat69] Cattermole, K. W., *Principles of Pulse-Code Modulation*, Elsevier, New York, 1969.

[CCI86] Radio Paging Code No. 1, *The Book of the CCIR*, RCSG, 1986.

[Chu87] Chuang, J., "The Effects of Time Delay Spread on Portable Communications Channels with Digital Modulation," *IEEE Journal on Selected Areas in Communications*, Vol. SAC-5, No. 5, pp. 879-889, June 1987.

[Cla68] Clarke, R. H.,"A Statistical Theory of Mobile-radio Reception," *Bell Systems Technical Journal,* Vol. 47 pp. 957-1000, 1968.

[Col89] Coleman, A., et.al., "Subjective Performance Evaluation of the REP-LTP Codec for the Pan-European Cellular Digital Mobile Radio System," *Proceedings of ICASSP*, pp. 1075-1079, 1989.

[Coo86] Cooper, G. R., and McGillem, C. D., *Probabilistic Methods of Signal and System Analysis*, Holt, Rinehart, and Winston, New York, 1986.

[Cou93] Couch, L. W., *Digital and Analog Communication Systems*, 4th edition, Macmillan, New York, 1993.

[Cox72] Cox, D. C., "Delay Doppler Characteristics of Multipath Delay Spread and Average Excess Delay for 910 MHz Urban Mobile Radio Paths," *IEEE Transactions on Antennas and Propagation*, Vol. AP-20, No. 5, pp. 625-635, September 1972.

[Cox75] Cox, D. C., and Leck, R. P., "Distributions of Multipath Delay Spread and Average Excess Delay for 910 MHz Urban Mobile Radio Paths," *IEEE Transactions on Antennas and Propagation*, Vol.AP-23, No.5, pp. 206-213, March 1975.

[Cox83a] Cox, D. C., "Antenna Diversity Performance in Mitigating the Effects of Portable Radiotelephone Orientation and Multipath Propagation," *IEEE Trans. Commun.*, Vol.COM-31, No. 5, pp. 620-628, May 1983.

[Cox83b] Cox, D. C., Murray, R. R., and Norris, A. W., "Measurements of 800 MHz Radio Transmission into Buildings with Metallic Walls," *Bell Systems Technical Journal,* Vol. 62, No. 9, pp. 2695 - 2717, November 1983.

[Cox84] Cox, D. C., Murray, R., and Norris, A., "800 MHz Attenuation Measured in and around Suburban Houses," *AT&T Bell Laboratory Technical Journal*, Vol. 673, No. 6, July-August 1984.

[Cox87] Cox, D. C., Arnold, W., and Porter, P. T., "Universal Digital Portable Communications: A System Perspective," *IEEE Journal on Selected Areas of Communications,* Vol. SAC-5, No. 5, pp. 764, 1987.

[Cox89] Cox, D. C., "Portable Digital Radio Communication — An Approach to Tetherless Access," *IEEE Communication Magazine,* pp. 30-40, July 1989.

[Cox92] Cox D. C., "Wireless Network Access for Personal Communications," *IEEE Communications Magazine*, pp. 96-114, December 1992.

[Cro76] Crochiere R. E., et.al., "Digital Coding of Speech in Sub-bands," *Bell Systems Technical Journal*, Vol.55, No.8, pp. 1069 - 1085, October 1976.

[Cro89] Crozier, S. N., Falconer, D. D., and Mahmoud, S., "Short Block Equalization Techniques Employing Channel Estimation for Fading, Time Dispersive Channels," *IEEE Vehicular Technology Conference*, San Francisco, pp. 142-146, 1989.

[CTI93] Cellular Telphone Industry Association, *Cellular Digital Packet Data System Specification*, Release 1.0, July 1993.

[Dad75] Dadson, C. E., Durkin, J., and Martin, E., "Computer Prediction of Field Strength in the Planning of Radio Systems," *IEEE Transactions on Vehicular Technology,* Vol. VT-24, No. 1, pp. 1-7, February 1975.

[deB72] deBuda, R., "Coherent Demodulation of Frequency Shift Keying with Low Deviation Ratio," *IEEE Transactions on Communications*, Vol. COM-20, pp. 466-470, June 1972.

[Dec93] Dechaux, C., and Scheller, R., "What are GSM and DECT ?", *Electrical Communication*, pp. 118-127, 2nd quarter, 1993.

[Del93] Deller, J. R., Proakis, J. G., and Hansen, J. H. L., *Discrete-time Processing of Speech Signals*, Macmillan Publishing Company, New York, 1993.

[DeR94] DeRose, J. F., *The Wireless Data Handbook*, Quantum Publishing, Inc., 1994.

[Det89] Dettmer, R., "Parts of a Speech transcoder for CT2," *IEE Review*, September 1989.

[Dev86] Devasirvatham, D. M. J., "Time Delay Spread and Signal Level Measurements of 850 MHz Radio Waves in Building Environments," *IEEE Transactions on Antennas and Propagation*, Vol. AP-34, No. 2, pp. 1300-1305, November 1986.

[Dev90a] Devasirvatham, D. J., Krain, M. J., and Rappaport, D. A., "Radio propagation measurements at 850 MHz, 1.7 GHz, and 4.0 GHz inside two dissimilar office buildings," *Electronics Letters*, Vol. 26, No. 7, pp. 445-447, 1990.

[Dev90b] Devasirvatham, D. M. J., Banerjee, C., Krain, M. J., and Rappaport, D. A., "Multi-frequency radiowave propagation measurements in the portable radio environment," *IEEE International Conference on Communications*, pp. 1334-1340, 1990.

[Dey66] Deygout J., "Multiple Knife-edge Diffraction of Microwaves," *IEEE Transactions on Antennas and Propagation*, Vol. AP-14, No. 4, pp. 480-489, 1966.

[Dix84] Dixon, R. C., *Spread Spectrum Systems*, 2nd Edition, John Wiley and Sons, New York, 1984.

[Dix94] Dixon, R. C., *Spread Sprectrum Systems with Commercial Applications*, 3rd Edition, John Wiley & Sons Inc., New York, 1994.

[Don93] Donaldson, R. W., "Internetworking of Wireless Communication Network," *Proceedings of the IEEE*, pp. 96-103, 1993.

[Dur73] Durante, J.M., "Building Penetration Loss at 900 MHz," *IEEE Vehicular Technology Conference*, 1973.

[Edw69] Edwards, R., Durkin, J., "Computer Prediction of Service Area for VHF Mobile Radio Networks," *Proceedings of the IEE*, Vol. 116, No. 9, pp. 1493-1500, 1969.

[EIA90] EIA/TIA Interim Standard, "Cellular System Dual Mode Mobile Station — Land Station Compatibility Specifications", IS-54, *Electronic Industries Association*, May 1990.

[EIA91] EIA/TIA Interim Standard, "Cellular System Mobile Station — Land Station Compatibility Specification IS-88," Rev. A, November 1991.

[EIA92] "TR 45: Mobile Station - Base Station Compatibility Standard for Dual-mode Wideband Spread Spectrum Cellular System," PN-3118, *Electronics Industry Association*, December 1992.

[Eng93] Eng, T., and Milstein, L. B., "Capacities of Hybrid FDMA/CDMA Systems in Multipath Fading", *IEEE MILCOM Conference Records*, pp. 753-757, 1993.

[Eps53] Epstein, J., and Peterson, D. W., "An Experimental Study of Wave Propagation at 840 MC," *Proceedings of the IRE*, 41, No. 5, pp. 595-611, 1953.

[Est77] Estaban, D., and Galand, C., "Application of Quadrature Mirror Filters to Split Band Voice Coding Schemes," *Proceedings of ICASSP*, pp. 191 - 195, May 1977.

[EUR91] European Cooperation in the Field of Scientific and Technical Research EURO-COST 231, "Urban Transmission Loss Models for Mobile Radio in the 900 and 1800 MHz Bands," Revision 2, The Hague, September 1991.

[Fan63] Fano, R. M., "A Heuristic Discussion of Probabilistic Coding," *IEEE Transactions on Information Theory*, Vol. IT-9, pp. 64-74, April 1963.

[FCC91] *FCC Notice of Inquiry for Refarming Spectrum below 470 MHz*, PLMR docket 91-170, November 1991.

[Feh91] Feher, K., "Modems for Emerging Digital Cellular Mobile Radio Systems," *IEEE Transactions on Vehicular Technology*, Vol. 40, No. 2, pp. 355-365, May 1991.

[Feu94] Feuerstein, M. J., Blackard, K. L., Rappaport, T. S., Seidel, S. Y., and Xia, H. H., "Path Loss, Delay Spread, and Outage Models as Functions of Antenna Height for Microcellular System Design," *IEEE Transactions on Vehicular Technology*, Vol. 43, No. 3, pp. 487-498, August 1994.

[Fil95] Filiey, G. B., and Poulsen, P. B., "MIRS Technology: On the Fast Track to Making the Virtual Office a Reality", *Communications*, pp. 34-39, January 1995.

[Fla79] Flanagan, J. L., et.al., "Speech coding," *IEEE Transactions on Communications*, Vol. COM-27, No.4, pp. 710 - 735, April 1979.

[For78] Forney, G. D., "The Viterbi Algorithm," *Proceedings of the IEEE*, Vol. 61, No. 3, pp. 268 -278, March 1978.

[Fun93] Fung, V., Rappaport, T. S., and Thoma, B., "Bit Error Simulation for $\pi/4$ DQPSK Mobile Radio Communication using Two-ray and Measurement-based Impulse Response Models," *IEEE Journal on Selected Areas in Communication*, Vol. 11, No. 3, pp. 393-405, April 1993.

[Gan72] Gans, M. J., "A Power Spectral Theory of Propagation in the Mobile Radio Environment," *IEEE Transactions on Vehicular Technology*, Vol. VT-21, pp. 27-38, February 1972.

[Gar91] Gardner, W. A., "Exploitation of Spectral Redundancy in Cyclostationary Signals," *IEEE Signal Processing Magazine*, pp. 14-36, April 1991.

[Gar95] Gardner, W., QUALCOMM Inc., personal correspondence, June 1995.

[Ger82] Geraniotis, E. A., and Pursley, M. B., "Error Probabilities for Slow Frequency-Hopped Spread Spectrum Multiple-Access Communications Over Fading Channels," *IEEE Transactions on Communications*, Vol. COM-30, No.5, pp.996-1009, May 1982.

[Ger90] Gerson, I. A., and Jasiuk, M. A., "Vector Sum Excited Linear Prediction (VSELP): Speech Coding at 8 kbps," *Proceedings of ICASSP*, pp. 461 - 464, 1990.

[Gil91] Gilhousen, et.al., "On the Capacity of Cellular CDMA System," *IEEE Transactions on Vehicular Technology*, Vol. 40, No. 2, pp. 303-311, May 1991.

[Git81] Gitlin, R. D., and Weinstein, S. B., "Fractionally Spaced Equalization : An Improved Digital Transversal Filter," *Bell Systems Technical Journal*, Vol. 60, pp.275-296, February 1981.

[Gol49] Golay, M. J. E., "Notes on Digital Coding," *Proceedings of the IRE*, Vol. 37, pp. 657, June 1949.

[Goo89] Goodman, D. J., Valenzula, R.A., Gayliard, K.T., and Ramamurthi, B., "Packet Reservation Multiple Access for Local Wireless Communication," *IEEE Transactions on Communications*, Vol. 37, No. 8, pp. 885-890, August 1989.

[Goo90] Goodman, D. J., "Cellular Packet Communications," *IEEE Transactions on Communications*, Vol. 38, No. 8, pp. 1272-1280, August 1990.

[Goo91] Goodman D. J., "Trends in Cellular and Cordless Communications," *IEEE Communications Magazine*, pp. 31-39, June 1991.

[Gos78] Gosling, W., McGeehan, J.P., and Holland, P. G., "Receivers for the Wolfson SSB/VHF Land Mobile Radio System," *Proceedings of IERE Conference on Radio Receivers and Associated Systems*, Southampton, England, pp. 169-178, July 1978.

[Gow93] Gowd K., et. al, "Robust Speech Coding for Indoor Wireless Channel," *AT&T Technical Journal*, Vol. 72, No. 4, pp. 64 - 73, July/August 1993.

[Gra84] Gray, R.M., "Vector Quantization," *IEEE ASSP Magazine*, pp. 4 - 29, April 1984.

[Gri87] Griffiths, J., *Radio Wave Propagation and Antennas*, Prentice Hall International, 1987.

[Gud92] Gudmundson, B., Skold, J., and Ugland, J. K, "A Comparison of CDMA and TDMA systems," *Proceedings of the 42nd IEEE Vehicular Technology Conference*, Vol. 2, pp. 732- 735, 1992.

[Ham50] Hamming, R. W., "Error Detecting and Error Correcting Codes," *Bell System Technical Journal*, April 1950.

[Has93] Hashemi, H., "The Indoor Radio Propagation Channel," *Proceedings of the IEEE*, Vol. 81, No. 7, pp. 943-968, July 1993.

[Hat90] Hata, Masaharu, "Empirical Formula for Propagation Loss in Land Mobile Radio Services," *IEEE Transactions on Vehicular Technology*, Vol. VT-29, No. 3, pp. 317-325, August 1980.

[Haw91] Hawbaker, D. A., *Indoor Wideband Radio Wave Propagation Measurements and Models at 1.3 GHz and 4.0 GHz*, Masters Thesis, Virginia Tech, Blacksburg, May 1991.

[Hay86] Haykin, S., *Adaptive Filter Theory*, Prentice Hall, Englewood Cliffs, NJ, 1986.

[Hay94] Haykin, S., *Communication Systems*, John Wiley and Sons, New York, 1994.

[Hel89] Hellwig, K., Vary P., Massaloux, D., Petit, J. P., Galand, C., and Rasso, M., "Speech Codec for the European Mobile Radio Systems," *IEEE Global Telecommunication Conference & Exhibition*, Vol. 2, pp. 1065-1069, 1989.

[Ho94] Ho, P., Rappaport, T. S., and Koushik, M. P., "Antenna Effects on Indoor Obstructed Wireless Channels and a Deterministic Image-Based Wide-Band Propagation Model for In-Building Personal Communication Systems," *Internation Journal of Wireless Information Netowrks*, Vol. 1, No. 1, pp. 61-75, January 1994.

[Hod90] Hodges, M. R. L., "The GSM Radio Interface," *British Telecom Technological Journal*, Vol. 8, No. 1, pp. 31-43, January 1990.

[Hol92] Holtzman, J. M., "A Simple, Accurate Method to Calculate Spread-Spectrum Multiple-Access Error Probabilities," *IEEE Transactions on Communications*, Vol. 40, No. 3, March 1992.

[Hor86] Horikishi, J., et. al., "1.2 GHz Band Wave Propagation Measurements in Concrete Buildings for Indoor Radio Communications," *IEEE Transactions on Vehicular Technology*, Vol. VT-35, No. 4, 1986.

[Hua91] Huang, W., "*Simulation of Adaptive Equalization in Two-Ray, SIRCIM and SMRCIM Mobile Radio Channels*", Masters Thesis in Electrical Engineering, Virginia Tech, December 1991.

[IEE91] "Special Issue on Satellite Communications Systems and Services for Travelers," *IEEE Communications Magazine*, November 1991.

[Ish80] Ishizuka, M., and Hirade, K., "Optimum Gaussian filter and Deviated-Frequency-Locking Scheme for Coherent Detection of MSK," *IEEE Transactions on Communications*, Vol. COM-28, No.6, pp. 850-857, June 1980.

[ITU93] *ITU World Telecommunications Report*, December 1993.

[ITU94] *ITU Documents of TG8/1 (FPLMTS),* International Telecommunications Union, Radiocommunications sector, Geneva, 1994.

[Jac94] Jacobsmeyer, J., "Improving Throughput and Availability of Cellular Digital Packet Data (CDPD)," *Virginia Tech 4th Symposium on Wireless Personal Communications*, pp. 18.1-18.12, June 1994.

[Jak70] Jakes, W. C., "New Techniques for Mobile Radio," *Bell Laboratory Rec.*, pp. 326-330, December 1970.

[Jak71] Jakes, W. C., "A Comparision of Specific Space Diversity Techniques for Reduction of Fast Fading in UHF Mobile Radio Systems," *IEEE Transactions on Vehicular Technology*, Vol. VT-20, No. 4, pp. 81-93, November 1971.

[Jak74] Jakes, W. C. Jr., *Microwave Mobile Communications*, Wiley-Interscience, 1974.

[Jay84] Jayant, N. S., Noll, P., *Digital Coding of Waveforms*, Prentice-Hall, Englewood Cliffs, NJ, 1984.

[Jay86] Jayant, N. S., "Coding Speech at Low Bit Rates," *IEEE Spectrum*, pp.58 - 63, August 1986.

[Jay90] Jayant, N. S., "High Quality Coding of Telephone Speech and Wideband Audio," *IEEE Communications Magazine*, pp. 10 - 19, January 1990.

[Jay92] Jayant, N. S., "Signal Compression: Technology, Targets, and Research Directions," *IEEE Journal on Selected Areas of Communications*, Vol.10, No.5, pp. 796 - 815, June 1992.

[Joh82] Johnson, L. W., and Riess, R. D., *Numerical Analysis*, Addison-Wesley, 1982.

[JTC95] JTC Standards Project 066: "Baseline Text for TAG #3 PACS - UB," Motorola Inc., February 1995.

[Kah54] Kahn, L., "Ratio Squarer," *Proceedings of IRE (Correspondence)*, Vol. 42, pp. 1074, November 1954.

[Kle75] Kleinrock, L., and Tobagi, F. A., "Packet Switching in Radio Channels, Part 1: Carrier Sense Multiple-Access Models and Their Throughput-Delay Characteristics", *IEEE Transactions on Communications*, Vol. 23, No.5, pp. 1400-1416, 1975.

[Kor85] Korn, I., *Digital Communications*, Van Nostrand Reinhold, 1985.

[Koz85] Kozono, S., et al, "Base Station Polarization Diversity Reception for Mobile Radio," *IEEE Transactions on Vehicular Technology*, Vol. VT-33, No. 4, pp. 301-306, November 1985.

[Kra50] Krauss, J. D., *Antennas*, McGraw-Hill, New York, 1950.

[Kre94] Kreuzgruber, P., et al, "Prediction of Indoor Radio Propagation with the Ray Splitting Model Including Edge Diffraction and Rough Surfaces," *1994 IEEE Vehicular Technology Conference,* Stockholm, Sweden, pp. 878-882, June 1994.

[Kuc91] Kucar, A. D., "Mobile Radio — An Overview," *IEEE Communications Magazine*, pp. 72-85, November 1991.

[Lam80] Lam, S. S., "A Carrier Sense Multiple Access Protocol for Local Networks", *Computer Networks*, Vol. 4, pp. 21-32, 1980.

[Lan92] Landron, O., *Microwave multipath resolution in microcellular channels*, Masters Thesis, Virginia Tech, August 1992.

[Lee72] Lee, W. C. Y., and Yeh, S. Y.," Polarization Diversity System for Mobile radio," *IEEE Transactions on Communications*, Vol. 20, pp. 912-922, October 1972.

[Lee85] Lee, W. C. Y., *Mobile Communications Engineering*, McGraw Hill Publications, New York, 1985.

[Lee86] Lee, W. C. Y., "Elements of Cellular Mobile Radio systems," *IEEE Transactions on Vehicular Technology,* Vol. VT-35, No. 2, pp. 48-56, May 1986.

[Lee89a] Lee, W. C. Y., "Spectrum Efficiency in Cellular," *IEEE Transactions on Vehicular Technology*, Vol. 38, No. 2, pp. 69-75, May 1989.

[Lee89b] Lee, W. C. Y., *Mobile Cellular Telecommunications Systems*, McGraw Hill Publications, New York, 1989.

[Lee91a] Lee, W. C. Y., "Overview of Cellular CDMA," *IEEE Transactions on Vehicular Technology*, Vol. 40, No. 2, May 1991.

[Lee91b] Lee, W. C. Y., "Smaller Cells for Greater Performance," *IEEE Communications Magazine*, pp. 19-23, November 1991.

[Leh87] Lehnert, J. S., and Pursley, M. B., "Error Probabilities for Binary Direct-Sequence Spread-Spectrum Communications with Random Signature Sequences," *IEEE Transactions on Communications,* Vol. COM-35, No. 1, January 1987.

[Lem91] Lemieux, J. F., Tanany, M., and Hafez, H. M., "Experimental Evaluation of Space/Frequency/Polarization Diversity in the Indoor Wireless Channel," *IEEE Transactions on Vehicular Technology*, Vol. 40, No. 3, pp. 569-574, August 1991.

[Li93] Li, Y., *Bit Error Rate Simulation of a CDMA System for Personal Communications*, Masters Thesis in Electrical Engineering, Virginia Tech, 1993.

[LiC93] Li, C., Greenstein L. J., and Gitlin R.D., "A Microcell/Macrocell Cellular Architecture for Low- and High Mobility Wireless Users," *IEEE Vehicular Technology Transactions,* pp. 885-891, August 1993.

[Lib94a] Liberti, J. C., Jr., "CDMA Cellular Communication Systems Employing Adaptive Antennas", *Preliminary Draft of Research Including Literature Review and Summary of Work-in-Progress*, Virginia Tech, March 1994.

[Lib94b] Liberti, J. C. Jr., Rappaport, T. S., "Analytical Results for Capacity Improvements in CDMA," *IEEE Transactions on Vehicular Technology,* Vol. 43, No. 3, pp. 680-690, August 1994.

[Lib95] Liberti, J. C. Jr., *Analysis of Code Division Multiple Access Mobile Radio Systems with Adapative Antennas,* Ph.D. Dissertation, Virginia Tech, Blacksburg, August, 1995.

[Lin83] Lin, S., and Costello, D. J. Jr., *Error Control Coding: Fundamentals and Applications*, Prentice-Hall, Englewood Cliffs, NJ, 1983.

[Lin84] Ling, F., Proakis, J. G., "Nonstationary Learning Characteristics of Least Squares Adaptive Estimation Algorithms," *Proceedings ICASSP84*, San Diego, California, pp.3.7.1-3.7.4, 1984.

[Liu89] Liu, C. L., Feher, K., "Noncoherent Detection of $\pi/4$-Shifted Systems in a CCI-AWGN Combined Interference eEnvironment," *Proceedings of the IEEE 40th Vehicular Technology Conference*, San Fransisco, 1989.

[Liu91] Liu, C., Feher, K., "Bit Error Rate Performance of $\pi/4$ DQPSK in a Frequency Selective Fast Rayleigh Fading Channel," *IEEE Transactions on Vehicular Technology*, Vol. 40, No. 3, pp. 558-568, August 1991.

[Lo90] Lo, N. K. W., Falconer, D. D., and Sheikh, A. U. H., "Adaptive Equalization and Diversity Combining for a Mobile Radio Channel", *IEEE Globecom*, San Diego, December 1990.

[Lon68] Longley, A G., and Rice, P. L., "Prediction of Tropospheric Radio Transmission Loss Over Irregular Terrain; A Computer Method," *ESSA Technical Report*, ERL 79-ITS 67, 1968.

[Lon78] Longley, A. G., "Radio Propagation in Urban Areas," *OT Report*, pp. 78-144, April 1978.

[Luc65] Lucky, R. W., "Automatic Equalization for Digital Communication", *Bell System Technical Journal*, Vol. 44, pp. 547-588, 1965.

[Luc89] Lucky, R. W., *Silicon Dreams: Information, Man and Machine*, St. Martin Press, New York, 1989.

[Lus78] Lusignan, B. B., "Single-sideband Transmission for Land Mobile Radio," *IEEE Spectrum*, pp. 33-37, July 1978.

[Mac79] MacDonald, V. H., "The Cellular Concept," *The Bell Systems Technical Journal*, Vol. 58, No. 1, pp. 15-43, January 1979.

[Mac93] Maciel, L. R., Bertoni, H. L., and Xia, H. H., "Unified Approach to Prediction of Propagation Over Buildings for all Ranges of Base Station Antenna Height," *IEEE Transactions on Vehicular Technology*, Vol. 42, No. 1, pp. 41-45, February 1993.

[Mak75] Makhoul, J., "Linear Prediction: A Tutorial Review," *Proceedings of IEEE*, Vol. 63, pp. 561 - 580, April 1975.

[Mal89] Maloberti, A., "Radio Transmission Interface of the Digital Pan European Mobile System," *IEEE Vehicular Technology Conference*, Orlando, FL, pp. 712-717, May 1989.

[Mal92] Malyan, A. D., Ng, L. J., Leung, V. C. M., and Donaldson, R. W., "A Microcellular Interconnection Architecture for Personal Communication Networks," *Proceedings of IEEE Vehicular Technology Conference*, pp. 502-505, May 1992.

[Man93] Mansfield, D. R., Millsteed, G., and Zukerman, M., "Congestion Controls in SS7 Signaling Networks," *IEEE Communications Magazine*, pp. 50-57, June 1993.

[Mar90] Marr, F. K., "Signaling System No.7 in Corporate Networks," *IEEE Communications Magazine*, pp. 72-77, July 1990.

[Max60] Max, J., "Quantizing for Minimizing Distortion," *IRE transactions on Information Theory*, March 1960.

[McG84] McGeehan, J. P., and Bateman, A. J., "Phase Locked Transparent Tone-in-band (TTIB): A New Spectrum Configuration Particularly Suited to the Transmission of Data over SSB Mobile Radio Networks," *IEEE Transactions on Communications*, Vol. COM-32, No. 1, pp. 81-87, January 1984.

[Mei92] Meier-Hellstern, K. S., Pollini, G. P., and Goodman, D., "Network Protocols for the Cellular Packet Switch," *Proceedings of IEEE Vehicular Technology Conference*, Vol. 2, No. 2, pp. 705-710, 1992.

[Mei93] Meier-Hellstern, K. S., et. al., "The Use of SS7 and GSM to support High Density Personal Communications," *Wireless Communications: Future Directions*, Kluwer Academic Publishing, 1993.

[Mil62] Millington, G., Hewitt, R., and Immirzi, F. S., "Double Knife-edge Diffraction in Field Strength Predictions," *Proceedings of the IEE*, 109C, pp. 419-429, 1962.

[Mod92] Modarressi, A. R., and Skoog, R. A., "An Overview of Signal System No.7," *Proceedings of the IEEE*, Vol. 80, No. 4, pp. 590-606, April 1992.

[Mol91] Molkdar, D., "Review on Radio Propagation into and Within Buildings," *IEE Proceedings*, Vol. 138, No. 1, pp. 61-73, Febuary 1991.

[Mon84] Monsen, P., "MMSE Equalization of Interference on Fading Diversity Channels," *IEEE Transactions on Communications*, Vol. COM-32, pp. 5-12, January 1984.

[Mor89a] Moralee, D., "CT2 a New Generation of Cordless Phones," *IEE Review,* pp 177 - 180, May 1989.

[Mor89b] Morrow, R. K., Jr., and Lehnert, J. S., "Bit-to-Bit Error Dependence in Slotted DS/SSMA Packet Systems with Random Signature Sequences," *IEEE Transactions on Communications*, Vol. 37, No. 10, October, 1989.

[Mou92] Mouly, M., and Pautet, M. B., *The GSM System for Mobile Communication*, ISBN: 2-9507190-0-7, 1992.

[Mul91] Mulder, R. J., "DECT — A Universal Cordless Access System," *Philips Telecommunications Review*, Vol. 49, No. 3, pp 68 - 73, September 1991.

[Mur81] Murota, K., and Hirade, K., "GMSK Modulation for Digital Mobile Radio Telephony," *IEEE Transactions on Communications*, Vol. COM-29, No. 7, pp. 1044-1050, July 1981.

[NAC94] North American Cellular Network, "*An NACN Standard*", Rev. 2.0, December 1994.

[Nar90] Narasimhan, A., Chennakeshu, S., and Anderson, J. B., "An Adaptive Lattice Decision Equalizer for Digital Cellular Radio," *IEEE 40th Vehicular Technology Conference*, pp. 662-667, May 1990.

[Nob62] Noble, D., "The History of Land-Mobile Radio Communications," *IEEE Vehicular Technology Transactions*, pp. 1406-1416, May 1962.

[Nyq28] Nyquist, H., "Certain topics in telegraph transmission theory," *Transactions of the AIEE*, Vol. 47, pp. 617-644, Febuary 1928.

[Och89] Ochsner, H., "DECT — Digital European Cordless Telecommunications," *IEEE Vehicular Technology 39th Conference*, pp 718 -721, 1989.

[Oet83] Oeting, J., "Cellular Mobile Radio — An Emerging Technology," *IEEE Communications Magazine*, pp. 10-15, November 1983.

[Oga94] Ogawa, K., et. al., "Toward the Personal Communication Era - the Radio Access Concept from Japan," *International Journal on Wireless Information Networks,* Vol. 1, No. 1, pp.17-27, January 1994.

[Oku68] Okumura, T., Ohmori, E., and Fukuda, K., "Field Strength and Its Variability in VHF and UHF Land Mobile Service," *Review Electrical Communication Laboratory*, Vol. 16, No. 9 - 10, pp. 825-873, September-October 1968.

[Oss64] Ossana, J. Jr., "A Model for Mobile Radio Fading due to Building Reflections: Theoretical and Experimental Fading Waveform Power Spectra," *Bell Systems Technical Journal*, Vol. 43, No. 6, pp. 2935-2971, November 1964.

[Owe91] Owen, F. C. and Pudney, C., "DECT: Integrated Services for Cordless Telecommunications," *IEE Conference Publications*, No.315, pp 152 -156, 1991.

[Owe93] Owens, F. J., *Signal Processing of Speech*, McGraw Hill, New York, 1993.

[Pad94] Padovani, R., "Reverse Link Performance of IS-95 Based Cellular Systems," *IEEE Personal Communications*, pp. 28-34, 3rd quarter, 1994.

[Pad95] Padyett, J., Gunther, E., and Hattari, T.,"Overview of Wireless Personal Communications," *IEEE Communications Magazine*", January 1995.

[Pah95] Pahlavan, K., and Levesque, A.H., *Wireless Information Networks*, Chapter 5, John Wiley & Sons, New York, 1995.

[Pap91] Papoulis, A., *Probability, Random Variables, and Stochastic Processes*, 3rd Edition, McGraw Hill, New York, 1991.

[Par76] Parsons, J. D., et. al., "Diversity Techniques for Mobile Radio Reception," *IEEE Transactions on Vehicular Technology*, Vol. VT-25, No. 3, pp. 75-84, August 1976.

[Pas79] Pasupathy, S., "Minimum Shift Keying: A Spectrally Efficient Modulation," *IEEE Communications Magazine*, pp. 14-22, July 1979.

[Pec92] Pecar, J. A., O'Conner, R. J., and Garbin, D. A., *Telecommunications Factbook*, McGraw Hill, New York, 1992.

[Per92] Personal Digital Cellular, Japanese Telecommunication System Standard, RCR STD 27.B, 1992.

[Per93] Personal Handy Phone System, Japanese Telecommunication System Standard, RCR-STD 28, December 1993.

[Pic91] Pickholtz, R. L., Milstein, L. B., and Schilling, D., "Spread Spectrum for Mobile Communications," *IEEE Transactions on Vehicular Technology*, Vol.40, No.2, pp. 313-322, May 1991.

[Pri58] Price, R., Green, P. E., "A Communication Technique for Multipath Channel," *Proceedings of the IRE*, pp. 555-570, March 1958.

[Pro89] Proakis, J. G., *Digital Communications*, McGraw-Hill, New York, 1989.

[Pro91] Proakis, J., "Adaptive Equalization for TDMA Digital Mobile Radio," *IEEE Transactions on Communications*,Vol. 40, No. 2, pp 333-341, May 1991.

[Pur77] Pursley, M. B., Sarwate, D. V., and Stark, W. E., "Performance Evaluation for Phase-Coded Spread-Spectrum Multiple-Access Communication - Part II: Code Sequence Analysis," *IEEE Transactions on Communications*, Vol. COM-25, No. 8, August 1987.

[Qur77] Qureshi, S. U. H., and Forney, G. D., "Performance properities of a T/2 equalizer", *IEEE Globecom,* pp. 11.1.1-11.1.14, Los Angeles, CA, December 1977.

[Qur85] Qureshi, S. U. H., "Adaptive equalization," *Proceeding of IEEE*, Vol. 37, No. 9, pp. 1340-1387, September, 1985.

[Rai91] Raith, K., and Uddenfeldt, J., "Capacity of Digital Cellular TDMA Systems," *IEEE Transactions on Vehicular Technology*, Vol. 40, No. 2, pp. 323-331, May 1991.

[Ram65] Ramo, S., Whinnery, J.R., and Van Duzer, T., *Fields and Waves in Communication Electronics*, John Wiley & Sons, New York, 1965.

[Rap89] Rappaport, T.S., "Characterization of UHF Multipath Radio Channels in Factory Buildings," *IEEE Transactions on Antennas and Propagation*, Vol. 37, No. 8, pp. 1058-1069, August 1989.

[Rap90] Rappaport, T.S., Seidel, S.Y., and Singh, R., "900 MHz Multipath Propagation Measurements for U.S. Digital Cellular Radiotelephone," *IEEE Transactions on Vehicular Technology,* pp. 132-139, May 1990.

[Rap91a] Rappaport, T. S., et. al., "Statistical Channel Impulse Response Models for Factory and Open Plan Building Radio Communication System Design," *IEEE Transactions on Communications*, Vol. COM-39, No. 5, pp. 794-806, May 1991.

[Rap91b] Rappaport, T. S., and Fung, V., "Simulation of Bit Error Performance of FSK, BPSK, and $\pi/4$ DQPSK in Flat Fading Indoor Radio Channels Using a Measurement-based Channel Model," *IEEE Transactions on Vehicular Technology,* Vol. 40, No. 4, pp. 731-739, November 1991.

[Rap91c] Rappaport, T. S., "The Wireless Revolution," *IEEE Communications Magazine*, pp. 52-71, November 1991.

[Rap92a] Rappaport, T. S., and Hawbaker, D. A., "Wide-band Microwave Propagation Parameters Using Circular and Linear Polarized Antennas for Indoor Wireless Channels," *IEEE Transactions on Communications*, Vol. 40, No. 2, pp. 240-245, February 1992.

[Rap92b] Rappaport, T.S., and Milstein, L. B., "Effects of Radio Propagation Path Loss on DS-CDMA Cellular Frequency Reuse Efficiency for the Reverse Channel," *IEEE Transactions on Vehicular Technology,* Vol. 41, No. 3, pp.231-242, August 1992.

[Rap93a] Rappaport, T.S., Huang, W., and Feuerstein, M.J., "Performance of decision feedback equalizers in simulated urban and indoor radio channels," Special issue on land mobile/portable propagation, *IEICE Transactions on Communications*, Vol. E76-B, No. 2, Febuary 1993.

[Rap93b] Rappaport, S. S., "Blocking, hand-off and traffic performance for cellular communication systems with mixed platforms," *IEE Proceedings,* Vol. 140, No. 5, pp. 389 - 401, October 1993.

[Rap95] *Cellular Radio & Personal Communications: Selected Readings*, edited by Rappaport T. S., IEEE Press, New York, ISBN: 0-7803-2283-5, 1995.

[Ree60] Reed, I. S., and Solomon, G., "Polynomial Codes Over Certain Finite Fields," *Journal of the Society for Industrial and Applied Mathematics,* June 1960.

[Reu74] Reudink, D. O., "Properties of Mobile Radio Propagation Above 400 MHz," *IEEE Transactions on Vehicular Technology,* Vol. 23, No.2, pp. 1-20, November 1974.

[Rhe89] Rhee, M. Y., *Error Correcting Coding Theory,* McGraw-Hill, New York, 1989.

[Ric48] Rice, S. O., "Mathematical Analysis of Random Noise," *Bell Systems Technical Journal,* Vol. 23, pp. 282-332, July 1944; Vol. 24, pp. 46-156, January 1945; and Rice, S. O., "Statistical Properties of a Sine Wave Plus Random Noise," *Bell Systems Technical Journal*, Vol. 27, pp. 109-157, January 1948.

[Ric67] Rice, P. L., Longley, A. G., Norton, K. A., and Barsis, A. P., "Transmission Loss Predictions for Tropospheric Communication Circuits," *NBS Tech Note 101*; two volumes; issued May 7, 1965; revised May 1, 1966; revised January 1967.

[Rob94] Roberts, J.A., and Bargallo, J.M., "DPSK Performance for Indoor Wireless Rician Fading Channels," *IEEE Transactions on Communications*, pp. 592-596, April 1994.

[Roc89] Roca, R. T., "ISDN Architecture," *AT&T Technical Journal*, pp. 5-17, October 1989.

[Ros93] Rossi, J. and Levi, A., "A Ray Model for Decimetric Radiowave Propagation in an Urban Area," *Radio Science*, Vol. 27, No. 6, pp. 971- 979, 1993.

[Rus93] Russel, T. A., Bostian, C. W., and Rappaport, T. S., "A Deterministic Approach to Predicting Microwave Diffraction by Buildings for Microcellular Systems," *IEEE Transactions on Antennas and Propagation*, Vol.41, No. 12, pp. 1640 - 1649, December 1993.

[Sal87] Saleh, A. A. M., and Valenzula, R. A., "A Statistical Model for Indoor Multipath Propagation," *IEEE Journal on Selected Areas in Communication*, Vol. JSAC-5, No. 2, pp. 128-137, Febuary 1987.

[Sal91] Salmasi, A., and Gilhousen, K. S., "On the System Design Aspects of Code Division Multiple Access (CDMA) Applied to Digital Cellular and Personal Communications Networks," *IEEE*, pp. 57-62, 1991.

[San82] Sandvos, J. L., "A Comparison of Binary Paging Codes," *IEEE Vehicular Technology Conference*, pp. 392-402, 1982.

[Sch85a] Schroeder, M. R., "Linear Predictive Coding of Speech: Review and Current Directions," *IEEE Communications Magazine*, Vol. 23, No. 8, pp. 54 - 61, August 1985.

[Sch85b] Schroeder, M.R., and Atal, B.S., "Code-excited Linear Prediction (CELP): High Quality Speech at Very Low Bit Rates," *Proceedings of ICASSP*, pp. 937 - 940, 1985.

[Sch92] Schaubach, K. R., Davis, N. J. IV, and Rappaport, T. S., "A Ray Tracing Method for Predicting Path Loss and Delay Spread in Microcellular Environments," in *42nd IEEE Vehicular Technology Conference*, Denver, pp. 932-935, May 1992.

[Sei91] Seidel, S.Y., Rappaport, T.S., Jain, S., Lord, M., and Singh, R., "Path Loss, Scattering and Multipath Delay Statistics in Four European Cities For Digital Cellular and Microcellular Radiotelephone," *IEEE Transactions on Vehicular Technology*, Vol. 40, No. 4, pp. 721-730, November 1991.

[Sei92a] Seidel, S. Y., et.al., "The Impact of Surrounding Buildings on Propagatiion for Wireless Inbuilding Personal Communications System Design," *1992 IEEE Vehicular Technology Conference*, Denver, pp. 814-818, May 1992.

[Sei92b] Seidel, S. Y., and Rappaport, T. S., "914 MHz path loss prediction models for indoor wireless communications in multifloored buildings," *IEEE Transactions on Antennas and Propagation*, Vol. 40, No. 2, pp. 207-217, Febuary 1992.

[Sei94] Seidel, S. Y., and Rappaport, T. S., "Site-Specific Propagation Prediction for Wireless In-Building Personal Communication System Design," *IEEE Transactions on Vehicular Technology*, Vol. 43, No. 4, November 1994.

[Sha48] Shannon, C. E., "A mathematical theory of communications," *Bell Systems Technical Journal*, Vol. 27, pp.379 - 423 and 623 - 656, 1948.

[Skl93] Sklar, B., "Defining, Designing, and Evaluating Digital Communication Systems," *IEEE Communications Magazine*, pp. 92-101, November 1993.

[Smi57] Smith, B., "Instantaneous Companding of Quantized Signals," *Bell System Technical Journal*, Vol. 36, pp. 653 - 709, May 1957.

[Smi75] Smith, J. I., "A Computer Generated Multipath Fading Simulation for Mobile Radio," *IEEE Transactions on Vehicular Technology*, Vol. VT-24, No. 3, pp. 39-40, August 1975.

[Sta86] Stark, H., and Woods, J. W., *Probability, Random Variables, and Estimation Theory for Engineers*, Prentice Hall, Englewood Cliffs, N.J. 1986.

[Sta90] Stallings W., *Local Networks*, Macmillan Publishing Company, New York, 1990.

[Ste87] Stein, S., "Fading Channel Issues in System Engineering," *IEEE Journal on Selected Areas in Communications*, Vol. SAC-5, No.2, February 1987.

[Ste90] Steedman, R., "The Common Air Interface MPT 1375," in *Cordless Telecommunications in Europe*, W. H. W. Tuttlebee, editor, Springer-Verlag, 1990.

[Ste92] Steele, R., *Mobile Radio Communications*, IEEE Press, 1992.

[Ste93] Steele, R., "Speech codecs for personal communications," *IEEE Communications Magazine*, pp. 76 - 83, November 1993.

[Ste94] Steele, R. ed., *Mobile Radio Communications*, IEEE Press, 1994.

[Stu81] Stutzman, W. L., and Thiele, G. A., *Antenna Theory and Design,* John Wiley & Sons, New York, 1981.

[Stu93] Stutzman, W. L., *Polarization in Electromagnetic Systems*, Artech House, Boston, 1993.

[Sun86] Sundberg, C., "Continuous Phase Modulation," *IEEE Communications Magazine*, Vol. 24, No.4, pp. 25-38, April 1986.

[Sun94] Sung, C. W., and Wong, W. S., "User Speed Estimation and Dynamic Channel Allocation in Hierarchical Cellular System," *Proceedings of IEEE 1994 Vehicular Technology Conference*, Stockholm, Sweden, pp. 91-95, 1994.

[Tan81] Tanenbaum, A. S., *Computer Networks*, Prentice Hall Inc., 1981.

[Tek91] Tekinay, S., and Jabbari, B., "Handover and Channel Assignment in Mobile Cellular Networks," *IEEE Communications Magazine*, pp. 42-46, November 1991.

[TIA93] TIA/EIA Interim Standard-95, "Mobile Station — Base Station Compatibility Standard for Dual-Mode Wideband Spread Spectrum Cellular System," July 1993.

[Tob75] Tobagi, F. A., and Kleinrock, L., "Packet Switching in Radio Channels, Part II: The Hidden-Terminal Problem in Carrier Sense Multiple Access and the Busy-Tone Solution," *IEEE Transaction on Communication*, Vol. 23, No. 5, pp. 1417-1433, 1975.

[Tre83] Treichler, J. R., and Agee, B. G., "A New Approach to Multipath Correction of Constant Modulus Signals," *IEEE Transactions on Acoustics, Speech, and Signal Processing*, Vol. ASSP-31, pp. 459-471, 1983.

[Tri79] Tribolet, J. M., and Crochiere, R. E., "Frequency domain coding of speech," *IEEE Transactions on Acoustics, Speech, and Signal Processing*, Vol. ASSP-27, pp. 512 - 530, October 1979.

[Tuc93] Tuch, B., "Development of WaveLAN, and ISM Band Wireless LAN," *AT&T Technical Journal,* pp. 27-37, July/August 1993.

[Tur87] Turkmani, A. M. D., Parson, J. D., and Lewis, D. G., "Radio Propagation into Buildings at 441, 900, and 1400 MHz," *Proceedings of the 4th International Conference on Land Mobile Radio*, December 1987.

[Tur92] Turkmani, A.M.D., Toledo, A.F., "Propagation into and within buildings at 900, 1800, and 2300 MHz," *IEEE Vehicular Technology Conference,* 1992.

[Ung87] Ungerboeck, G., "Trellis Coded Modulation With Redundant Signal Sets Part 1: Introduction," *IEEE Communication Magazine*, Vol. 25, No. 2, pp. 5-21, February 1987.

[Val93] Valenzuela, R. A., "A Ray Tracing Approach to Predicting Indoor Wireless Transmission," *IEEE Vehicular Technology Conference Proceedings*, pp. 214-218, 1993.

[Van92] Van Nielen, M. J. J., "UMTS: A Third Generation Mobile System," *IEEE Third International Symposium on Personal, Indoor & Mobile Radio Communications*, pp. 17-21, 1992.

[Van87] Van Rees, J., "Measurements of the Wideband Radio Channel Characteristics for Rural, Residential and Suburban areas", *IEEE Transactions on Vehicular Technology*, Vol. VT-36, pp.1-6, February 1987.

[Var88] Vary, P., et.al., "Speech Codec for the Pan-European Mobile Radio System," *Proceedings of ICASSP*, pp. 227 - 230, 1988.

[Vau90] Vaughan, R.,"Polarization Diversity in Mobile Communications," *IEEE Trans on Vehicular Technology*, Vol. 39, No. 3, pp. 177-186, August 1990.

[Vio88] Violette, E. J., Espeland, R. H., and Allen, K. C., "Millimeter-Wave Propagation Characteristics and Channel Performance for Urban-Suburban Environments," *National Telecommunications and Information Administration*, NTIA Report 88-239, December 1988.

[Vit67] Viterbi, A. J., "Error Bounds for Convolutional Codes and an Asymptotically Optimum Decoding Algorithm," *IEEE Transactions on Information Theory,* Vol. IT-13, pp. 260-269, April 1967.

[Vit79] Viterbi, A. J., and Omura, J. K., *Principles of Digital Communication and Coding*, Mc-Graw Hill, New York, 1979.

[Von54] Von Hipple, A.R., *Dielectric Materials and Applications*, Publication of MIT Press, MA, 1954.

[Wag94] Wagen, J., and Rizk, K., "Ray Tracing Based Prediction of Impulse Responses in Urban Microcells", *1994 IEEE Vehicular Technology Conference,* Stockholm, Sweden, pp 210-214, June 1994.

[Wal88] Walfisch, J., and Bertoni, H. L., "A Theoretical Model of UHF Propagation in Urban Environments," IE*EE Transactions on Antennas and Propagation*, Vol. AP-36, pp. 1788-1796, October, 1988.

[Wal92] Walker, E. H., "Penetration of Radio Signals into Buildings in Cellular Radio Environments," *IEEE Vehicular Technology Conference*, 1992.

[Wel78] Wells, R., "SSB for VHF Mobile Radio at 5 kHz Channel Spacing," *Proceedings of IERE Conference on Radio Receivers and Associated Systems*, Southampton, England, pp. 29-36, July 1978.

[Wid66] Widrow, B., "Adaptive Filter, 1: Fundamentals," *Stanford Electronics Laboratory*, Stanford University, Stanford, CA, Tech. Rep. 6764-6 December 1966.

[Wid85] Widrow, B., and Stearns, S. D., *Adaptive Signal Processing*, Prentice Hall, 1985.

[Woe94] Woerner, B. D., Reed, J. H., and Rappaport, T. S., "Simulation Issues for Future Wireless Modems," *IEEE Communications Magazine,* pp. 19-35, July 1994.

[Xia92] Xia, H., and Bertoni, H. L., "Diffraction of Cylindrical and Plane Waves by an Array of Absorbing Half Screens," *IEEE Transactions on Antennas and Propagation*, Vol. 40, No. 2, pp. 170-177, February 1992.

[Xia93] Xia H., et. al, "Radio Propagation Characteristics for Line-of-Sight Microcellular and Personal Communications," *IEEE Transactions on Antennas and Propagation*, Vol. 41, No. 10, pp. 1439-1447, October 1993.

[Xio94] Xiong, F., "Modem Techniques in Satellite Communications," *IEEE Communications Magazine*, pp. 84-97, August 1994.

[Yac93] Yacoub, M. D., *Foundations of Mobile Radio Engineering*, CRC Press, 1993.

[Yao92] Yao, Y. D., and Sheikh, A. U. H., "Bit Error Probabilities of NCFSK and DPSK Signals in Microcellular Mobile Radio Systems," *Electronics Letters*, Vol. 28, No. 4, pp. 363-364, February 1992.

[You79]Young, W.R., "Advanced Mobile Phone Service : Introduction, Background, and Objectives," *Bell Systems Technical Journal*, Vol. 58, pp. 1-14, January 1979.

[Zag91a] Zaghloul, H., Morrison, G., and Fattouche, M., "Frequency Response and Path Loss Measurements of Indoor Channels," *Electronics Letters*, Vol. 27, No. 12, pp. 1021-1022, June 1991.

[Zag91b] Zaghloul, H., Morrison, G., and Fattouche, M., "Comparison of Indoor Propagation Channel Characteristics at Different Frequencies," *Electronics Letters*, Vol. 27, No. 22, pp. 2077-2079, October 1991.

[Zho90] Zhou, K., Proakis, J. G. and Ling, F., "Decision Feedback Equalization of Time Dispersive Channels with Coded Modulation," *IEEE Transactions on Communications*, Vol. 38, pp., 18-24, January 1990.

[Zie90] Ziemer, R. E., and Peterson, R. L., *Digital Communications*, Prentice Hall, Englewood Cliffs, NJ, 1990.

[Zie92] Ziemer, R. E., and Peterson, R. L., *Introduction to Digital Communications*, Macmillan Publishing Company, 1992.

[Zog87] Zogg, A., "Multipath Delay Spread in a Hilly Region at 210 MHz", *IEEE Transacations on Vehicular Technology*, Vol. VT-36, pp. 184-187, November 1987.

Index

R

S

POSTAGE
REQUIRED
Post Office
will not deliver
without proper
postage

Virginia Tech Intellectual Properties, Inc.
1900 Kraft Drive, Suite 107
Blacksburg, VA 24060

Fold Here

WIRELESS SYSTEM DESIGN AND SIMULATION TOOLS

Outdoor and Indoor Channel Modelling, Wireless Link Design and Simulation Software
Please send me more information about licensing the design and simulation software for small-scale and large-scale propagation channels, bit error rate simulation, and wireless system design, as provided by Virginia Tech Intellectual Properties, Inc.

- ❑ Please send me technical information on:
  - ❑ BERSIM, A Wireless Link Bit Error Simulator
  - ❑ SMCHIM, An Outdoor Macro and Microcellular Radio Channel Simulator
  - ❑ SIRCIM, An Indoor Radio Channel Simulator
  - ❑ SMT Plus and SiteBuilder, An Indoor Site Modeling and Planning Tool
- ❑ Please send information on individual and site licenses for universities

Fold Here

- ❑ Please have a Technical Sales Consultant call

Name _____ Title _____

Company Name _____

Street Address-Line 1 _____

Street Address-Line 2 _____

City _____ State _____ Country _____ ZIP _____

Phone _____ e-mail _____

Electrical Engineering
Communications

WIRELESS COMMUNICATIONS

Principles & Practice

Theodore S. Rappaport

As cellular telephones become commonplace business tools, interest in wireless technology is booming. This book responds to that demand with a comprehensive survey of the field, suitable for educational or technical use. Materials are drawn from academic and business sources, numerous journals, and an IEEE professional reader. Extensively illustrated, **Wireless Communications** is filled with examples and problems, solved step by step and clearly explained.

Wireless Communications covers the design fundamentals of cellular systems, including issues of frequency reuse, channel assignments, radio propagation, and both analog and digital modulation techniques. Speech coding, channel coding, diversity, spread spectrum, and multiple access are also discussed. A separate chapter is devoted to wireless networking, including SS7 and ISDN.

Beyond theory, **Wireless Communications** offers practical reference sections, including:

- Complete technical standards for cellular, cordless telephone, and personal communications systems
- International standards for Europe, the Americas, and the Asia-Pacific region
- Noise figure calculations and Gaussian approximations of spread spectrum CDMA interference
- Mathematical tables, identities, and the Q, erf, and erfc functions
- Glossary of abbreviations and acronyms
- Full list of references

This book is designed for use in graduate and undergraduate classrooms, but is also suitable for use by professional engineers and technicians. It can be used for both teaching and reference, and is also appropriate for the interested cellular phone consumer who wants to understand the technology.

Theodore S. Rappaport is professor of Electrical Engineering at Virginia Tech. In 1990, he founded the Mobile and Portable Radio Research Group (MPRG), an educational research center dedicated to training students for the wireless communications industry. He is an active educator, researcher, and consultant for the industry, and has consulted with and conducted short courses for the IEEE and many companies throughout the world. Dr. Rappaport serves as technical editor for several wireless communications journals, has edited four books on the subject of wireless, and has developed over twenty commercial products that are now in daily use by cellular, paging and personal communications operators throughout the world.

PRENTICE HALL
Upper Saddle River, NJ 07458

ISBN 0-7803-1167-1
90000
9 780780 311671
IEEE ORDER NO. PC5641

Rappaport
WIRELESS COMMUNICATIONS
Principles & Practice
PTR
PH